Universitat Autònoma de Barcelona

Design of new ionic liquid-based electrolytes for lithium-oxygen battery

Etienne Knipping

Universitat Autònoma de Barcelona

Design of new ionic liquid-based electrolytes for lithium-oxygen battery

Etienne Knipping

PhD in Chemistry

Advisors:

Dr. Christophe Aucher

Dr. Laurent Aubouy

Dr. Gonzalo Guirado López

Department of Chemistry

Faculty of Science

2018

Memòria presentada per aspirar al Grau de Doctor per

Etienne Knipping

Vist i plau,

Christophe Aucher, PhD Principal researcher Leitat Technological Center	Laurent Aubouy, PhD R&D Director Leitat Technological Center	Gonzalo Guirado López, PhD Associate Professor Department of Chemistry Universitat Autònoma de Barcelona

Bellaterra, 15 de Maig de 2018

Direction certificate

Design of new ionic liquid-based electrolytes for lithium-oxygen battery

A thesis submitted in partial fulfillment of the requirements for the degree of

Doctor of Philosophy in Chemistry

by

Etienne Knipping

Department of Chemistry

Advisors:

Dr. Christophe Aucher, PhD. Principal Researcher, Leitat Technological Center.

Dr. Laurent Aubouy, PhD. R&D Director, Leitat Technological Center.

Dr. Gonzalo Guirado López, PhD. Associate Professor, Department of Chemistry, Universitat Autònoma de Barcelona.

À mon père

Acknowledgments

I would like to thank my directors Christophe Aucher, Laurent Aubouy and Gonzalo Guirado, who accepted to supervise this thesis at Leitat with the collaboration of the Universitat Autònoma de Barcelona. This work was carried out in the frame of the European project STABLE (FP7, Grant Agreement n°314508).

I also thank the members of the jury, Thierry Brousse (Université de Nantes - France), Sébastien Fantini (Solvionic, Toulouse - France) and Dino Tonti (ICMAB, Bellaterra - Spain).

Thanks especially to Christophe who is the mentor I could not even hope to have. His methods are not the most conventional but his availability and interest for my work were very helpful. I am also grateful to Laurent with his harsh but constructive remarks and Gonzalo for his kindness and his always positive attitude.

I would like to thank my teammates and ex-teammates too, Maziar who met me at the very beginning of this work, Ángel who gave me some technical but also supportive advice, Marc for its expertise in many fields, Mateu, Flavia, Luis, Gokhan, Belén, Sandra. This work would not have been possible without you but also without the contribution of the different interns, students and co-workers with who I worked and/or partied, Kévin, Simon, Ece, Robin, Antoine, Minerva, David, Sandra, Pau, Ana, Max, Aleix, François, Javi, Giuseppe. Thank you, guys, for your help!

Many other people participated to this achievement, maybe from a farther point of view but still important to notice. That is why I would also like to thank Kostas for his constant support and his trustworthy friendship, Stefanos for his exemplarity and relevance in all his projects, Sophia for her kindness and the revision of my first article, Christina and Simon, who I met more recently but who complete this Greek band with the same friendly and wonderful spirit. I am also thankful to my best men JB and Guillaume, the other "Zamis" Claire and Flavie, and the "Montluçon team" Thibaud, Séb, Clément and Alice. We are much less in contact since we took different directions but every time we meet is like we never split up.

Je remercie bien évidemment ma famille en commençant par ma femme Carolina, qui m'a vraiment donné tous les moyens pour réussir. On dit que derrière chaque grand homme, se cache une femme. Je ne sais pas si je suis un grand homme, ni si elle se cache, mais je suis sûr d'être avec la femme qui me fera réussir. Une autre personne que je remercie est bien sûr mon père qui n'est plus là pour voir cet aboutissement mais qui j'en suis convaincu, aurait été fier et heureux. Il ne me l'a jamais vraiment dit directement, mais je sais qu'il suivait avec attention mon parcours et qu'il faisait tout pour me soutenir. Ma mère, mes frères et sœur, leurs époux(se), Patricia, mes oncles et tantes, mes cousins et cousines, merci à vous aussi d'être là. Une mention spéciale à Sylvain qui, bien qu'il soit le plus éloigné géographiquement, est celui qui a le plus suivi ce travail, avec un point de vue plus décalé mais toujours utile.

Também quero agradecer à minha família portuguesa, Palmira, Pedro, Flávia, Carlos, Avó Lurdes, os tios e os primos. É sempre uma alegria estar com vocês, fico sempre mais positivo e com mais energia depois de estar com vocês. Muito obrigado a todos!

Abstract

The lithium-oxygen ($Li-O_2$) battery has received much interest in the last few years as global energy demand is growing and availability of fossil energies becomes limited. With its high theoretical energy density approaching that of gasoline, this technology is potentially one of the best solutions for electric vehicles (EV). However, this new technology will remain a research topic for at least the next 20 following years, due to the low cyclability, the limited electrical efficiency, the low rate capability and the difficulty of assembling a safe practical cell working in ambient atmosphere as good as at the laboratory scale under well-controlled conditions. Recently, Room Temperature Ionic Liquids (RTILs) attracted much attention. Indeed, their high thermal stability, non-flammability, low vapor pressure and wide potential window can offer an interesting alternative to the traditional organic solvents for $Li-O_2$ battery electrolyte. In this context, the chemical and physical properties of RTILs are determined in order to design a suitable RTIL-based electrolyte. The study of these parameters, compared to the electrochemical performance of the battery, enables to find a correlation between the viscosity, the lithium solvation of the electrolyte and the capacity of the battery. Given that RTILs viscosity is too high for adequate battery reaction kinetics, a mixture of an organic solvent and a RTIL is then studied. Electrolytes composed by dimethylsulfoxide (DMSO), 1-ethyl-3-methylimidazolium bis(trifluoromethylsulfonyl)imide (EMI TFSI) and $LiClO_4$ are characterized, evaluating the suitability of such electrolyte. The optimum concentration of EMI TFSI enables to reduce the overpotential from 1.43 V to 1.06 V, with a cyclability of 69 cycles with 200 mAh g^{-1} of limited capacity. Thereafter, a real-time synchrotron X-ray diffraction technique is applied to analyze the oxidation/reduction of lithium oxide derivatives in an operating battery cell. Four different electrolytes composed of DMSO, a RTIL and $LiClO_4$ are tested. This study proves that the lithium used as anode material is reacting with the RTIL, forming continuously LiOH, independently of the cycling stage. The comparisons between the different electrolytes provide insights for future investigation on the improvement of electrolyte design of this technology.

Resumen

Las baterías de litio-oxigeno (Li-O_2 o litio-aire) son un campo de gran interés y reciente actualidad ya que su densidad energética es teóricamente similar a la de la gasolina. Esta tecnología es potencialmente una de las mejores soluciones para el diseño y la construcción de vehículos eléctricos. Sin embargo, esta nueva tecnología seguirá sujeta a investigación al menos durante los próximos 20 años, debido a su baja ciclabilidad, su eficiencia eléctrica limitada y la dificultad para montar una celda real, segura, y capaz de funcionar en condiciones atmosféricas tan bien como a escala de laboratorio donde las condiciones son controladas. Recientemente, el uso de líquidos iónicos como disolventes verdes está captando la atención de muchos investigadores por características físico-químicas, tales como su casi nula inflamabilidad, su baja presión de vapor y su amplia ventana de potencial. En este sentido los líquidos iónicos ofrecen una alternativa interesante a los disolventes orgánicos tradicionales utilizados para los electrolitos de baterías de Li-O_2. En la presente tesis doctoral, se determinan las propiedades químico-físicas de varios líquidos iónicos para diseñar un electrolito adecuado basado en los mismos. El estudio de estos parámetros, comparados con las prestaciones electroquímicas de la batería, permite encontrar una correlación entre la viscosidad, la solvatación de litio en el electrolito y la capacidad de la batería. Dado que la viscosidad de los líquidos iónicos es demasiado alta para tener una cinética de reacción adecuada en la batería, se estudian mezclas con disolventes orgánicos. Posteriormente, se caracterizan estos electrolitos compuestos de dimetilsulfóxido (DMSO), 1-etil-3-metilimidazolio bis(trifluorometilsulfonil)imida (EMI TFSI) y $LiClO_4$, evaluando la idoneidad de cada formulación. La concentración óptima de EMI TFSI permite reducir el sobrepotencial de 1.43 V a 1.06 V, con una ciclabilidad de 69 ciclos, con una capacidad limitada a 200 mAh g^{-1}. Con estos resultados, se utiliza la difracción de rayos X en tiempo real con un sincrotrón, con el objetivo de analizar la oxidación/reducción de los derivados de óxidos de litio en una batería en funcionamiento. Este estudio demuestra que el litio utilizado como material anódico, reacciona con el líquido iónico, formando LiOH en continuo, independientemente del estado de carga. La comparación entre los diferentes electrolitos, permite incrementar el conocimiento sobre el funcionamiento interno de la batería, para futuras investigaciones sobre el desarrollo de electrolitos para baterías de Li-O_2.

Table of Contents

List of abbreviations

Abbreviation	Full name
AN	acceptor number
BEV	battery electric vehicles
BMI	1-butyl-3-methylimidazolium
BMI TFSI	1-butyl-3-methylimidazolium bis(trifluoromethylsulfonyl)imide
BMP	1-butyl-3methylpyridinium
BoL	beginning of life
Bu_4N	tetrabutylammonium
CN	coordination number
CNT	carbon nanotube
DEC	diethyl carbonate
DMC	dimethyl carbonate
DME	1,2-dimethoxyethane
DMPI TFSI	1,2-dimethyl-3-propylimidazolium bis(trifluoromethylsulfonyl)imide
DMSO	dimethyl sulfoxide
DN	donor number
DSC	differential scanning calorimetry
EC	ethylene carbonate
EMI	1-ethyl-3-methylimidazolium
EMI BF_4	1-ethyl-3-methylimidazolium tetrafluoroborate
EMI Cl	1-ethyl-3-methylimidazolium chloride
EMI PF_6	1-ethyl-3-methylimidazolium hexafluorophosphate
Et_4NBF_4	tetraethylammonium tetrafluoroborate
EV	electric vehicles
GDL	gas diffusion layer
ICE	internal combustion engine
MAD	minimum average duration
MOF	metallic-organic framework
MPT	N-methylphenothiazine
NA	numerical aperture
NCA	nickel-cobalt-aluminum oxide
NMC	nickel-manganese-cobalt
NMP	N-methyl-2-pyrrolidone
OER	oxygen evolution reaction
ORR	oxygen reduction reaction
PC	propylene carbonate
PeO	poly(ethylene oxide)
PHEV	plug-in hybrid electric vehicles
PHS	pumped hydro storage
PI	polyimide
PMI TFSI	1-methyl-3-propylimidazolium bis(trifluoromethylsulfonyl)imide
PP13 TFSI	1-methyl-1-propylpiperidinium bis(trifluoromethylsulfonyl)imide

PVDF	polyvinylidene fluoride
PYR13 TFSI	1-methyl-1-propylpyrrolidinium bis(trifluoromethylsulfonyl)imide
PYR14 TFSI	1-butyl-1-methylpyrrolidinium bis(trifluoromethylsulfonyl)imide
R&D	Research and Development
RTILs	Room Temperature Ionic Liquids
SEI	solid electrolyte interphase
SEM	Scanning Electron Microscopy
SHE	standard hydrogen electrode
SS	spot size
TEGDME	tetraethylene glycol dimethyl ether
TFSI	bis(trifluoromethylsulfonyl)imide
TGA	thermo gravimetric analysis
WD	working distance
XRD	X-ray diffraction

Chapter 1. Introduction

1.1. Li-air batteries

1.1.1. Applications and overview

Today fossil fuels are the main source of energy but because of their limited reserves and their impact on the climate, renewable energies are being more and more developed. Moreover, the global energy demand is in constant growth which encourages the countries to find alternatives. Renewable energies are mostly coming from sun and wind energies, that is to say that energy is produced when the sun is shining and the wind is blowing. As these phenomena are not necessarily matching the energy demand, the storage of this energy is necessary. Pumped hydro storage systems (PHS) are the most used energy storage options. They are the most effective for large amount systems but they require large capital costs and an appropriate geography. On the other hand, rechargeable batteries are mostly used for mobile applications because they have high energy density, which compensate their generally high cost per kWh.

Batteries are electrochemical cells that convert chemical energy into electrical energy. There are two types of batteries, the primary one which can only discharge and the secondary battery which is able to store energy and recharge for several cycles. The first battery was invented by Alessandro Volta in 1800 using a pile of copper and zinc electrodes separated with a felt paper soaked with sodium chloride as electrolyte. Since then, many other technologies have been developed such as the Lead-acid (Pb-acid), Nickel-Cadmium (Ni-Cd), Nickel Metalhydrate (Ni-MH) and more recently Li-ion batteries. Li battery was first proposed by M. S. Whittingham in the 1970s but this is with their Li-$LiCoO_2$ system that John Goodenough and Koichi Mizushima make the commercialization of this battery possible, occurring 12 years later, in 1991, by Sony. The production will then keep growing, reaching today an annual production of 6 billion cells, equivalent to 90 GWh, for a market of US$20 billion, mostly oriented to small electronic (laptops, smartphones, tablets…) and electrical mobility (PHEV, BEV). And the production will keep increasing as the forecast indicates 300 GWh produced in 2025 (Avicenne Energy 2016).

The energy density of Li-ion battery is since then still increasing with the optimization of the manufacturing and the development of new materials. Indeed, the development of

high voltage spinel or nickel rich cathode or others such as layered and cobalt based oxide (NMC, NCA) and higher capacity anode such as phosphides or Si composites enable to increase the energy density, which is proportional to the voltage and the capacity. Next Li-ion battery generations include also solid electrolytes and lithium metal as anode. However, the Li-ion technology is reaching its limit around 250-300 Wh kg^{-1} and 600-700 Wh L^{-1} due to its intrinsic features, as it can be seen in the Figure 1, where the different options of cathode and anode materials are mapped in function of their voltage and capacity. Moreover, several other concerns are met in the Li-ion battery sector. The cycle life of high voltage spinel and other high energy systems is quite low, typically losing 80% of the beginning of life (BoL) before 500 cycles [1]. The layer-structured cathode materials have generally low thermal stability leading to safety issues [2]. The cobalt used in the cathode is listed in the critical raw materials by the European Commission, as the resources are limited, coming for the most part from the Congo with serious environmental and ethical concerns. Miners are indeed using hand tools, under low safety standards and include also children [3].

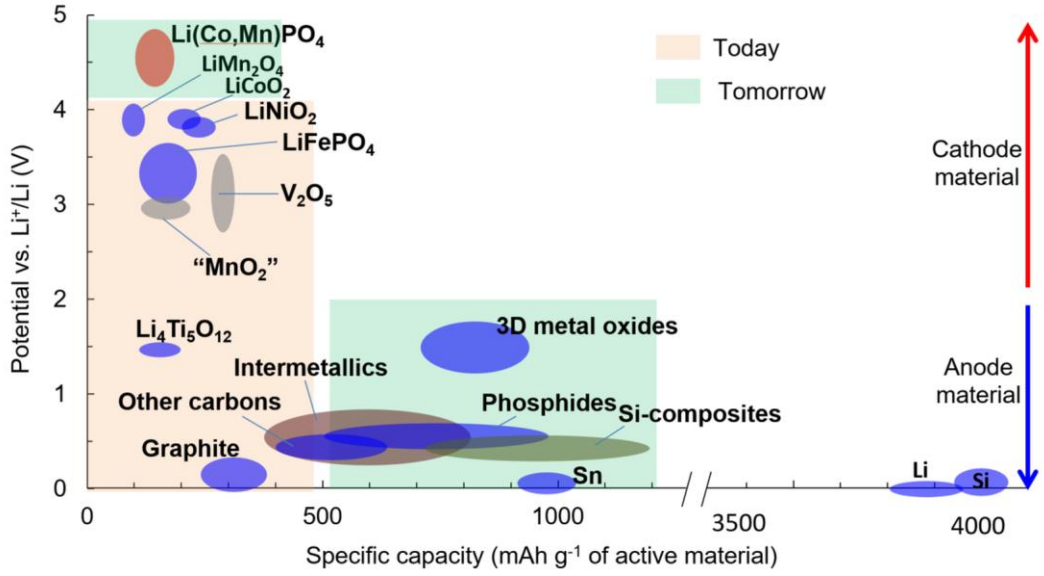

Figure 1: Current (Today) and future (Tomorrow) material options for Li-ion battery technology.

More recently, new technologies called Post Li-ion are emerging, such as Na-ion, Mg-ion, Al-ion, lithium-sulfur or lithium-air that present high theoretical energy density and would be excellent alternatives to Li-ion batteries for applications like electrical vehicles or grid support. Indeed, they give the possibility to develop low carbon footprint cell manufacturing with more abundant and accessible materials.

Among these Post Li-ion technologies, the Li-air battery has the highest theoretical energy density compared to all other battery chemistry (Figure 2), with 5217 Wh kg^{-1} [4,5]. Such value would offer a specific energy higher than 1000 Wh kg^{-1} [6] at the cell level, versus 250 Wh kg^{-1} at present for Li-ion battery, if several challenges can be overcome. The first paper on Li-air battery has been published in 1976 [7] where A. Galbraith presented a "Li-water-air battery" for automotive propulsion. Then, the first nonaqueous Li-air battery was published by K. Abraham et al. in 1996 [8] with a system including a polymer electrolyte membrane and a carbon composite electrode. But it is in the past decade that the interest has grown significantly, with more than 600 patents per years in the last five years, as global energy demand is growing and availability of fossil energies becomes limited. Moreover, the population growth and the European policy that targets to reduce the CO_2 emissions by 40% by 2030 [9] push to the transportation electrification. From this context and regarding the potential energy density of this new technology, which is close to the one of internal combustion engine technology (ICE) [10], the main application for Li-air battery would be electric vehicles (EV). The concept consists in developing an electric car that reduces the range-anxiety, complying with the same distance range as gasoline, cheaper and CO_2 emission free. Several companies including automotive manufacturers already applied for many patents on Li-air technology [11–26]. In particular, Toyota worked on new kind of electrolytes [13] and on a 2-compartment cell using lithium ion conductive membrane [21], Hyundai developed hybrid cell using both liquid and solid electrolytes [15] and Badding and coworkers [12] patented a Ni foam current collector that includes nanowire catalysts.

In the case of non-rechargeable Li-air batteries, their high energy density would enable a higher autonomy defined by the Minimum Average Duration (MAD) with respect to current commercial primary battery such as Zn-air batteries for small electronic (e.g. emergency devices or hearing aids) [4].

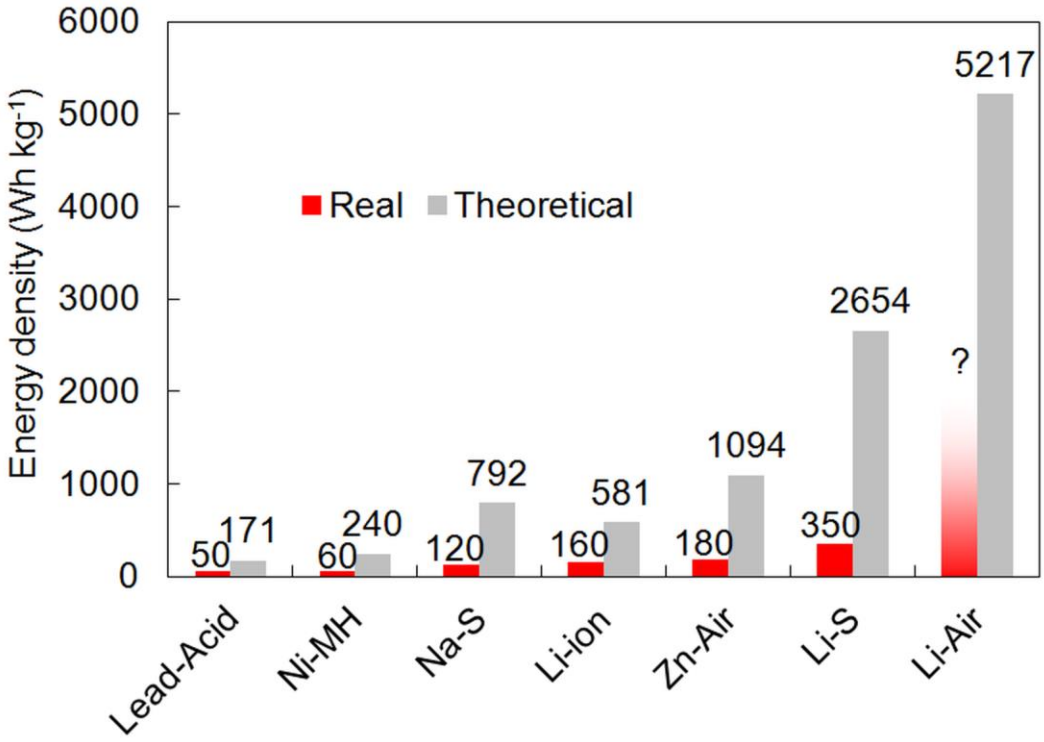

Figure 2: Specific energy density (Wh kg^{-1}) of different types of batteries. The theoretical values (grey bars) are based strictly on thermodynamics while the real values are indicated by the red bars.

While many researchers refer to "Li-air battery", most of their work actually focuses on the Li-O_2 battery, as O_2 is the true cathode active material and components in air such as H_2O and CO_2 can interfere with the electrochemical behavior of the battery. Four main architectures (aprotic, aqueous, solid state and mixed aqueous-aprotic) of Li-O_2 batteries can be highlighted, shown in the Figure 3. All four types consist of lithium metal anode and air (oxygen) cathode.

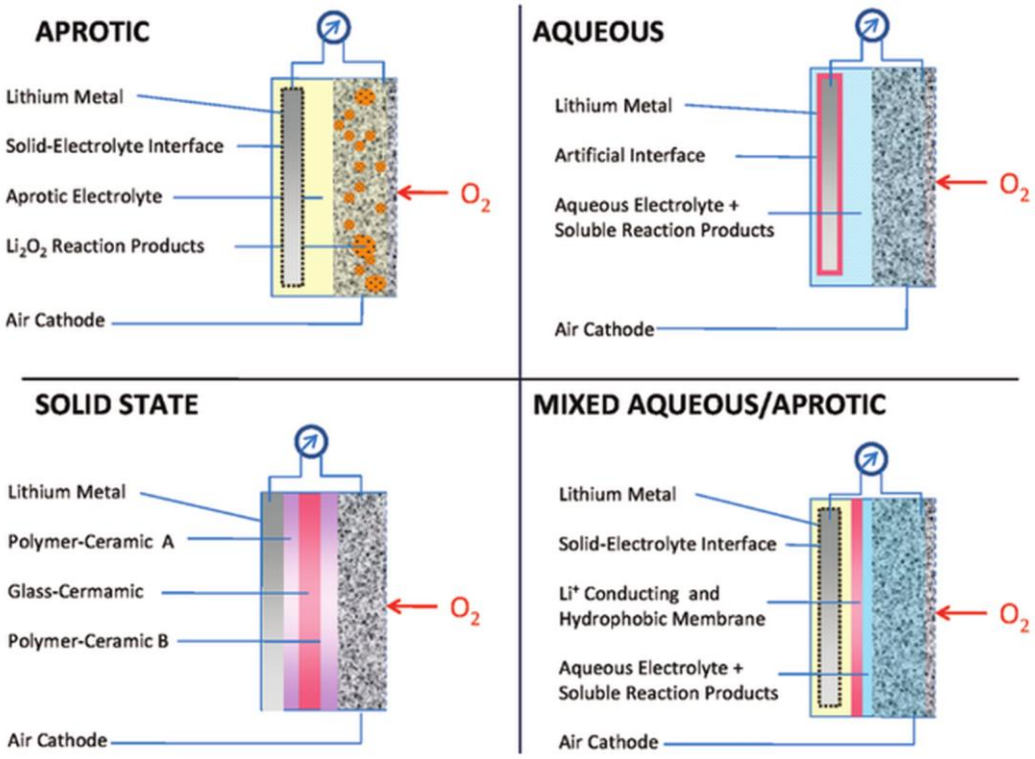

Figure 3: The four main architectures of Li-O_2 batteries [10].

The aqueous one is using water as electrolyte solvent and then a protective membrane on the lithium anode to protect it from oxidation. The main advantages are the high discharge potential of 3.4-4.3 V vs. Li^+/Li allowing a specific energy of 700 Wh kg^{-1}, the high round-trip efficiency and the solubility of the discharge products in the electrolyte [27]. The latter has also a higher conductivity than the most part of organic solvent. The main issue is the high reactivity of the lithium metal with water, which entails the use of protective, Li^+-conductive membranes. Glass ceramics (e.g. LISICON) are generally used but they are expensive, degrade with time and are not easy to fabricate [6]. This lead to complicated and challenging fabrication process.

The mixed aqueous / aprotic architecture combines both aqueous and aprotic architectures, taking advantage of the stable behavior of lithium ions in aprotic solvent and the high solubility of the discharge products in water. The inconvenient is the same as the aqueous system with the need of a Li^+-conductive membranes. The difference is that an aprotic solvent is in direct contact with the lithium anode, forming a natural solid electrolyte interphase (SEI). Visco *et al*. [22]. have developed an aprotic Li-O_2 cell with an artificial ceramic SEI to protect the anode, achieving 60 cycles in air with 50% relative humidity.

All-solid-state battery is using a solid or gel polymer electrolyte that enables the same performance than aprotic batteries but improving the safety of the device as the components are nonflammable and generally nontoxic [28]. Moreover, the protection of the lithium from moisture and CO_2 is increased. However the low ionic conductivity, the stability of the polymer electrolyte with the charge/discharge products and the interfacial chemistry between the components are the main issues of this architecture. Many material developments have to be done to achieve a practical solid-state battery.

The aprotic one has received most attention in literature due to the problems with important ohmic losses, low reversibility and low energy density observed in other systems. It is typically made of a Li metal anode, an aprotic solvent, a separator (e.g. glass fiber or polymer membrane) and a porous "air-cathode". For the latter, carbon material is an adequate choice considering their light weight, high conductivity, large surface area and oxygen channel flexibility [29]. A slurry is prepared by mixing a carbon black and a polymer binder in an organic solvent or water. This slurry is then coated on a metal grid/foam or a gas diffusion layer (GDL). This three-phase boundary electrode where meet the oxygen, the electrolyte and the reaction products, requires a high surface area, an appropriate pore volume and distribution, mostly mesoporous, a good electrical conductivity and should be designed for gas transport.

The reaction mechanism, which depends on the electrolyte, is described for each type in the Table 1.

Table 1: Types of Li-O_2 batteries with their cell reactions, advantages and disadvantages [30].

Type	Cell reactions	Advantages	Disadvantages
Aprotic [31]	$2Li^+ + 2e^- + O_2 = Li_2O_2$ (2.96 V)	High theoretical energy density, rechargeability	Insoluble discharge products, material challenges
Aqueous [32]	$4\ Li^+ + 4e^- + O_2 = 2Li_2O$ (2.90 V) $4Li + O_2 + 2H_2O = 4LiOH$ (alkaline electrolyte) $4Li + O_2 + 4H^+ = 4Li+ + 2H_2O$ (acidic electrolyte)	No pore clogging, no moisture effects as discharge products are soluble in aqueous system	Lack of Li-ion conducting membrane, undetermined charging behavior
Hybrid [22]	$4Li + O_2 + 2H_2O = 4LiOH$ (alkaline electrolyte) $4Li + O_2 + 4H^+ = 4Li^+ + 2H_2O$ (acidic electrolyte)	No pore clogging, no moisture effects, natural SEI formation on Li anode in aprotic electrolyte	Lack of solid Li-ion conducting membrane, undetermined charging behavior
Solid state [33]	$2Li^+ + 2e^- + O_2 = Li_2O_2$ (3.10 V)	Good stability, may use air, rechargeability, avoids dendrite formation	Low conductivity, capacity and energy density

As the discharge products generated in the aprotic system can be reversed into the original reagents, this system is more advantageous than the other three. The aprotic Li-O_2 battery has actually attracted the most attention worldwide compared to the other systems [31] and is the focus of this thesis.

1.1.2. Working principles of the aprotic Li-O_2 system

Li-O_2 batteries are open at the cathode side to allow oxygen inside the battery. During the discharge, the oxygen that diffused to the cathode is reduced to the superoxide ($O_2^{\cdot-}$) in a one-electron process, usually referred to the Oxygen Reduction Reaction (ORR). As a hard base, the superoxide tends to form ionic bonds with hard Lewis acids such as lithium [34]. The lithium superoxide (LiO_2) is then formed (Equation 1) but is unstable with a very short half-life and decomposes to lithium peroxide (Li_2O_2) and O_2 according to the chemical reaction described by the Equation 2 [34,35]. At the anode, the lithium oxidizes to form the Li^+ cations (Equation 3).

$O_2 + Li^+ + e^- \rightarrow LiO_2$	(E° = 3.0 V vs. Li^+/Li)	Equation 1
$2\ LiO_2 \rightarrow Li_2O_2 + O_2$	(E° = 3.0 – 3.5 V vs. Li^+/Li) [36]	Equation 2
$Li \rightarrow Li^+ + e^-$	(E° = -3.0401 V vs. SHE)	Equation 3

The Figure 4 represents the electrochemistry of the Li-O_2 battery.

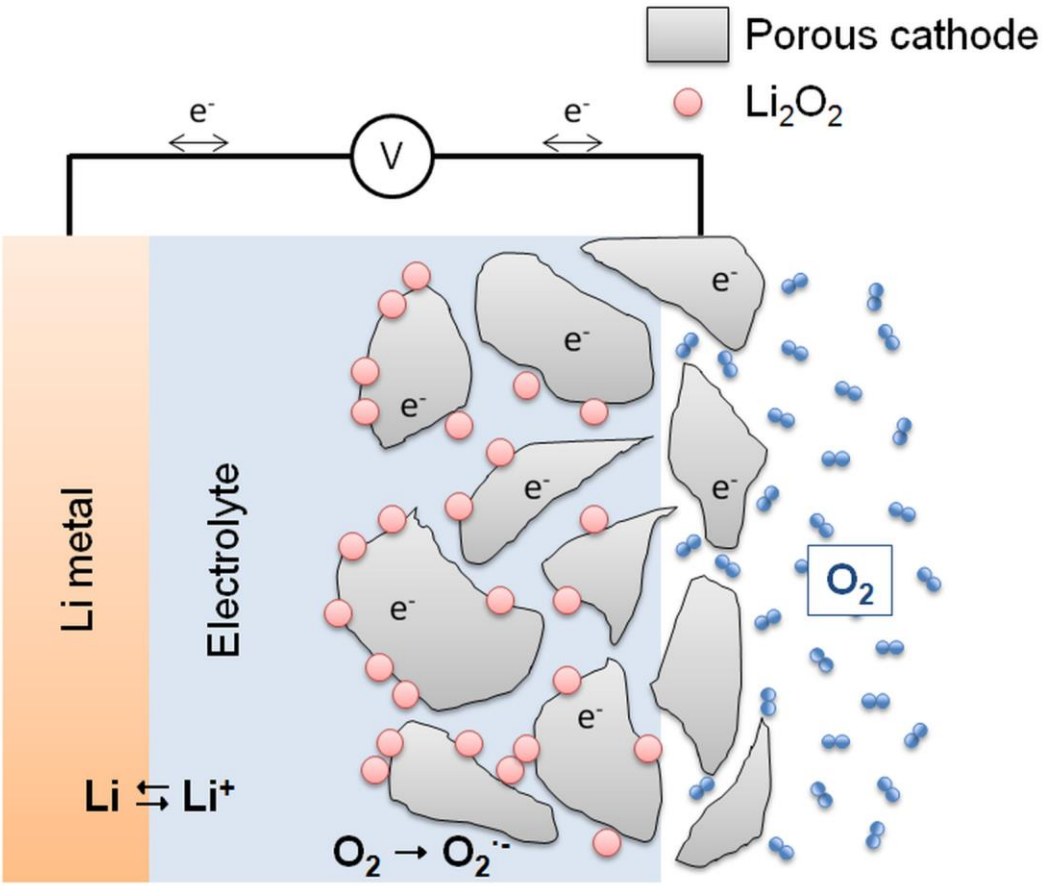

Figure 4: Schematic electrochemistry of an aprotic Li-O_2 battery.

The LiO_2 that survives decomposition is reduced to Li_2O_2 following the electrochemical reaction described by the Equation 4.

$$LiO_2 + Li^+ + e^- \rightarrow Li_2O_2 \qquad (E^\circ = 3.1 \text{ V vs. } Li^+/Li) \qquad \text{Equation 4}$$

Then the lithium peroxide possibly decomposes according to Equation 5.

$$Li_2O_2 + 2\,Li^+ + 2e^- \rightarrow 2\,Li_2O \qquad (E^\circ = 2.87 \text{ V vs. } Li^+/Li)\ [37] \qquad \text{Equation 5}$$

During the recharge, Li_2O_2 is oxidized at the cathode and O_2 is released (Equation 6), hence the so-called Oxygen Evolution Reaction (OER). At the anode, lithium is plated by reduction of the Li^+ (Equation 7).

$$Li_2O_2 \rightarrow 2\,Li^+ + 2e^- + O_2 \qquad \text{Equation 6}$$

$$Li^+ + e^- \rightarrow Li \qquad (E^\circ = -3.0401 \text{ V vs. SHE}) \qquad \text{Equation 7}$$

The specific capacity of a Li-O_2 battery is generally expressed in mAh g^{-1} where the weight is referring to the mass of carbon at the cathode although it is the not the active material. Indeed, unlike Li-ion batteries, the active material of Li-O_2 batteries (Li_2O_2) is essentially synthesized during the discharge process. But to form Li_2O_2, the triple junction where electrolyte, carbon and oxygen coexist is necessary. In other words, the more tri-phase regions, the more Li_2O_2 will be produced and therefore the higher the capacity obtained. This ideal electrochemical process has been quantitatively defined by Luntz *et al*. [38] as following:

(1) The yield of Li_2O_2 relative to that anticipated from the current and ideal cathode reaction $2\ Li^+ + 2\ e^- + O_2 \rightarrow Li_2O_2$ during discharge is 1. In other word, no other products are formed during discharge either on the cathode or in the electrolyte (e.g. LiOH, Li_2CO_3 [39], LiF, carboxylates, etc.).

(2) During discharge, the electrochemical current consumes only O_2, $(e^-/O_2)_{dis} = 2$. And during charge, all electrochemical current evolves O_2, $(e^-/O_2)_{ch} = 2$.

(3) No parasitic gas evolution (H_2, CO_2, etc.) occurs during the charge/discharge cycle.

(4) All O_2 consumed during discharge (ORR) is released during charge (OER) so that OER/ORR = 1.

The Li-O_2 battery is perfectly rechargeable if all these requirements are met.

1.1.3. Challenges in Li-O_2 batteries

Despite this promising performance, Li-O_2 technology will remain a research topic for at least the next two decades, due to the low cyclability, the limited electrical efficiency, the low rate capability and the difficulty of assembling a practical cell working in ambient atmosphere and not at the laboratory scale under well-controlled conditions (Figure 5).

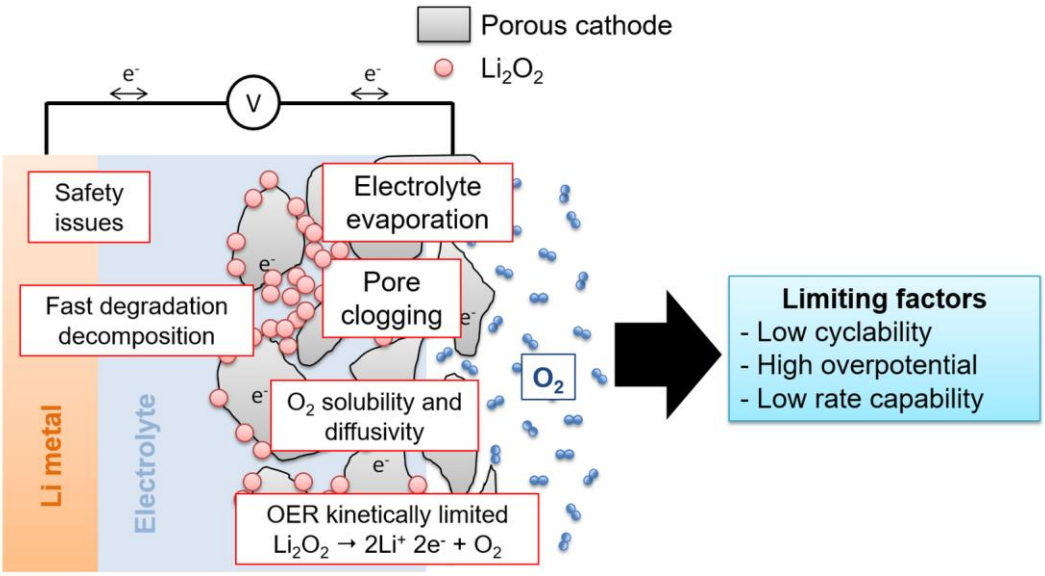

Figure 5: General challenges in current aprotic Li-O2batteries.

1.1.3.1. Development of cathode materials

Many works have been focused on the optimization of the cathode material, tuning the morphology, surface structure, surface area, pore distribution and the pore size [29,40–71]. For instance, Kuboki *et al*. [49] show that a mesoporosity of the carbon would be favorable to improve the discharge capacity. To extend the reaction of Li_2O_2 formation and then reach high specific capacity for a full discharge, Mei *et al*. [55] synthesized SnO_2-C core-shell nanoparticles that exhibits a capacity of 8500 mAh g^{-1} at 75 mA g^{-1}. Chawla *et al*. [40] investigated on cathodes using palladium filled carbon nanotubes that show a discharge capacity of 11000 mAh g^{-1} at 250 mA g^{-1}. Zhang *et* al. [71] fabricated mesoporous Ta_2O_5 nanoparticles as cathode catalyst and obtained 13000 mAh g^{-1} of specific capacity. Wu *et al*. [69] prepared a 3D porous boron-doped reduction graphite oxide material that achieves a capacity of 18000 mAh g^{-1} at 100 mA g^{-1}. Jung *et al*. [46] report a vertically aligned carbon nanotube-ruthenium dioxide core-shell cathode that increases the capacity up to 35000 mAh g^{-1} at 800 mA g^{-1}.

Such capacities seem to be quite high, which is why care must be taken in considering the test conditions, especially the carbon loading per unit area (mg cm^{-2}) of the cathode. The area-specific capacity (mAh cm^{-2}) is a more practical parameter to optimize the performance of the complete air-cathode in a practical Li-O_2 cell. Indeed, it is proportional to the area of the air-cathode exposed to the air and then to the specific

capacity per gram carbon (mAh g^{-1}) and the carbon loading per unit area. In the literature, authors generally use a carbon loading around 1 mg cm^{-2} but rarely above 2 mg cm^{-2} (Figure 6). With such low carbon loading, they obtain very high capacities, higher than 6000 mAh g^{-1} in most cases, which shows the high potential of such technology. However, in a real manufacturing process, the active material loading is usually higher than 2 mg cm^{-2}.

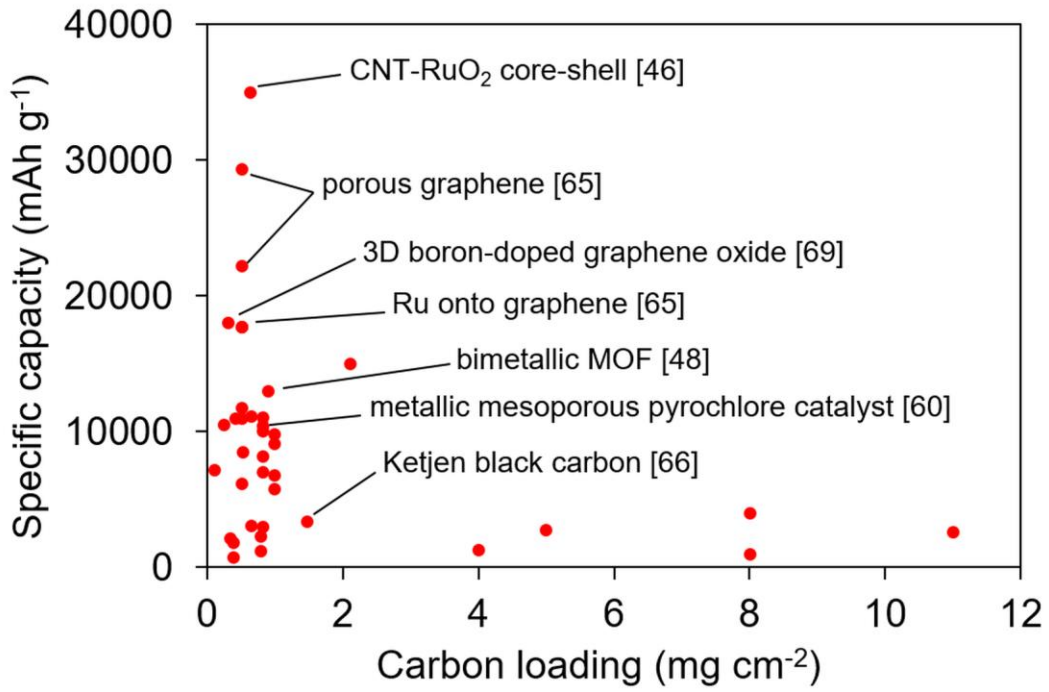

Figure 6: Specific capacity of Li-O_2 battery cells published in the literature in function of the carbon loading specified by the authors.

The major challenge for Li-O_2 battery system is the relatively poor cycle life. Indeed, the specific capacity of the battery drastically decreases after 10-20 cycles in most cases (Figure 7) [72].

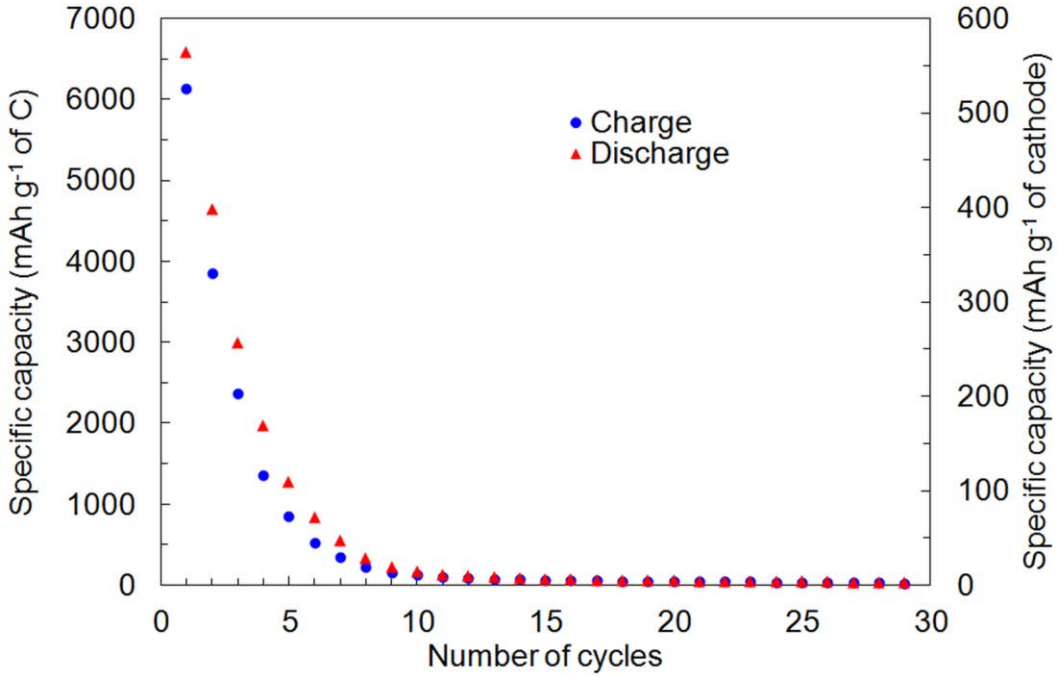

Figure 7: Typical cycling behavior of a Li-O_2 battery using a carbon air-cathode (loading of 2 mg cm^{-2}) at a constant current of 0.1 mA cm^{-2} and 100% of DOD.

Li_2O_2 and the other discharge products formed are insulating and insoluble in the aprotic electrolytes generally used, which leads to the clogging of the cathode pores and the capacity fading. By limiting the time of charge/discharge and using a relatively low current, cyclability of 100 cycles or more can be obtained. Gong *et al*. [73] obtained 112 cycles by limiting the capacity at 1000 mAh g^{-1} and Leng *et al*. [51] obtained a long-term stable cycling of 400 cycles with a limited capacity of 1000 mAh g^{-1} at 400 mA g^{-1}, using a nitrogen-doped reduced graphene oxide as cathode material. However, none of these materials is the ultimate choice and an effective catalyst has still to be identified.

1.1.3.2. Catalysts

Another challenge is the low coulombic efficiency of the battery showed by a high overpotential or polarization loss, i.e. a voltage gap between the discharge and charge processes that can reach almost 2 V (Figure 8).

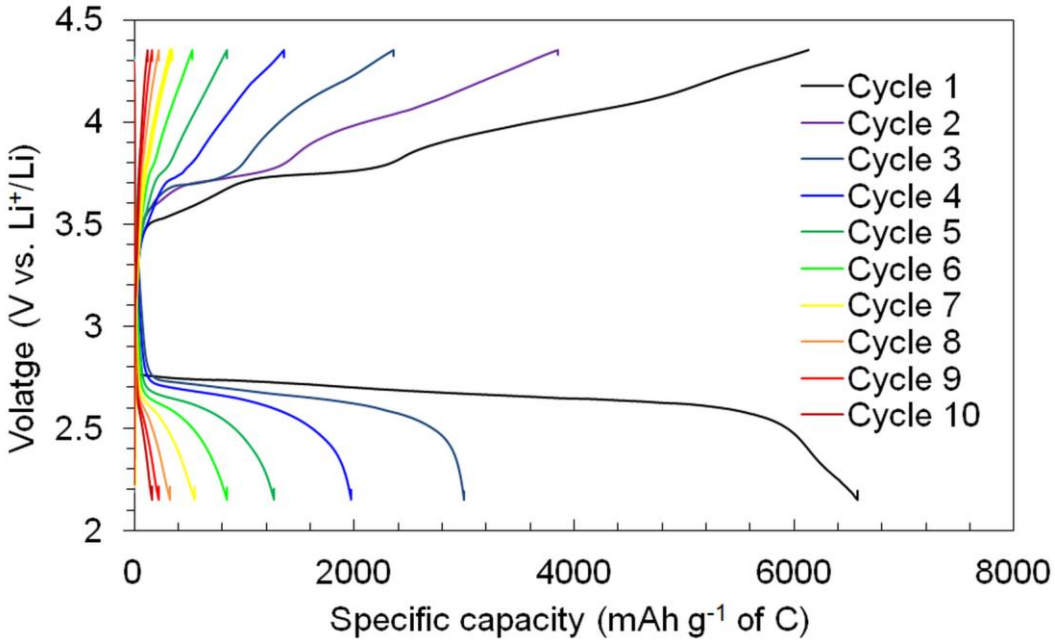

Figure 8: Typical charge and discharge curves of a Li-O_2 battery using a carbon air-cathode (loading of 2 mg cm^{-2}) at a constant current of 0.1 mA cm^{-2} and 100% of DOD.

This phenomenon is due to the Li_2O_2 OER that is kinetically limited by the energy barrier for the evolution of O_2 molecules [58]. Such challenge can be overcome by using effective catalysts. Many literature reports demonstrate that incorporation of metal or metal oxides catalysts in the cathode enhance the energy efficiency of the cell. Kim *et al*. [74] synthesized RuO_2 nanoparticles and manganite as OER and ORR bifunctional catalyst to reduce the charge potential from 4.3 to 3.9 V. Park *et al*. [75] used Ag electrodes, obtaining a charge potential of 3.6 V. Martinez *et al*. showed that carbon nanofibers doped with Pd nanoparticles enable to reduce the charge plateau from 4.2 V vs. Li^+/Li to 3.2 V [76].

Another way to improve the ORR and OER kinetics and reduce the overpotential is adding soluble redox mediators in the electrolyte. A redox mediator (M^{red}) is a molecule in solution that is oxidized directly at the electrode surface to give its oxidized form (M^{ox}) that in turn, oxidizes the discharge products by reducing itself back to M^{red} and so catalyzes the reaction. Some mediators such as tetrathiafluvalene (TTF) [77], LiI [78,79], CsI [80], 2,2,6,6-tetramethylpiperidinyloxyl (TEMPO) [81] and N-methylphenothiazine (MPT) [82] have already shown some improvements for Li-O_2 battery, reducing the overpotential and increasing the efficiency. In the latter case, the incorporation of MPT in the electrolyte results in a reduction of the charge plateau from 4.3 to 3.63 V.

A different approach is to take into consideration the Gutmann donor number (DN), which depicts the electron donating properties of a solvent and hence its ability to interact with acceptors such as Li^+ [83]. A high DN means high basicity of the solvent and then a strong interaction with hard Lewis acids like Li^+ [37]. In particular, electrolytes with high DN or acceptor number (AN) promote solvation of Li^+ or Li^+-containing species (e.g. LiO_2), resulting in the formation of Li_2O_2 through the solution-mediated pathway i.e. the one-electron pathway (Equation 2). On the other hand, in low DN solvents, LiO_2 is not solvated but adsorbed at the cathode surface where it is reduced to form a film of Li_2O_2 (Equation 4). In the former case, the formation of toroidal Li_2O_2 particles is promoted, leading to higher capacity than in the latter one. Thus, Aetukuri *et al*. [84] showed that H_2O, which has a strong acidity (AN = 54.8), promotes the solution-mediated mechanism when added in trace amount. Johnson *et al*. [85] demonstrated that high DN solvents favor also this mechanism, enabling high capacity and low overpotential. Cho *et al*. [86] used Pd_3Co nanoparticles as cathode additive to reduce the size of the toroidal Li_2O_2 particles and then improve the rechargeability of the cell. Indeed their high DN electrolyte led to the formation of crystalline Li_2O_2, showing poor rechargeability with a pristine carbon cathode. Matsuda *et al*. [87] showed that the addition of high AN species such as NH_4^+ in N,N-diethyl-N-(2-methoxyethyl)-N-methylammonium TFSI (DEME TFSI) electrolyte can improve the energy capacity of the battery. Nevertheless, the prolonged presence of LiO_2 in solution may negatively impacts on the stability of the electrolyte [88].

As shown in the previous paragraphs, many works are focused on the cathode development, optimizing the materials and their properties. Indeed, all the porous materials and all the catalysts based on metals or metal oxides offer an infinite number of possibilities. However, in the view of the practical application of the Li-O_2 battery in ambient atmosphere, much of the effort must be dedicated to the development of the lithium anode too, especially its protection.

1.1.3.3. Lithium anode

With its highest theoretical capacity (3860 mAh g^{-1}) and lowest electrochemical potential (-3.04 V vs. SHE), lithium metal is the anode of choice for a battery. But its high reactivity with moisture and CO_2 present in the air and/or in the electrolyte is a critical issue for

long-term operation. Firstly, this affects the safety of the battery and secondly, there is formation of lithium hydroxide (LiOH) in contact with the water coming from the ambient air and/or the electrolyte decomposition [72]. Even if the transport of Li^+ cation is maintained through porous channels in the LiOH layer, the metallic lithium is oxidized until it is completely consumed. Then, for the manufacturing of a practical cell, the protection of the Li anode is necessary. Li ion conducting ceramics (LISICON, LIPON) were widely studied to protect the anode from moisture [30] but they are more adapted to aqueous and solid-state systems. Liu *et al*. [89] developed a stable solid electrolyte interphase (SEI) film based on fluoro ethylene carbonate on the lithium anode, which tripled the number of cycles. Guo *et al*. [90] prepared a lithiated Al-carbon composite that show lower voltage gap between the charge and the discharge and better cycling performance in ambient air. Wu *et al*. [91] built a polyfluorocarbon SEI on a commercial Si particle-based anode to protect it against corrosion from oxygen side reactions and obtained more than 100 cycles. Lee *et al*. [92] designed a Al_2O_3/polymer composite as protective layer for a Li-O_2 cell that exhibited a stable cycling up to 175 cycles.

At laboratory scale, Li-O_2 battery cells generally have a massive excess of lithium. Then its degradation can occur without limiting the electrochemical assessment carried out in this work. This enable to study the other components such as the cathode and the electrolyte more accurately.

1.1.3.4. Development of electrolytes

The role of the electrolyte in a battery is to enable the ion transfer between the anode and the cathode. It is usually a solution (solvent) containing dissociated salts that insure this transfer. One of the biggest challenge to progress in Li-O_2 batteries is development of an electrolyte that requires the following characteristics: (i) compatibility with the anode, (ii) low volatility to avoid the evaporation of the solvent in open cell systems, (iii) high oxygen solubility and diffusivity, (iv) a low viscosity to ensure fast kinetics of mass transport and a high ionic conductivity and (v) a wide electrochemical stability window. Usual carbonate solvents, such as ethylene carbonate (EC), propylene carbonate (PC) and dimethyl carbonate (DMC) from the lithium-ion technology [93] would be good candidates with their stability at high potentials, their ability to form a stable “solid electrolyte interphase” (SEI) on lithium and their high polarity that enables to transport

lithium cations effectively. But they are also good substrates for the nucleophilic attack of the superoxide ($O_2^{\cdot-}$) coming from the ORR [94,95]. Then the decomposition of the carbonate, forming mostly lithium carbonate will result to the passivation of the cathode and a very poor cycle life of the battery. On the other hand, ether solvents are more stable to the superoxide and the discharge products and show the advantages of cathodic stability and low volatility [35]. Both 1,2-dimethoxyethane (DME) and tetraethylene glycol dimethyl ether (TEGDME) are the most-used ether solvents as they form the most of Li_2O_2 during discharge and evolved the most oxygen during charge [38]. However, the degradation of these electrolytes has been observed with the formation of side products like acetates, fomates and carbonates [39,94] (Figure 9), which makes them unsuitable for a practical commercial battery.

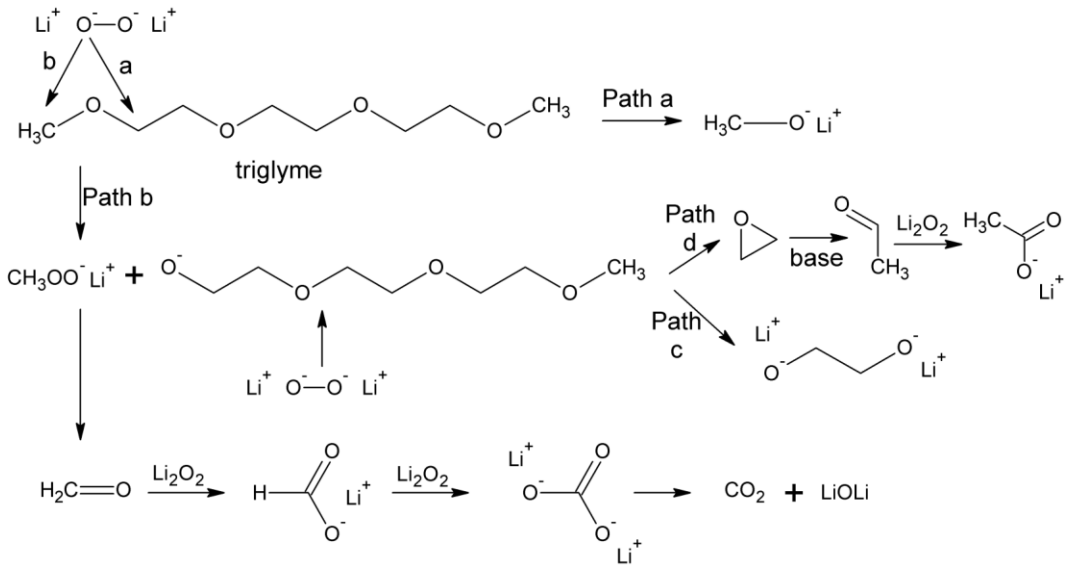

Figure 9: Proposed mechanism for the oxidative degradation of triglyme during ORRs in the presence of Li^+ cations [94].

Dimethyl sulfoxide (DMSO) is also a promising candidate for stable ORRs [66], as it shows longer cycling than the most part of ether solvents. Peng *et al*. [96] have obtained 100 cycles with a Li-O_2 battery cell using DMSO-based electrolyte and porous gold cathode. Ottakam *et al*. [97] also showed 100 cycles with DMSO electrolyte and TiC cathode. However, the DMSO may cause the formation of decomposition product when using the common carbon cathode [27]. Sharon *et al*. [98] investigated on the DMSO decomposition and proposed a mechanism (Figure 10) that may explain the formation of side-products such as LiOH, dimethyl sulfone ($DMSO_2$), Li_2SO_3 and Li_2SO_4.

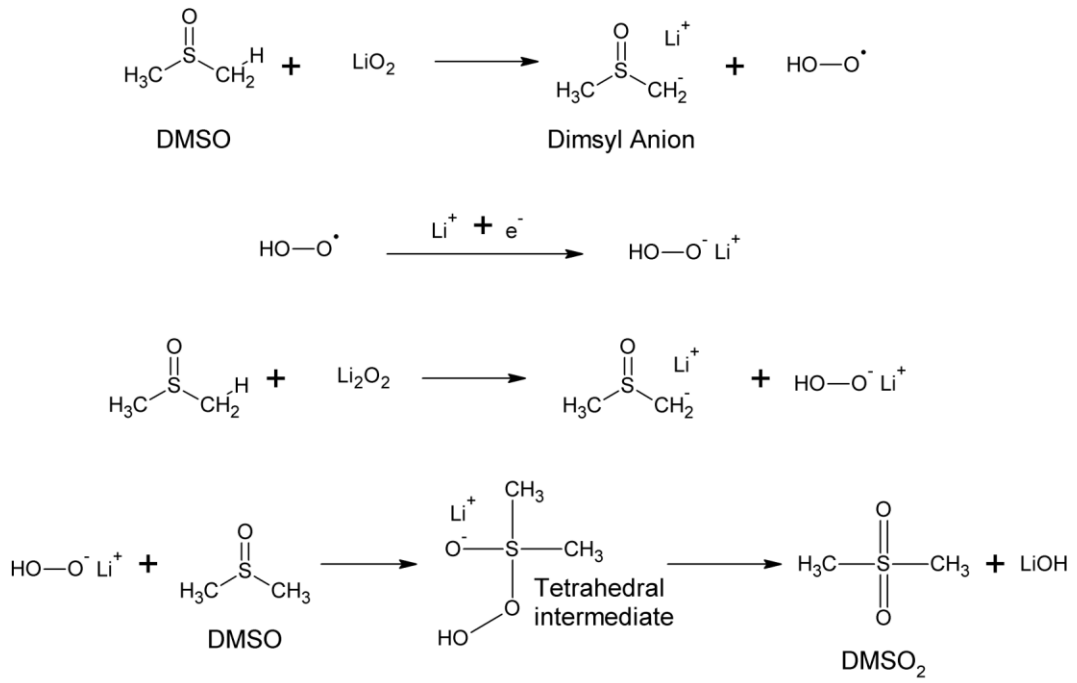

Figure 10: Proposed mechanism of DMSO during ORRs in the presence of Li^+ cations [98].

Concerning the salt, the study of its influence on the Li-O_2 battery operation is more sporadic than the solvent. Nevertheless, several systematic studies have been published, assessing the stability and the performance of various possible salts. Because it provides the best balance between ionic conductivity, thermal stability and formation of a proper SEI, $LiPF_6$ (dominant salt in commercial Li-ion batteries) would be an adequate candidate. However, several works show that this salt is unstable in Li-O_2 battery, decomposing in the presence of O_2^-, LiO_2 and Li_2O_2 [37]. Other salts are then mostly used such as Li triflate, Li TFSI or $LiClO_4$. Elia *et al.* [99] demonstrated the overpotential is affected by the anion nature of salt that alters the SEI resistance, the lithium transference number and the ionic conductivity of the electrolyte. Although their conclusion leans towards the lithium triflate, other salts such as lithium bis(trifluoromethylsulfonyl)imide (Li TFSI) and lithium perchlorate ($LiClO_4$) are also widely used. In particular, $LiClO_4$ is less reactive to oxygen or reduced oxygen [100].

The identification of an adequate solvent-salt combination is crucial to realize a rechargeable Li-O_2 system. Considering their instability, the carbonates solvents can be discarded, whereas the DMSO and ethers are acceptable candidates. The challenge is to identify more stable electrolyte, compatible with the cathode and that facilitates the Li_2O_2

formation. In this regard, an alternative to these electrolytes is the use of ionic liquids, whose characteristics, advantages and disadvantages are detailed in the next part.

1.2. Room Temperature Ionic Liquids (RTILs)

1.2.1. Overview

Room temperature ionic liquids are salts that are in liquid phase at standard temperature and pressure. They are also called room temperature molten salts or simply "ionic liquids" although the latter is generally defined as salts with melting temperatures below 100 ˚C.

This is in the mid-19th century that the first documented observation of ionic liquids appeared with a so-called "red oil" formed during Friedel-Crafts reactions [101]. This "red oil" would now be identified as a heptachlorodialuminate salt, which is a stable intermediate of the $AlCl_3$-catalyzed Friedel-Crafts reactions. The first RTIL, published in 1914, was the ethylammonium nitrate ($EtNH_3$-NO_3) with a melting point of 12 ˚C [102,103]. Then in the 1930s, a patent application described the dissolution of the cellulose in molten pyridinium salts above 130 ˚C [104]. Then some works were published in the 1940s [105,106] and later in the 1070s [107] on the electroplating of aluminum with N-alkylpyridinium chlorominates used as electrolyte. One of the first 1,3-dialkylimidazolium RTIL, obtained by mixing the 1-ethyl-3-methylimidazolium chloride (EMI Cl) with the aluminum trichloride ($AlCl_3$), was reported by Wilkes *et al*. [108] in the 1980s. This is only during the next decade that the EMI^+ cations was more extensively studied with for instance the 1-ethyl-3-methylimidazolium tetrafluoroborate (EMI BF_4) or the 1-ethyl-3-methylimidazolium hexafluorophosphate (EMI PF_6) that thanks to their better stability in air conditions, increase the possibilities for applications. Until 2001, the halogenoaluminates (III) and alkylhalogenoaluminates (III) ionic liquids have been the most widely studied [109]. Nowadays, imidazolium salts are one of the most popular classes of ionic liquids, especially for cellulose dissolution [110]. Other cations that are also more and more studied are the non-aromatic cyclic cations such as pyrrolidinium and piperidinium [111].

1.2.2. Properties of RTILs

The main properties that most of the ionic liquids present and that make them a subject of great interest, are their thermal, chemical and electrochemical stability [101]. Indeed they have the main advantages of molten salts but they avoid the disadvantages caused by high temperature. Then they can be used as solvent with the particularity to have a very wide liquidus range, low flammability and to be non-volatile as they have no measurable vapor pressure [112]. They can be considered as green solvents as they are compatible with a wide selection of organic and inorganic materials, generally highly polar yet non-coordinating and they offer an alternative for two-phase systems [109]. Other important properties are the wide electrochemical window that can reach 5-6 V versus 1.23 V for water (Figure 11), reasonable ionic conductivity (2-10 mS cm^{-1}) and high thermal stability (> 350 ˚C).

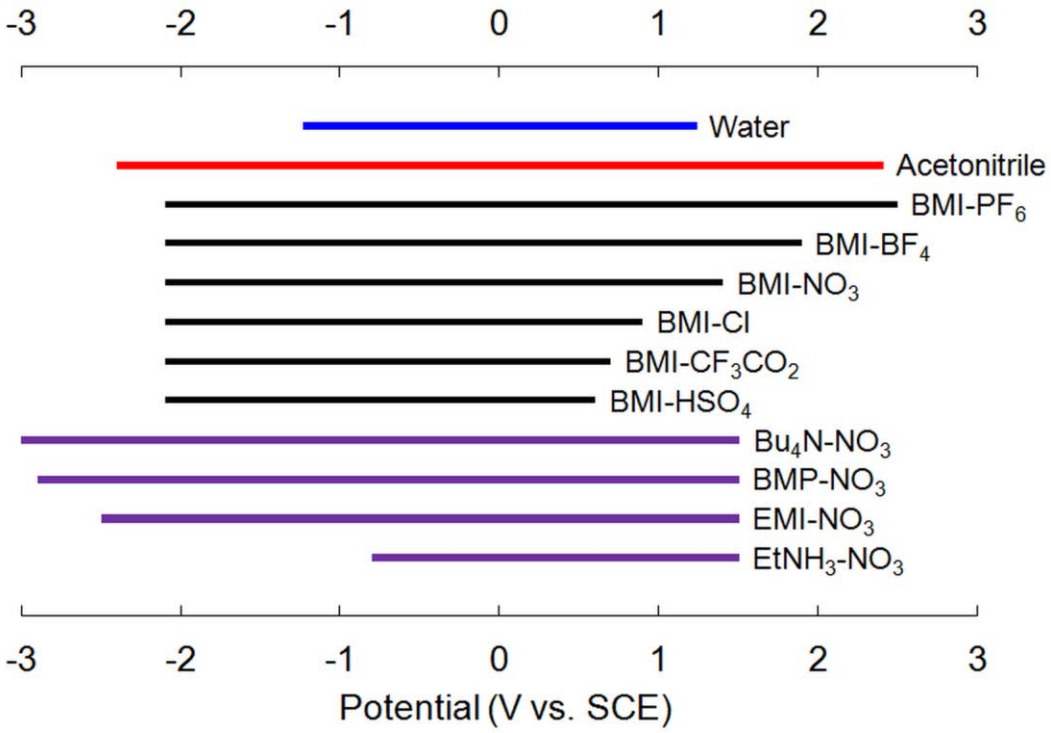

Figure 11: Electrochemical windows for some typical ionic liquids compared to water and acetonitrile (0.1 M Et_4NBF_4, Pt) [113]. BMI: 1-butyl-3-methylimidazolium, Bu_4N: tetrabutylammonium, BMP: 1-butyl-3methylpyridinium, EMI: 1-ethyl-3-methylimmidazolium.

Besides, some physical properties such as the melting point and the viscosity of the ionic liquid can be influenced by the size and the symmetry of the cation. For example, the tetraalkylphosphonium hexafluorophophate (P_{nnnn}-PF_6) shows a maximum melting point

for the symmetric cation P_{6666} (Figure 12). On the other hand, the anion influences more generally the chemical properties and the reactivity. This means there is the possibility to tune the properties of the ionic liquid by combining the adequate cation and anion. One million simple ionic liquids can be easily prepared in the laboratory versus about 600 conventional solvents used in industry. Then there are one billion binary combinations and one trillion ternary systems possible. With only about 300 ionic liquids commercialized at the moment, there are still many opportunities in this field.

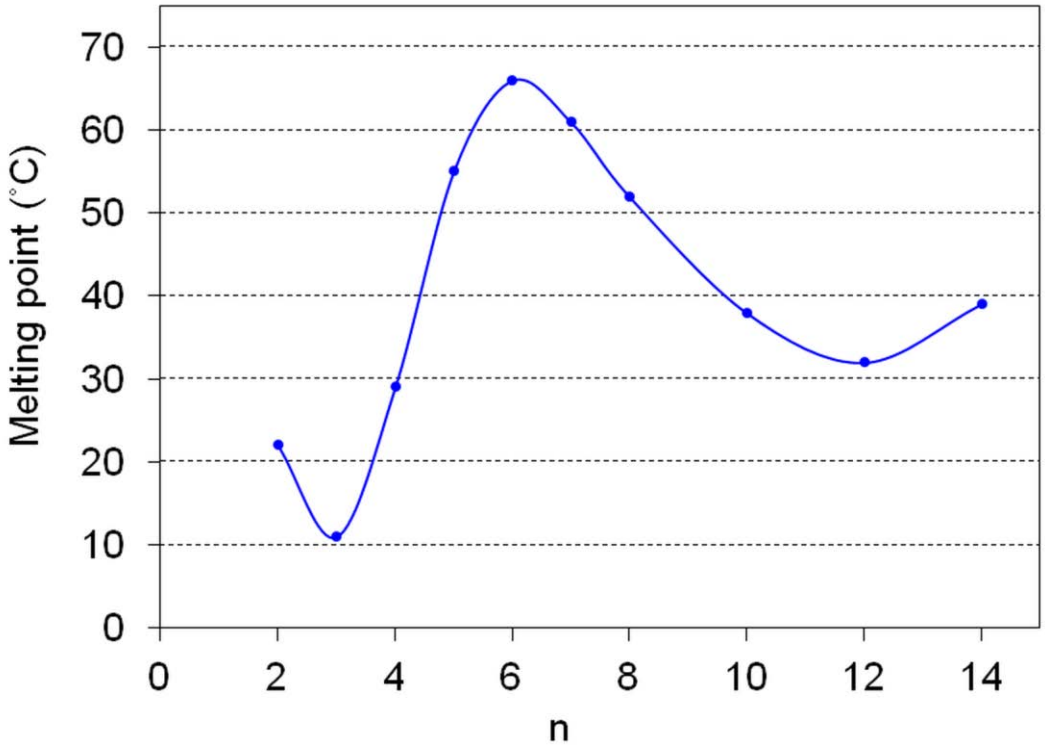

Figure 12: Melting points of P_{666n}-PF_6 as a function of n [114].

1.2.3. Applications of RTILs

Thanks to these particular properties, ionic liquids have many applications, especially in synthesis materials [115,116], sensors [117,118], extraction and separation [119,120], as lubricants [121,122] or in electrochemical processes and devices [123,124]. For instance as dye-sensitized solar cell electrolyte, different ionic liquids have been tested in order to improve the conversion efficiency [125]. Promising results were obtained with a fast diffusion of triiodide but the efficiency is still lower than with traditional solvent like acetonitrile, mainly due to the high viscosity of the ionic liquids. Such electrolyte was also used for electrochemical double layer capacitors [126] allowing higher voltage (up

to 5 V) and then higher energy compared to aqueous (1 V) or organic system (2.5 V). They are also advantageous to operate fuel cells at room temperature although the sensitivity to water contamination remains an issue [127].

Concerning Li batteries, traditional carbonate-based electrolytes are perfectly compatible with lithium anode as they form a protective passivation layer on its surface and enable an excellent diffusion of the Li^+ cations in the electrolyte. However they generate safety issues as they are highly volatile and flammable. That is why using ionic liquid is interesting for this application too. Several findings have brought ionic liquids closer to a practical Li-ion battery [128,129] but they also attract research interest for other battery technology such as Li-S [130–132], Al-ion [133–135], Zn-air [136,137] and Li-O_2 [29,87,95,138–155].

Concerning the latter, Nakamoto *et al*. [95] showed the advantage of the RTILs stability against electrochemical oxidation vs. Li^+/Li and O_2 redox reversibility. Cai *et al*. [142] proved that ionic liquid could show higher specific capacity (1160 mA g^{-1}) compared to carbonate solvent electrolyte (1030 mAh g^{-1}). Cechetto *et al*. [143] observed a decrease of 0.4 V of the overpotential by mixing ionic liquids with an ether-based electrolyte. Asadi *et al*. [140] used also a mixed electrolyte but with EMI BF_4 and DMSO, achieving 700 cycles in simulated air atmosphere with a molybdenum disulfide cathode. Yamagata *et al.* [155] have shown that the interface between the ionic liquid electrolyte and the anode can be stabilized and protected from the ionic liquid decomposition, using an organic additive such as ethylene carbonate and vinylene carbonate. Using cyclic voltammetry and AC impedance measurements, they proposed an electrode/electrolyte interface structure that depends on the ionic liquid used and the coordination of the lithium cation with the anions in solution.

The main families of ionic liquid cations and anions used for Li-O_2 batteries are shown in the Figure 13. The main advantage of these RTILs is their hydrophobicity that reduces the problem of compatibility with the Li anode [156]. Then, other properties will depend on the cation or anion family. As an example, for a given anion, the ionic conductivity decreases in the order: imidazolium > pyrrolidinium > ammonium [157] but the pyrrolidinium- and piperidinium-based cations are more stable against peroxide radical attack than imidazolium-based cations [144]. By changing the anion, other properties can

be altered such as the oxygen solubility that is higher for the TFSI than for the hexafluorophosphate (PF_6) and the tetrafluoroborate (BF_4) [158]. The TFSI anion is also widely used for its high hydrophobicity and stability [159].

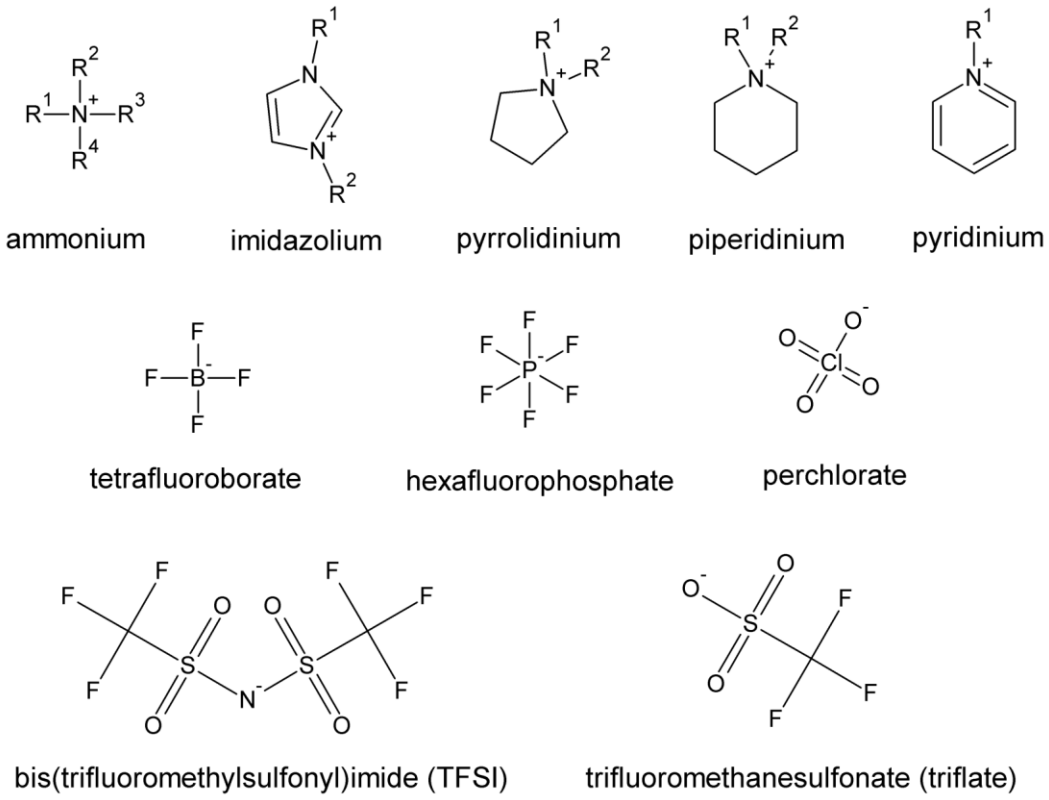

Figure 13: Typical cations and anions used in ionic liquid-based electrolytes. R groups may take one hydrogen atom or different alkyl groups.

However the main drawback associated with RTILs is related to their high viscosity, which results in lower conductivity and therefore in lower capacity compared to the organic solvents. Moreover, they generally decompose at the negative electrode which can lead to a lack of reversibility of the battery reaction [144].

1.3. About this work

1.3.1. Thesis objectives

The Li-O_2 battery has received much interest in the last few years as the global energy demand is growing and the availability of fossil energies becomes limited. In this context and regarding the potential energy density of this new technology, which is close to the

one of internal combustion engine technology (ICE), the project STABLE ("STable high-capacity lithium-Air Batteries with Long cycle life for Electric cars" FP7-NMP, Grant agreement nº 314508) aimed to conceive, from innovative materials, a full electrical vehicle with the best performances and the lowest cost possible. The objective was to obtain a Li-O_2 battery with a specific capacity higher than 2000 mAh g^{-1} with a cyclability of 100-150 cycles. A multidisciplinary work team employed his expertise in material synthesis, characterization and cell assembly to achieve the following tasks: (i) nanostructuration of the Li-anode by electrodeposition, (ii) fabrication of nanostructured carbon cathode and (iii) preparation of ionic liquid-based electrolyte.

The present PhD thesis was carried out in the frame of this project and focused on the development of new electrolytes based on ionic liquids in the final goal to improve both the capacity and cycling life of the battery. It is important to highlight that in 2014, i.e. at the beginning of this work, Cai *et al*. [142] presented a battery using an ionic liquid electrolyte with a capacity of 1160 mAh g^{-1} and Elia *et al*. [145] achieved 30 cycles using a PYR14 TFSI-LiTFSI electrolyte. The main research objectives of the PhD thesis are listed below.

(1) To understand better the working principles of the Li-O_2 battery.

(2) To identify the most suitable RTILs for Li-O_2 battery electrolyte and then to build a Li-O_2 battery cell using only an ionic liquid and a Li salt as electrolyte that presents a specific capacity of at least 1500 mAh g^{-1} at a current density of 0.1 mA cm^{-2} and 100% DOD.

(3) To design a Li-O_2 battery electrolyte partially or fully composed of ionic liquids that allows a cyclability of 100 cycles with limited capacity of 600 mAh g^{-1} at 200 mA g^{-1}.

(4) To determine the nature of the products formed during the battery cycling in order to propose the mechanisms of the Li-O_2 battery reactions that involves ionic liquids. Although there are many results reported on this subject, a few of them were obtained in such medium.

1.3.2. Thesis organization

This thesis has been validated to be presented as a compendium of publications shown in the appendices. The main body is consisted of four chapters written with the following arrangement.

Chapter 1 introduces both Li-O_2 battery and the use of Room Temperature Ionic Liquids as electrolyte for this specific technology. Li-O_2 is described as a potential candidate to replace both primary and secondary system due to its high energy density. In this section, the working principle, the challenges of the electrolytes and the possible prospects of using RTILs are highlighted. Besides these, the research objectives and the thesis organization of this study are also stated.

Chapter 2 describes the experimental procedures, including the apparatus and methods for characterization techniques used to study the electrolytes prepared.

Chapter 3 reports on the results obtained and the corresponding discussion. In a first part, new electrolytes fully composed of ionic liquids in Li-O_2 battery are studied. The thermal and electrochemical stability, the non-volatility and non-flammability of the ionic liquids make them an ideal candidate for Li-O_2 battery electrolyte. They would resolve the problem of safety that present the current battery containing flammable and explosive solvents. That is why a first selection of ionic liquids has been done according to their commercial availability, hydrophobicity and potential window. These ionic liquids were tested as electrolytes in Li-O_2 battery cell and compared to organic solvents to find a correlation between the physicochemical properties of the electrolytes and the rechargeability of the Li-O_2 battery. The results were published in New Journal of Chemistry with an article entitled “Room Temperature Ionic Liquids versus organic solvents as lithium-oxygen battery electrolytes” [160].

The second part of the work presents a study of blended EMI TFSI / DMSO electrolytes. The ion mobility is a key factor for improving the battery performance and consequently, an ionic liquid that generally presents a high viscosity, is limited. That is why blended ionic liquid/organic solvent electrolytes were tested, taking advantage of both liquids properties to achieve better capacity and better cyclability. Some of these mixtures

showed indeed some improvements that would come from the alteration of the reactions medium and therefore the products formed.

The nature of these products has been investigated in the final part where the products formed during the Li-O_2 battery cycling are studied. An *in situ* synchrotron X-ray diffraction was employed to obtain more information on the chemical species involved in the electrochemical process of the battery, which is essential to identify the obstacles to achieve high performance. The results were published in New Journal of Chemistry in the article entitled "*In operando* X-ray diffraction of lithium-oxygen battery using ionic liquid as electrolyte co-solvent" [161].

Finally, it also includes the perspectives of this technology.

Chapter 4 summarizes the results obtained and their interpretation.

Chapter 2. Materials and methods

2.1. Materials

The lists of the solvents, reactants and other materials used, including their provider are presented in the Table 2, Table 3 and Table 4 respectively. Ionic liquids, 99% pure, were purchased from Solvionic or IoLiTec (Ionic Liquids Technologies GmbH). TEGDME, DMSO, EC and DEC were purchased from Sigma Aldrich with purity higher than 99% as well as the salts of lithium bis(trifluoromethanesulphonyl)imide (LiTFSI – 99.95%), lithium perchlorate ($LiClO_4$ – 99.99%) and lithium hexafluorophosphate ($LiPF_6$ – 99.99%). The molecular structure of the solvents and RTILs used are shown in the Figure 14. Electrolytes are prepared by direct mixing of appropriate amount of salt with either a RTIL or a solvent to reach the molar fraction or the concentration desired. The water content of all samples is measured by Karl Fischer (Coulometer KF 831) titration, before and after drying the electrolyte with 4 Å molecular sieves (Aldrich) for two days and stored in argon filled glove box (H_2O < 1 ppm, O_2 < 1 ppm). To exclude the influence of water contamination in the electrolyte, which could affect its stability and the cyclability of the battery [142], the water content of the ionic liquids is lowered until it reaches values below 500 ppm. The same range as for the organic solvents is then obtained.

Table 2: List of the solvents used.

Solvents	Name	Provider	Reference
BMI TFSI	1-butyl-3-methylimidazolium bis(trifluoromethylsulfonyl)imide, 99%	Iolitec	IL-0029-HP
DEC	diethyl carbonate, 99%	Sigma Aldrich	517135
DMPI TFSI	1,2-dimethyl-3-propylimidazolium bis(trifluoromethylsulfonyl)imide, 99%	Iolitec	IL-0134-HP
DMSO	dimethyl sulfoxide, 99.5%	Sigma Aldrich	D5879
EC	ethylene carbonate, 99%	Sigma Aldrich	676802
EMI TFSI	1-ethyl-3-methylimidazolium bis(trifluoromethylsulfonyl)imide, 99%	Solvionic	Im0208c
NMP	N-methyl-2-pyrrolidone, 99.5%	Sigma Aldrich	328634
PMI TFSI	1-methyl-3-propylimidazolium bis(trifluoromethylsulfonyl)imide, 99%	Iolitec	IL-0024-HP
PP13 TFSI	1-methyl-1-propylpiperidinium bis(trifluoromethylsulfonyl)imide, 99%	Iolitec	IL-0045-HP
PYR13 TFSI	1-methyl-1-propylpyrrolidinium bis(trifluoromethylsulfonyl)imide, 99%	Iolitec	IL-0044-HP
PYR14 TFSI	1-butyl-1-methylpyrrolidinium bis(trifluoromethylsulfonyl)imide, 99%	Iolitec	IL-0035-HP
TEGDME	tetraethylene glycol dimethyl ether, 99%	Sigma Aldrich	172405

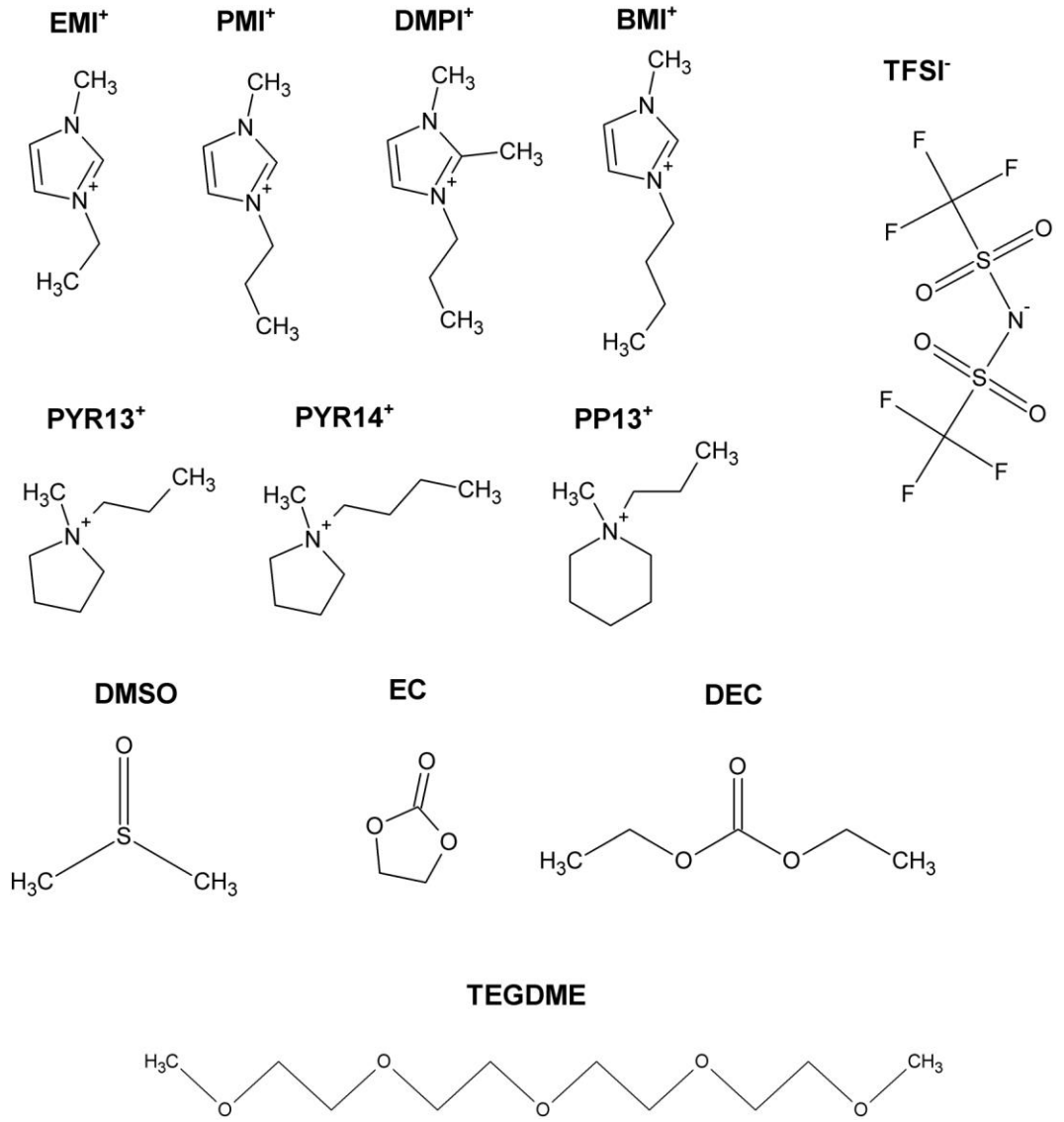

Figure 14: Molecular structure of solvents and RTIL ions used. EMI: 1-ethyl-3-methylimidazolium; PMI: 1-methyl-3-propylimidazolium; DMPI: 1,2-dimethyl-3-propylimidazolium; BMI: 1-butyl-3-methylimidazolium; PYR13: 1-methyl-1-propylpyrrolidinium; PYR14: 1-butyl-1-methylpyrrolidinium; PP13: 1-methyl-1-propylpiperidinium; TFSI: bis(trifluoromethylsulfonyl)imide; DMSO: dimethylsulfoxide; EC: ethylene carbonate; DEC: diethyl carbonate; TEGDME: tetraethylene glycol dimethyl ether

Table 3: List of the reactants used.

Reactants	Description	Provider	Reference
Li chip	lithium chips for anode	MTI Corp.	EQ-Lib-LiC25
Li ribbon	lithium ribbon for electrochemical cell	Sigma Aldrich	265985
Li TFSI	lithium bis(trifluoromethanesulphonyl)imide, 99.95%	Sigma Aldrich	544094
$LiClO_4$	lithium perchlorate, 99.99%	Sigma Aldrich	634565
$LiPF_6$	lithium hexafluorophosphate, 99.99%	Sigma Aldrich	450227
Oxygen	Oxygen gas, 99.995% pure	Air Products	Oxygen Premier
PICAtif carbon	activated carbon	PICA	PICAtif

Table 4: List of the other materials used.

Materials	Description	Provider	Reference
PVDF	polyvinylidene fluoride	Arkema	Kynar ADX 161
Pt electrode	platinum electrode, 3 mm diameter	Bio-Logic	A-002422
Al_2O_3 suspension 0.05µm	Suspension of alumina 0.05 µm	Buehler	40-10083
Al_2O_3 suspension 1µm	Suspension of alumina 1 µm	Buehler	40-10081
Cell	electrochemical Li-O_2 test cell	EL-Cell	ECC-Air
PI tube	polyimide tube, 3mm diameter	Goodfellow	278-183-54
GDL24BA	gas diffusion layer, 190 µm thick	SGL Group	24BA
GDL24BC	gas diffusion layer, 235 µm thick	SGL Group	24BC
GF/A separator	Glass-fiber filter paper Whatman sheets GF/A	Sigma Aldrich	WHA1820866

2.2. Preparation of the cathode

As explained in the introduction, many works are focused on the development of better cathode for Li-O_2 battery. In this thesis, the objectives are related to the improvement of the Li-O_2 battery via the development of new electrolytes. Therefore, in order to test the different electrolytes studied in comparable and reproducible conditions, the same cathode using an activated carbon (PICAtif) coated on a GDL is used. No catalyst neither any kind of additive is used in the cathode coating, so that the improvement of the electrolyte can be observed more easily when tested in the full cell. Then the cathode is prepared from a mixture of PICAtif (PICA) as active material, polyvinylidene fluoride (PVdF Kynar ADX 161, Arkema) as binder and N-methyl-2-pyrrolidone (NMP, 99.5%, Sigma-Aldrich) as solvent. The weight percentage of each component is given in the Table 5.

Table 5: Composition of the ink used for the cathode preparation.

Ink components	Weight % (wet)	Weight % (dry)
PICAtif	11.2	90
PVDF	1.3	10
NMP	87.5	-

The PICAtif is an activated carbon with a mesoporous volume of 0.68 cm^3 g^{-1}, suitable for Li-O_2 battery cathode [45]. A full description of this material is given by Brousse *et al*. [162]. Once the PICAtif is weighted in a vial, the PVDF, previously dissolved in NMP, is added in the same vial. Then the rest of NMP needed is added and the whole mixture is homogenized in a sonication bath for 30 min. The resulting slurry is tape casted on a Gas Diffusion Layer (GDL SIGRACET 24BC – SGL Company) using the doctor blade technique with a wet thickness of 100 µm. The coating is then dried at 70°C under vacuum for 12 hours, resulting to a coating thickness between 20 and 30 µm. Subsequently, 18 mm-diameter disks are punched and weighted, reaching a mass up to a PICAtif loading of 1.5 ± 0.2 mg cm^{-2}. Although the GDL may participate to the overall capacity of the battery [163], only the mass of PICAtif is taken into account to normalize the specific capacity calculated. The different layers that compose the cathode are presented in the Figure 15.

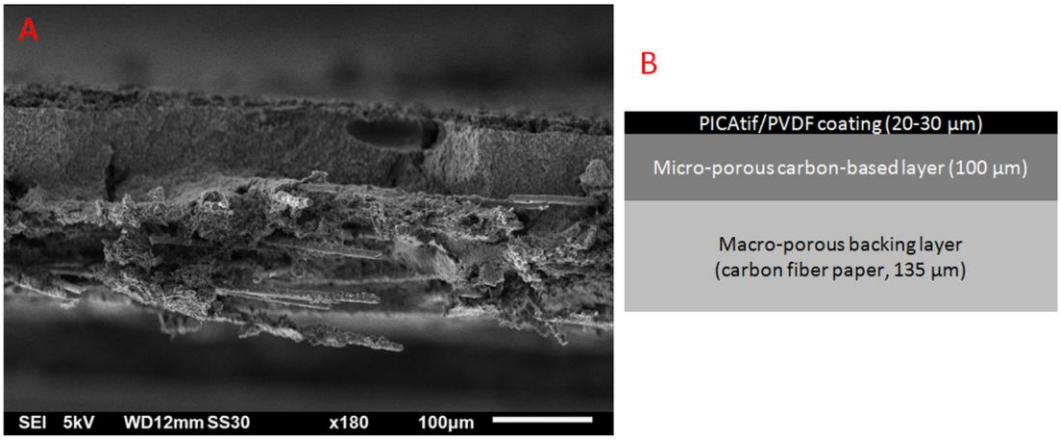

Figure 15: A) SEM image of the transversal cut of the cathode obtained. B) Schematic representation of the different cathode layers.

2.3. Instrumentation and methodology

2.3.1. Ionic conductivity

The ionic conductivity is measured with a titanium tip (Ref. 50 73) on an EC Meter Basic 30+ conductimeter from Crison Instrument (Figure 16).

Figure 16: Photo of the EC Meter Basic 30+ conductimeter (Crison Instrument).

The tip is composed of four electrodes with well-defined surface area *S* and distance between them *d*. A current *i* is applied between the outer pair of electrodes and a potential *E* between the inner electrodes is measured. Then the Ohm's law (Equation 8) enables to determine the resistivity ρ, which is the inverse of the conductivity.

$$\frac{E}{i} = \frac{d}{S}\rho \qquad \text{Equation 8}$$

But generally, for accuracy, a calibration is employed using standard solutions of well-known conductivity.

Thus, the apparatus was first calibrated thanks to the three standard solutions at 147 µS cm^{-1}, 1413 µS cm^{-1} and 12.88 mS cm^{-1} respectively. Then, the samples are measured under constant magnetic steering in a range of temperature from -10 °C to 80 °C. For the

temperature below 0 °C, the vial containing the sample is placed in a mixture of ice and salt. Then the sample is heated using a hot plate. The temperature is stabilized for 30 min before running each measurement.

2.3.2. Viscosity

The viscosities are measured using a Malvern Bohlin CVO 100-901 rheometer (Figure 17).

Figure 17: Photo of the Malvern Bohlin CVO 100-901 rheometer.

The rheometer is used to measure the way in which some liquid flows in response to applied forces. Generally, it is used to measure the evolution of the viscosity of this liquid in function of the shear stress applied i.e. its rheology. In this work, the volume of the sample is limited, especially due to the cost of the RTILs. Then the use of a viscometer that requires at least 10-20 mL per sample is not viable.

With the rheometer, a quantity of around 1 mL of sample is placed on the metallic disk until the whole surface area is covered. Then, shear rates are varied between 0.1 s^{-1} and 10 s^{-1} in air, at room temperature. No shear thinning behavior due to the variation of the shear rate is observed. Hence, the viscosities are determined from the plateau value at high shear rates (Figure 18), 76.1 cP in the case of PYR14 TFSI.

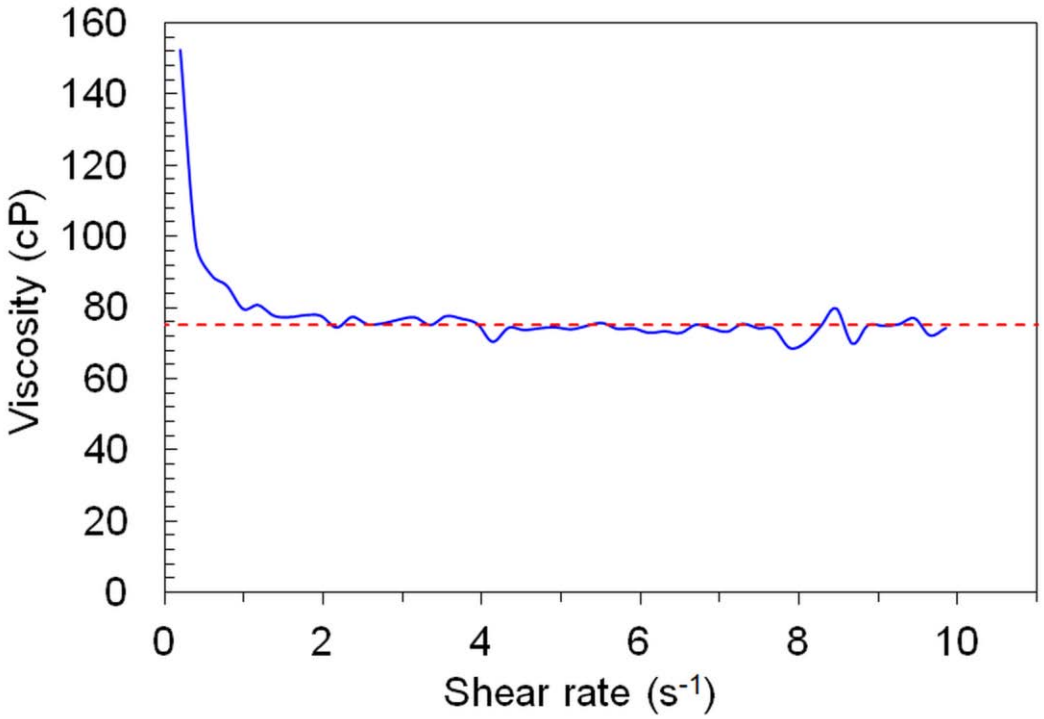

Figure 18: Evolution of the viscosity of PYR14 TFSI sample in function of the shear rate applied.

2.3.3. Thermal stability

Thermogravimetric analysis (TGA) is done with a TA Instruments Q500 apparatus (Figure 19). The TGA consists in measuring the variation of a sample mass over time as the temperature changes. This technique enables to give information about physical phenomena such as phase transitions, degradation temperature and oxidation kinetics of the material studied.

Figure 19: Photo of TGA TA Instruments Q500 apparatus.

Using a Pasteur pipette, a drop of around 5-10 mg is placed in a platinum pan, which is then hanged on the hook above the furnace. When the furnace is closed, a ramp of 10 ºC min^{-1} is applied until 800 ºC in O_2 and then in N_2 atmosphere. In the case of the BMI TFSI, the loss of 100% of the mass at 405°C, highlighted by the peak of the derivative (Figure 20) indicates that it degrades at this temperature.

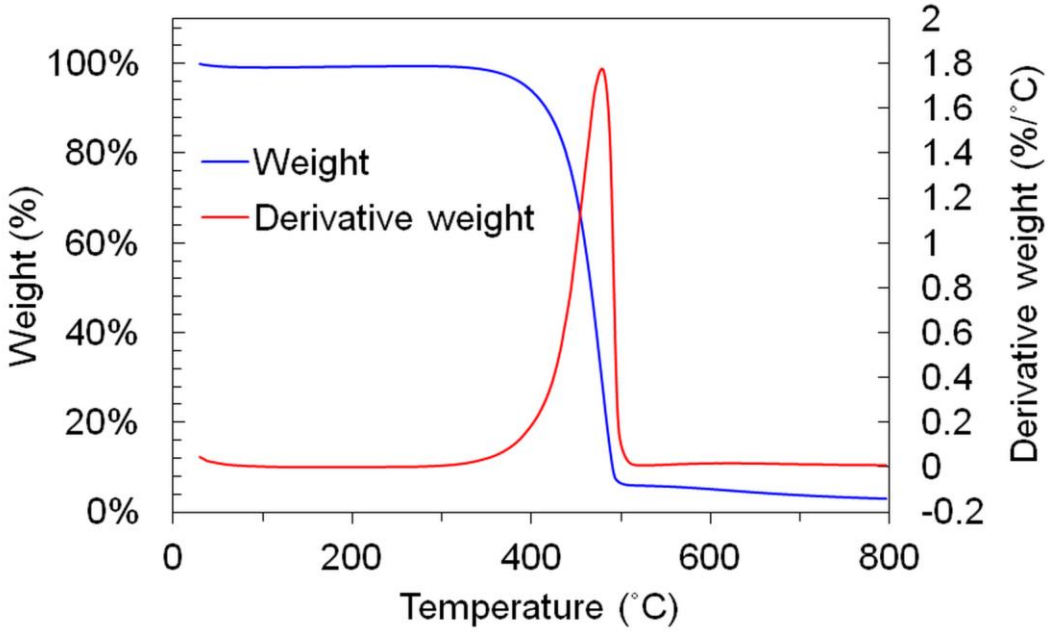

Figure 20: TGA spectra of BMI TFSI measured under nitrogen atmosphere.

Differential scanning calorimetry (DSC) results are obtained using a TA Instruments Q20 apparatus (Figure 21). The DSC is a technique of thermal analysis that consists in measuring the differences of heat exchanges between a sample and a reference (generally the air). It enables to determine the phase transitions of a sample i.e. glass transition, melting point and crystallization temperature.

Figure 21: Photo of DSC TA Instruments Q20 apparatus.

Samples weighting 5-14 mg are hermetically sealed in Al pans and cooled to -90˚C followed by heating to 200˚C applying a scan rate of 10 ˚C min^{-1}. Finally, the samples are cooled back to -90˚C at the same scan rate. As shown in the case of the DMSO/$LiClO_4$ mixture (Figure 22), the positive peak indicates exothermic reaction, here the crystallization, and the negative peak an endothermic reaction like the melting point.

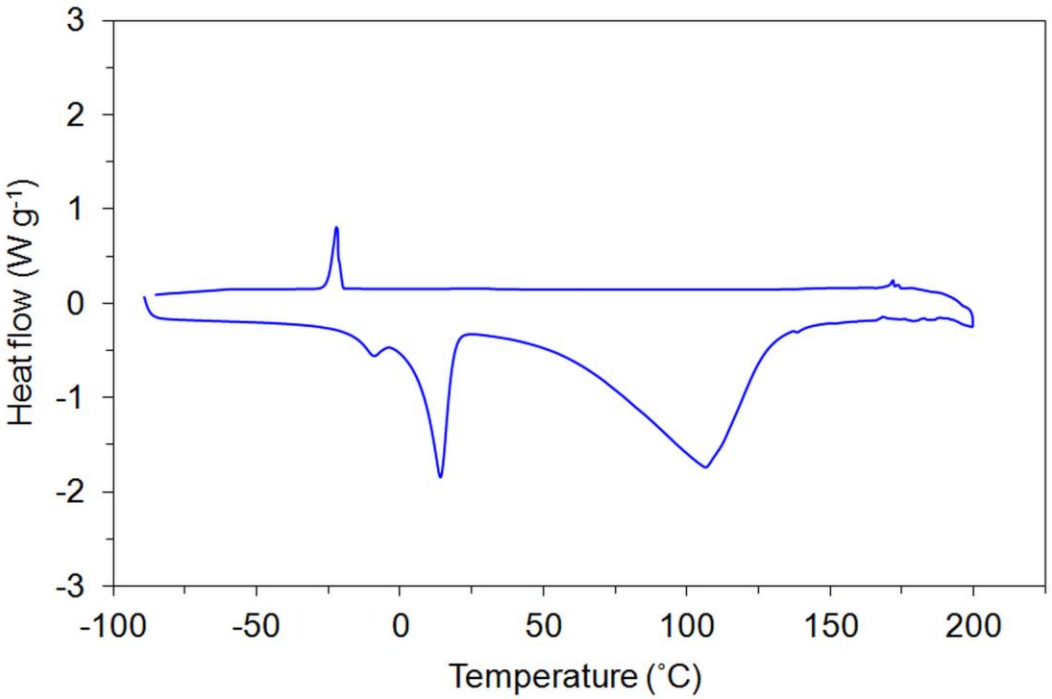

Figure 22: DSC profiles of DMSO/$LiClO_4$ mixture.

2.3.4. Raman spectroscopy

The Raman spectroscopy is a characterization technique used to observe vibrational, rotational and other low-frequency modes in a system to identify molecules and study chemical bonding. The technique consists in illuminating the sample with a laser beam and analyzing the light diffused. When the light passes through the sample, the frequency is slightly modified, which corresponds to an exchange of energy and is called the Raman effect. This technique is complementary to the Infrared spectroscopy that enables to study the vibrational modes of a molecule too but with a different selection rules. For instance the carbon dioxide, a linear symmetrical molecule, shows only one vibrational band at 1388 cm^{-1} with the Raman spectroscopy, corresponding to symmetrical elongation of two bonds [164]. On the other hand, two vibrational bands are observed with Infrared spectroscopy at 2349 and 667 cm^{-1}, which corresponds to the antisymmetric elongation and bond angle deformation respectively.

The Raman spectra are recorded using a Bruker RFS/100 FT-Raman spectrometer with a Nd-YAG laser (wavelength of 1064 nm). The collected spectra are the average of 512 scans at an optical resolution of 2 cm^{-1}. The samples are sealed in glass ampoules under argon and measured at room temperature. For a detailed analysis of the region 730-770

cm^{-1}, the RTILs spectra are fit with the multipeak fitting package in IGOR PRO 6.37 using a Voigt function with a fixed Lorentzian/Gaussian ratio, following the procedure of Lassègues *et al*. [165]. The lithium coordination number *CN* is calculated for each RTIL electrolyte from the deconvoluted spectra, dividing the area $A_{coordinating}$ of the band corresponding to Li^+-coordinated anions with the total band area (including also the contributions from "free" anion $A_{non\text{-}coord}$) and the molar fraction of Li salt *x* (Equation 9).

$$CN = \frac{A_{coordinating}}{(A_{coordinating} + A_{non-coord})x} \qquad \text{Equation 9}$$

For instance, with the PYR13 TFSI with Li TFSI salt at a molar fraction of 0.2, the peak at 742 cm^{-1} is deconvoluted in two peaks, one at 742.1 cm^{-1} with an area of $A_{non\text{-}coord}$ = 9.59 and another one at $A_{coordinating}$ = 748.4 cm^{-1} with an area of 4.41 (Figure 23). Then the lithium coordination number is 1.57.

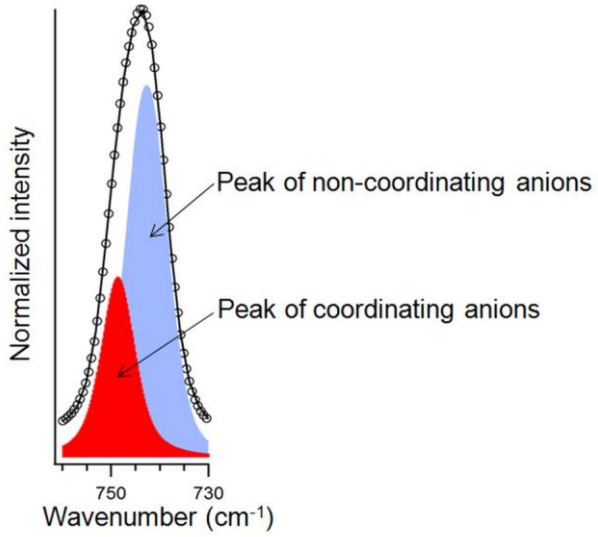

Figure 23: Raman spectra of a solution containing LiTFSI (molar fraction 0.2) and PYR13 TFSI in the range between 760 and 730 cm^{-1}.

2.3.5. Scanning Electron Microscopy

The SEM consists in producing a magnified image of a sample from the interactions of an electron beam with atoms at various depths within the sample. The use of an electron beam enables to produce very high-resolution images of the sample surface, revealing details less than 1 nm in size. Indeed, the wavelength of the electrons in a SEM is in the

range of 10-15 pm and according to the Abbe diffraction limit (Equation 10), the smaller is the beam wavelength λ, the smaller is the spot size *SS*.

$$SS = \frac{\lambda}{2n \sin \theta} \qquad \text{Equation 10}$$

The portion of the denominator $n \sin \theta$, where n is the refractive index and θ is the half-angle of the spot, is called the numerical aperture (NA). As a comparison, an optical microscope uses a beam of light i.e. with a wavelength of 400-700 nm, obtaining a *SS* around 250 nm. In the SEM, the electron beam is emitted from an electron gun fitted with a heated filament (generally made of tungsten) and focused by one or two condenser lenses to a spot from 0.4 to 5 nm in diameter. The beam passes through deflector plates in the electron column which deflect the beam in the x and y axes so that it scans over a rectangular area of the sample surface. The interaction of the primary electrons with the sample results in the reflection of high-energy electrons by elastic scattering, emission of secondary electrons by inelastic scattering and the emission of electromagnetic radiation (Figure 24). Each emission/reflection is detected by specialized detectors. The secondary electron detector collects the low energy (< 50 eV) secondary electrons that are ejected from the sample, giving a qualitative information of the sample morphology. The backscattered electron detector detects the electrons coming from the elastic collisions with the atoms nuclei of the sample. As they present the same energy as the primary electrons and then higher energy than secondary electrons, they enter deeper in the sample and give more information in the chemical nature of the sample.

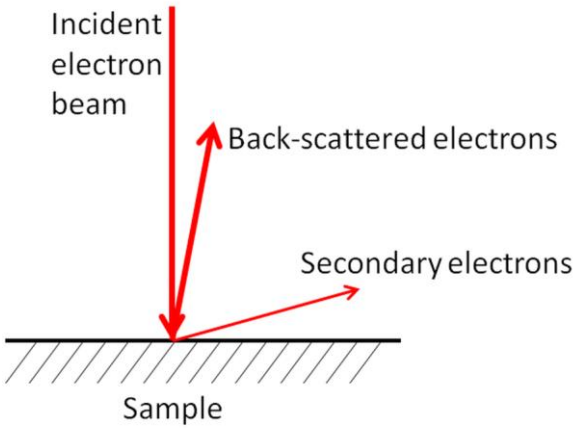

Figure 24: Schematic representation of electron beams involved in a SEM.

Only a part of the incident electrons are back-scattered or resulting to secondary electron emission. The sample needs then to be electrically conductive and electrically grounded to prevent the accumulation of electrons, leading to image artifacts. The non-conductive samples are generally coated with a thin layer of gold deposited by sputtering. Once the sample is ready and placed under vacuum in the equipment, different parameters are adjusted in order to optimize the resolution of the image in function of the nature and the morphology of the sample. The voltage, that controls the acceleration of the electrons, is increased until good enough resolution is obtained without penetrating too much in the sample. The working distance (WD) is adjusted in function of the morphology of the sample. If the sample is flat, the adapted WD is the distance between the sample and the detector. For a sample with high relief, a higher working distance is needed in order to "see" the sample from a farther point of view, then with a better resolution. The type of detector, either secondary electron or backs-scattered electron detector, is selected in function of the nature of the sample and what information needs to be highlighted. The secondary electron detector is used if high resolution of the relief is needed. The back-scattered electron detector enables to see better the differences of density in the material (e.g. metallic coating). The SS can be adjusted too. It corresponds to the aperture of the lens enabling to control the percentage of electron beam reaching the sample. Increasing the SS leads to less signal noise but diminishes the resolution.

In this work, the morphology of the cathodes is examined using a scanning electron microscope (SEM, JEOL JSM-6010LV) at accelerating voltage of 15 kV and WD of 12 mm. Indeed the sample is flat enough to work with a WD equivalent to the sample-detector distance. The secondary electron detector is used as the materials observed are homogenously distributed. Besides, the carbon is conductive enough to use the sample as it is, without preparing it before.

2.4. Electrochemical techniques

All the electrochemical characterizations were carried out using a multichannel VMP3 potentiostat/galvanostat from Biologic. This equipment enables to measure in a 20 V range adjustable from [-20 V; 0 V] to [0 V; +20 V] with a current ranging from 10 µA up to 400 mA and a current resolution of 760 pA. The data acquisition time is 20 µs, using a control software named EC-Lab®. This software enables to setup the different

techniques, adjusting the conditions parameters, display and analyze the results obtained. The techniques used are detailed in the following paragraphs.

2.4.1. Voltammetry

The voltammetry is an electrochemical technique that enables to identify the chemical reactions occurring in an electrolyte at different potentials. The current is measured as the potential is varied at a defined scan rate.

In the present work, the electrochemical stability window of different electrolytes is determined by linear sweep voltammetry between 2 electrodes, carried out in glovebox (oxygen and moisture content below 1 ppm). The working electrode is a 3 mm-diameter platinum disk, which is manually polished before the measure to remove possible contaminants and ensure the control of the electrode dimensions. Two suspensions of alumina are used on a soft pad, first a 1 µm-size and then 0.05 µm-size particles. The counter and reference electrode is a band of lithium metal. In the electrolyte is added potassium ferricyanide ($K_3[Fe(CN)_6]$) at a concentration of 5 mM. This salt is typically used in electrochemistry as redox probe as it presents fast and reversible redox reactions (Equation 11).

$$[Fe(CN)_6]^{3-} + e^- \leftrightarrows [Fe(CN)_6]^{4-} \qquad (E^\circ = 0.358 \text{ V vs. SHE}) \qquad \text{Equation 11}$$

Applying a ramp of potential in function of the time (Figure 25), the potential and the current of the corresponding peak enable to check there is no potential shift and that the surface area of the working electrode remains the same from a measure to another.

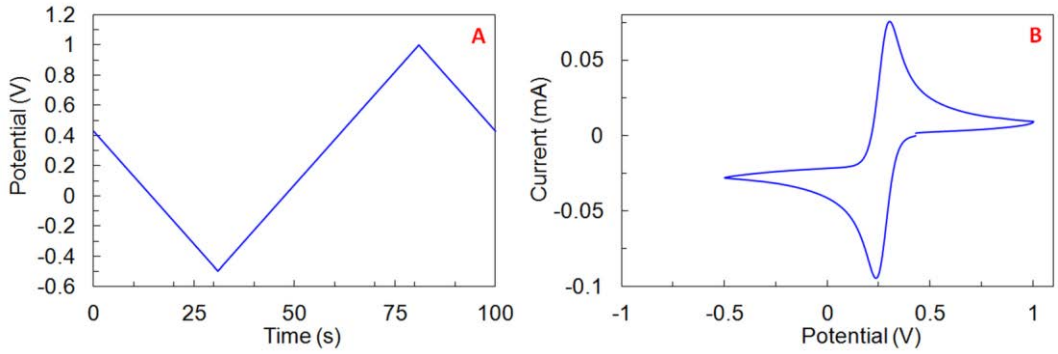

Figure 25: A) Representation of the scan rate applied and B) the resulting voltammogram of potassium ferricyanide.

The potential between both working and counter electrodes is swept at a scanning rate of 1 mV s^{-1} from the open circuit voltage toward positive and negative potentials to evaluate the anodic and cathodic limit respectively.

2.4.2. Galvanostatic

Li-O_2 batteries are assembled inside an Ar-filled glove box using ECC-air cell (EL-Cell - Figure 26). This cell was conceived for electrochemical characterization of gas diffusion electrodes in aprotic electrolytes. The upper diffusion electrode, i.e. the cathode, is contacted by a perforated stainless steel plate on top. The gas is circulated continuously inside the cell above the plate via two ports in the cell lid.

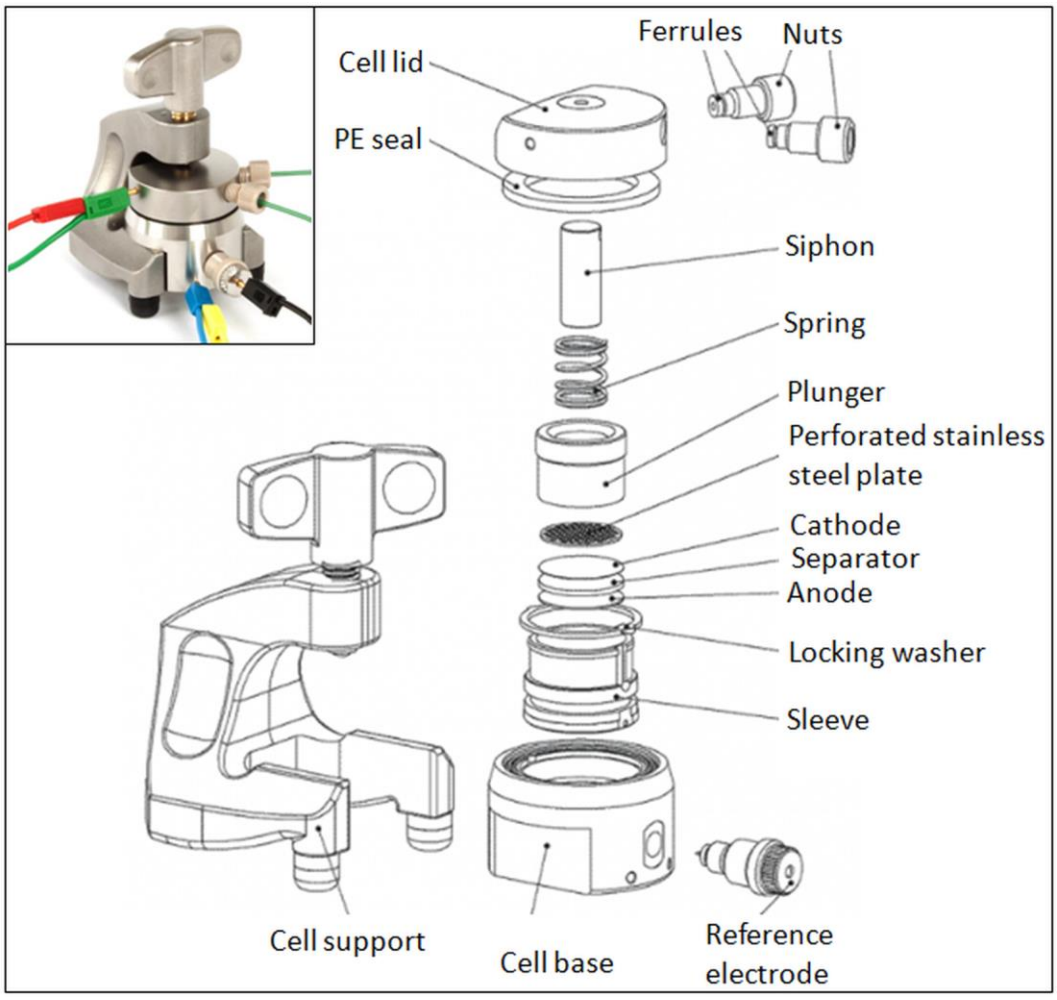

Figure 26: Photo of an ECC-Air cell and split view of the different components.

The cathode used is prepared as explained before. A circular lithium chip (Ref: EQ-Lib-LiC25, MTI Corp.) is used as the anode. The separator is a glass fiber membrane

(Whatman GF/A) soaked for 15 min with the tested electrolyte. The thickness of 260 µm is ensuring that the electrolyte is in excess with around 100 µL. Prior applying any current, the cell is maintained under O_2 flow (8 mL min^{-1}) up to stabilize the open circuit voltage after 10 hours. The gas entered through the inlet nut, goes down following the external part of the siphon until the perforated stainless steel plate, then leaves the cell through the siphon and the outlet nut (Figure 27). This system enables a constant flow above the cathode through which the oxygen can diffuse.

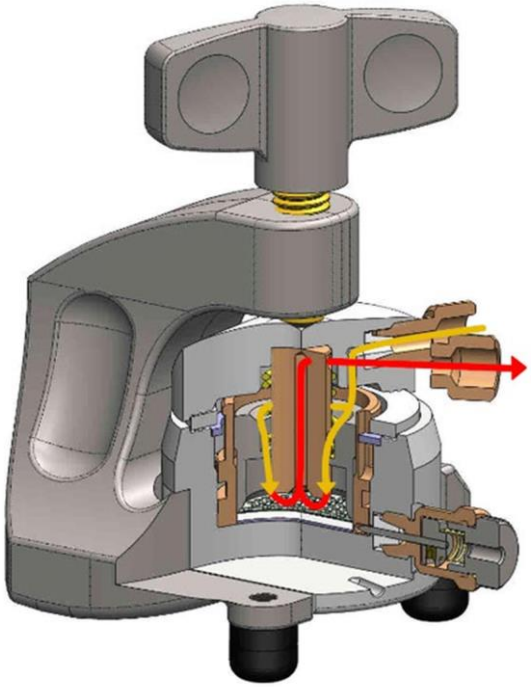

Figure 27: Schematic view of the gas flow inside the ECC-Air cell.

For the full initial discharge measurement, galvanostatic tests are performed with a current of 100 µA cm^{-2} applied until 2.15 V vs. Li^+/Li with an oxygen flow rate of 8 mL min^{-1}. For the cycling test, discharge and recharge curves are recorded at a constant specific current applied between 2.15 V and 4.35 V and limiting in time then limited in capacity, specified for each experiment.

2.4.3. Li/Li stripping/plating

Lithium/lithium stripping/plating tests are carried out in CR2032 coin cells (Figure 28) using lithium chip (Ref: EQ-Lib-LiC25, MTI Corp.) as anode and cathode and a glass fiber membrane (Whatman GF/A) as separator. A quantity of 150 µL of the electrolyte

studied is used. Then, a spring and a spacer are placed in the coin cell before sealing it with a press, so that good electrical contacts are assured. A galvanostatic cycling test is then performed with an applied current of 10 mA cm^{-2} with limited charge/discharge time of one hour and a cut-off voltage limit of +/- 1 V vs. Li^+/Li. This typical test in battery study enables to evaluate the chemical compatibility of an electrolyte with the anode material and its electrochemical compatibility i.e. its ability to host the reduction and oxidation reactions of the species.

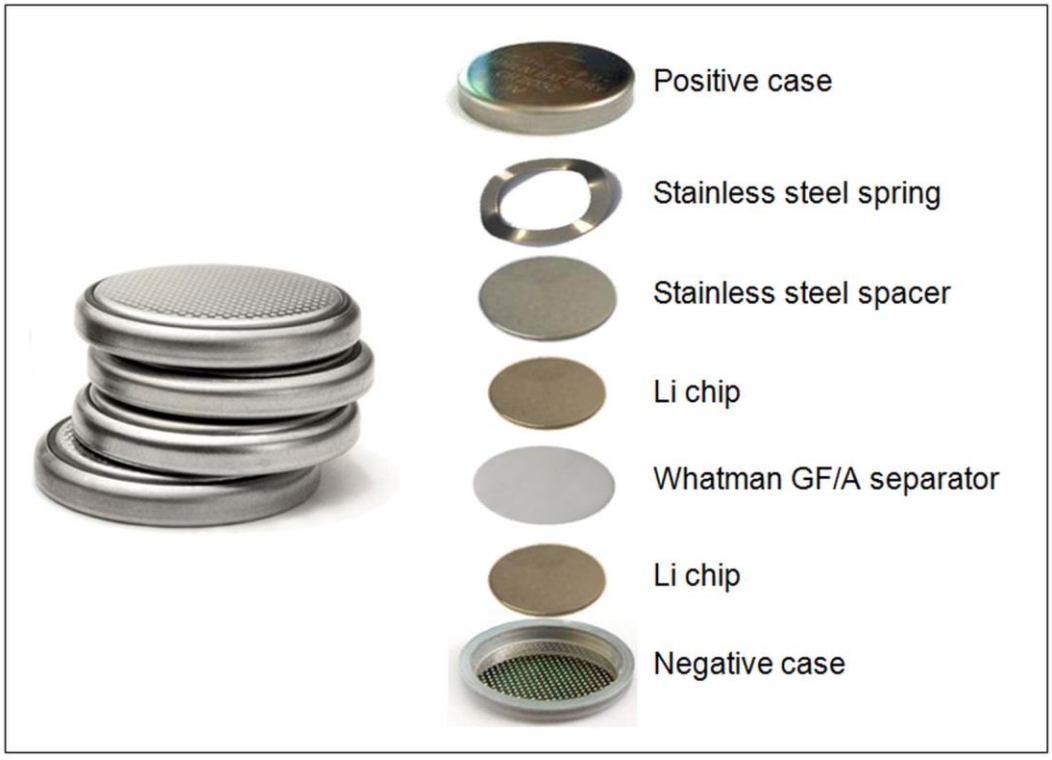

Figure 28: Photo of a CR2032 coin cell and its components for the Li stripping/plating test.

2.5. Synchrotron experiment setup

2.5.1. Cell preparation

Li-O_2 batteries are assembled in an Ar-filled glovebox by sandwiching a 200 µm-thick carbon-coated Gas Diffusion Layer cathode (GDL Sigracet 24BA from SGL Group), a 260 µm-thick glass fiber separator (Whatman GF/A) soaked with the studied electrolyte and a 250 µm-thick Li foil (MTI Corp.) in a polyimide tube (diameter: 3 mm) as shown in Figure 29-A and Figure 29-B. The electrolyte is in excess in the cell as the quantity brought with the soaked separator is more than enough for the battery to work. Then the

parasitic degradation reactions will not affect the electrochemical measurements. The cathode current collector is a stainless steel tube filled with pure O_2 and a stainless steel rod was used at the anode side. Both rod and tube fit exactly in the polyimide tube, although a Teflon tape was used to wrap the junctions for a better impermeability.

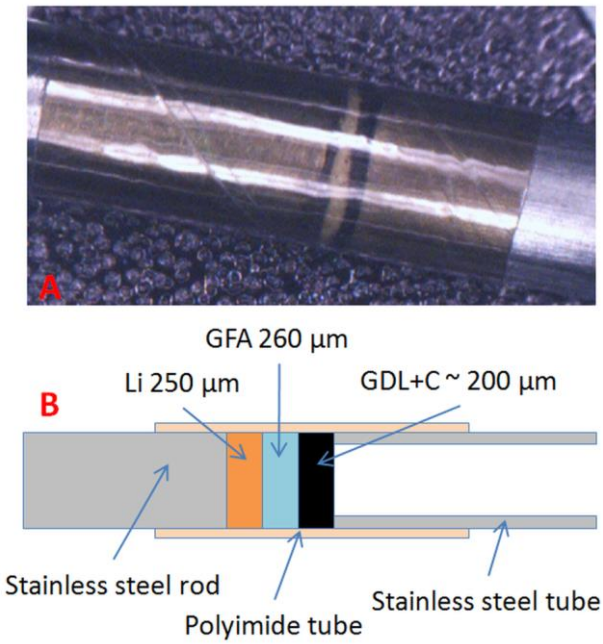

Figure 29: A) Photo (x24) of the anode/separator/cathode stack between the stainless steel tube and rod in the polyimide tube. B) Schematic representation of the cell.

2.5.2. Electrochemical setup

The chemical aging has been carried out as well as electrochemical studies with the following setup. The discharge/recharge cycling of the cell is controlled by a VSP potentiostat (Bio-Logic) under a current density of 20 mA g^{-1} between 2.15 and 4.35 V vs. Li^+/Li as cut-off voltage for discharge and recharge respectively, with discharge/recharge cycle duration of 5h each. Four different battery configurations (DMSO, DET, DPT and DBT) are tested, changing only the electrolyte (Table 6).

Table 6: List of electrolytes tested and their composition.

Sample name	Electrolyte composition
DMSO	DMSO : $LiClO_4$ (95:5 mol%)
DET	DMSO:EMIM TFSI:$LiClO_4$ (87:8:5 mol%)
DPT	DMSO:PMIM TFSI:$LiClO_4$ (87:8:5 mol%)
DBT	DMSO:BMIM TFSI:$LiClO_4$ (87:8:5 mol%)

2.5.3. X-ray diffraction (XRD)

While recording the battery voltage, diffraction scans were continuously registered every minute. *Operando* microdiffraction measurements are performed at the synchrotron MSPD beamline [166], using transmission geometry with the beam going through the battery cell from its side. A set of several XRD data points at different cathode layer depths is collected by moving the battery for every selected state-of-charge. As the cathode-electrolyte-anode stack has a thickness of 760 μm, the number of scans per set is 8 data points taken along the cell's stack from the anode to the cathode. To achieve such data points, the measurements are performed on the HP/MD station of the BL04_MSPD beamline able to deliver a 15 x 15 μm FWHM beam size matching the size of the probed sample. The operating energy selected is 23.22 keV (Rh K-edge, the choice of a specific absorption edge is for calibration purpose). The corresponding wavelength is long enough to minimize Bragg peak overlap and has the interesting peaks in optimum detector range (2θ angle between 6 and 14 degrees). Data are collected using the 2D Rayonix CCD detector positioned within a distance range of 200-300 mm. A suitable support is built to mount in horizontal position the electrochemical cell on the HP/MD stages in compliance with the beamline staff (Figure 30).

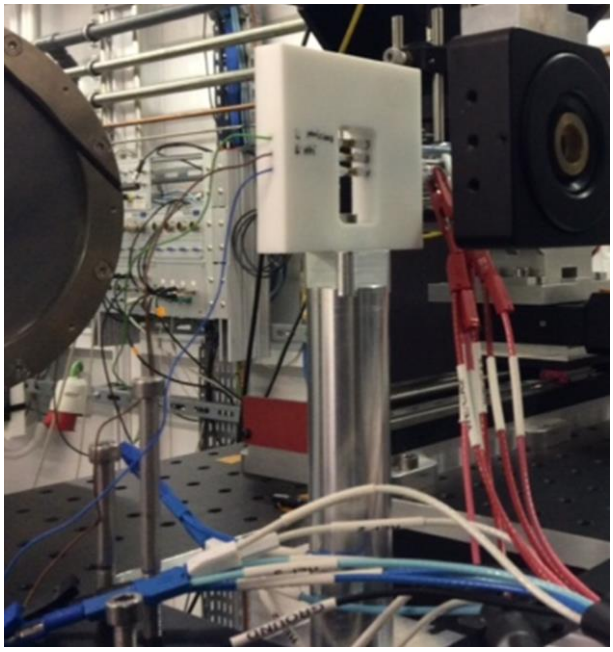

Figure 30: Picture of the cell support placed in the beam line.

The interaction of an incident X-ray beam with the structure of a crystal causes its diffraction into many specific directions. The measure of the diffracted beam angles and intensities enables to identify the lattice planes of the crystal thanks to the Bragg's law (Equation 12):

$$2d \sin\theta = n\lambda \qquad \text{Equation 12}$$

Here, d is the spacing between diffracting planes, θ is the incident angle, n is the order of diffraction and λ is the wavelength of the beam.

The atomic planes are defined by the Miller indices (hkl) (Figure 31). Each plan on which the X-ray beam is scattered is characterized by a peak on the XRD pattern. This pattern represents the intensity of these peaks in function of the angle and is characteristic of a crystalline structure that can be compared to the Joint Committee on Powder Diffraction Standards of the International Centre for Diffraction Data (JCPDS-ICDD) to identify the crystal.

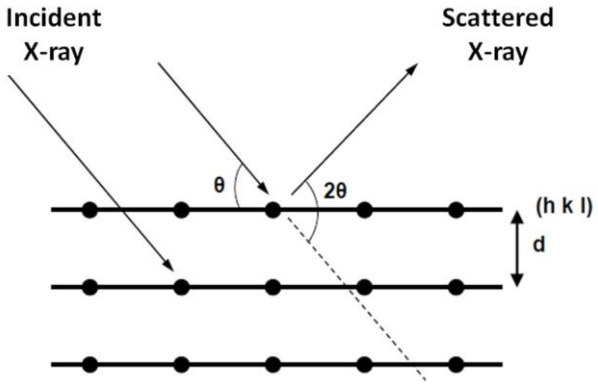

Figure 31: X-ray diffraction phenomenon on atomic planes indexed with the Miller indices (hkl).

Synchrotron radiations are more powerful X-ray beams, generated by synchrotrons that accelerate electrically charged particles, often electrons, to nearly the speed of light and confine them in a circular loop using magnetic fields. Thus, X-rays with energy from 20 to 80 keV can be generated, which enables the analysis of samples through a solvent like an electrode in an electrolyte. Indeed, common XRD typically uses Cu-Kα source generating beam with an energy of 8 keV. As the X-rays intensity is diminished through scattering by the solvent molecules, a more powerful beam is needed to perform such *in situ* analysis.

Chapter 3. Results & Discussion

The objective of this thesis is to design an electrolyte composed of ionic liquids to enhance the performance of Li-O_2 batteries. In a first time, electrolytes composed only of RTIL and a Li salt are characterized to evaluate their physicochemical properties and tested in Li-O_2 batteries cell. As a comparison, two typical electrolytes of Li-ion and Li-O_2 battery respectively, are also characterized. This study enables to identify the key parameters to select the adequate electrolyte.

In a second time, RTILs are evaluated as co-solvent, i.e. in blended RTIL/organic solvent electrolytes. Indeed, RTILs are generally too viscous compared to organic solvents, which makes them unsuitable for the battery. That is why a study of electrolytes containing different amount of RTIL is carried out.

Finally, in order to understand better the behavior of the battery and especially the influence of RTILs in the electrolyte, a characterization of the product formed during cycling is needed. That is why an *in situ* XRD is performed at different positions between the anode and the cathode of the battery, at different states-of-charge. The results enable to identify the chemical reactions occurring in the battery and then to refine the selection of the electrolyte components.

3.1. RTILs versus organic solvents as Li-O_2 battery electrolytes

The results were published in New Journal of Chemistry with an article entitled "Room Temperature Ionic Liquids versus organic solvents as lithium-oxygen battery electrolytes" [160].

The first part of the work consists in evaluating the physical and chemical properties of 7 RTIL-based electrolytes and 2 organic solvent-based electrolytes. The lithium salt used is LiTFSI as it is the common salt used in Li-O_2 battery, known for its stability and hydrophobicity [159]. Only the carbonate electrolyte (EC:DEC) contains $LiPF_6$, in order to have a typical Li-ion battery electrolyte for comparison. The characterization of these electrolytes enables to determine their thermal stability, ionic conductivity, viscosity, lithium cation solvation and electrochemical stability window.

The TGA of the different electrolytes (Figure 32) shows that organic electrolytes evaporate at relatively low temperature, 150 ˚C in the case of the TEGDME-LiTFSI. On the other hand, RTILs electrolytes show higher thermal stability between 350 and 450 ˚C. This result represents a real advantage of these electrolytes for the safety of the battery.

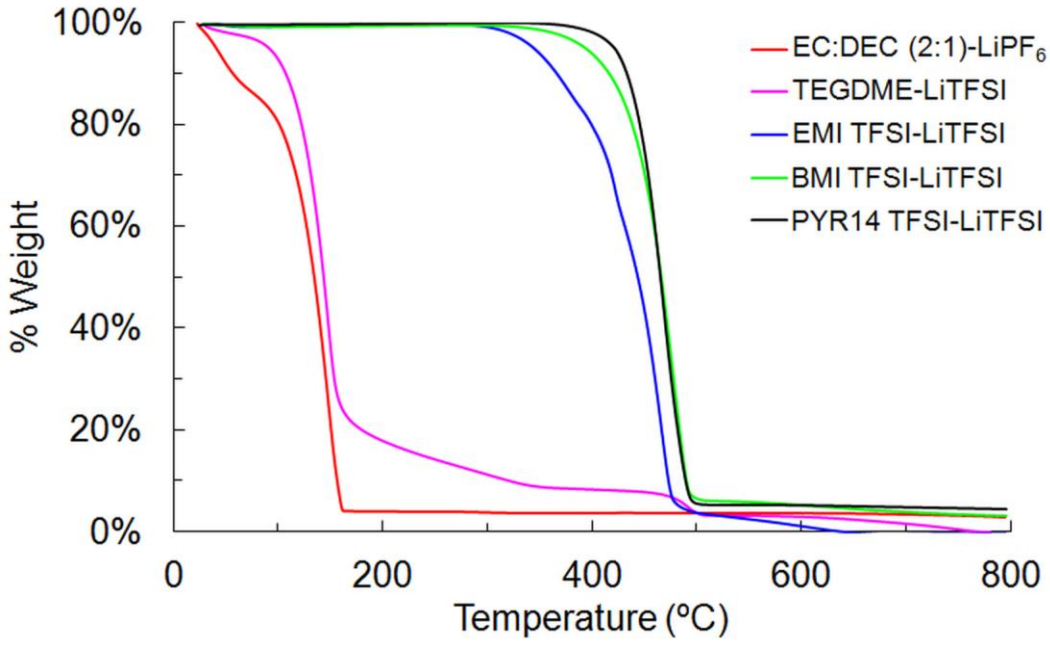

Figure 32: TGA spectra of ionic liquids and organic electrolytes measured under nitrogen atmosphere.

The ionic conductivity of the electrolytes is also studied (Figure 33), showing that the conductivity of the RTIL electrolytes is in the same range that the one of the organic electrolytes, i.e. between 1 and 8 mS cm^{-1}. A particularity observed for the RTILs is that the ionic conductivity increases with the temperature, whereas ionic conductivity of organic solvent is stable from room temperature to higher temperature.

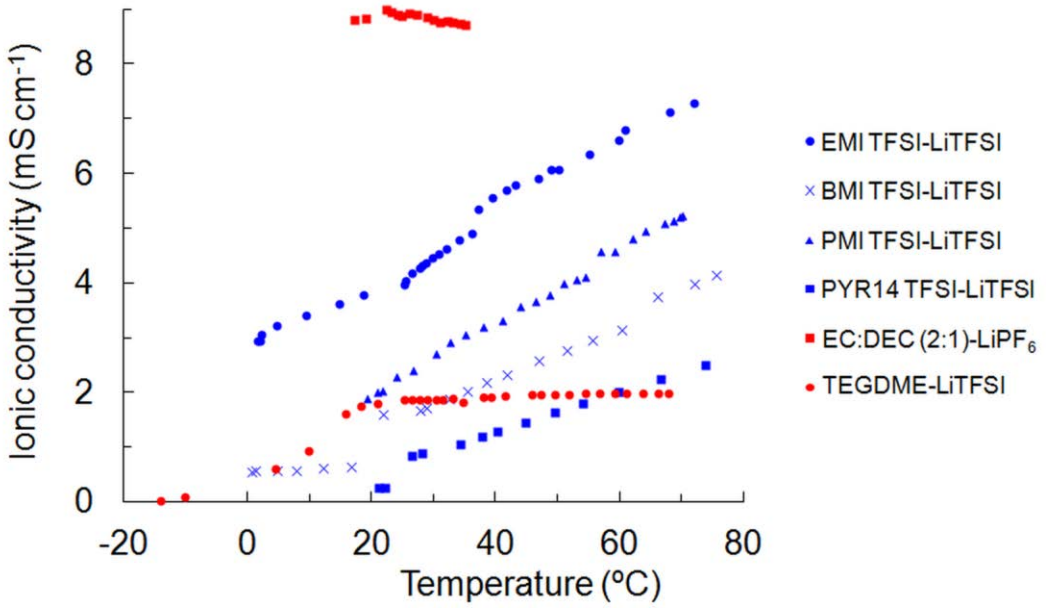

Figure 33: Ionic conductivity versus temperature for different families of electrolytes: in blue the RTILs and in red the organic solvents.

The Li coordination number of the RTIL electrolytes, which quantify the lithium cation solvation, was also measured by Raman spectroscopy. This value indicates how strong the interaction between the anion and the cation of a RTIL is and gives some information on the lithium cation mobility. In TFSI-based RTILs the coordination of the anion $[TFSI]^-$ can be evaluated considering the peak at a wavenumber of ≈ 742 cm^{-1}. Such a peak is associated to the anion expansion and contraction. In the presence of Li^+ cations, the $TFSI^-$ anions coordinating with Li^+ generate an additional signal, which is shifted to higher wavenumbers in the Raman spectra (Figure 34). As shown, the areas $A_{coordinating}$ of this peak and $A_{non\text{-}coord}$ of the non-coordinating $TFSI^-$ peak are strongly dependent on the cation-anion interaction occurring in the RTIL. The comparison of both areas is used to determine the lithium coordination number of the electrolyte (Table 7). The stronger is the anion-cation interaction occurring in the RTIL, the lower is the lithium coordination number. Thus, the Li coordination number increases in the following order PMI TFSI-

LiTFSI < PYR13 TFSI-LiTFSI < BMI TFSI-LiTFSI < EMI TFSI-LiTFSI < PYR14 TFSI-LiTFSI < DMPI TFSI-LiTFSI < PP13 TFSI-LiTFSI. The number of protons, the ring size of the cation and the length of the alkyl chain may influence these ion interactions.

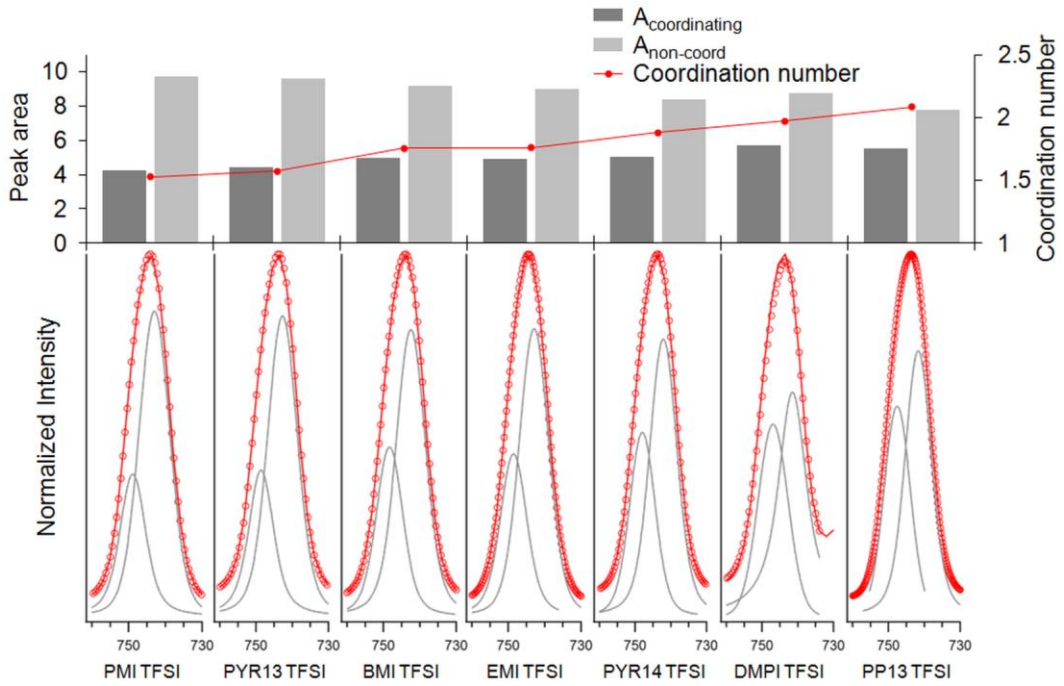

Figure 34: Raman spectra of solutions containing LiTFSI (molar fraction 0.2) and RTILs in the range between 760 and 730 cm^{-1}. The red lines represent the measured data, the circles represent the fitted curve and the grey lines represent the two individual fitted peaks for coordinated and non-coordinated $[TFSI]^-$ anions.

Additionally to these parameters, the water content, the viscosity and the potential window of these electrolytes are measured and presented in the Table 7.

Table 7: Composition, degradation temperature, H_2O content, ionic conductivity, potential window and Li coordination number of the studied electrolytes.

Solvent / RTIL	Salt (x = 0.2)	Degradation temperature (ºC)		H_2O content (ppm)		Ionic conductivity at 25°C (mS cm^{-1})	Viscosity at 25°C (cP)	Potential window (V vs. Li^+/Li)	Lithium coordination number
		Under N_2	Under O_2	Before drying	After drying				
TEGDME	Li TFSI	118	115	851	156	1.79	14.2	[0.1 ; 4.9]	-
PMI TFSI	Li TFSI	411	406	1062	33.1	2.3	102	[1.1 ; 5.4]	1.53
EMI TFSI	Li TFSI	407	369	3800	46	3.22	85.2	[1.3 ; 5.4]	1.76
EC:DEC (2:1vol)	Li PF_6	88	75	22	-	8.87	5.1	[0.0 ; 5.7]	-
BMI TFSI	Li TFSI	405	362	110	43	1.42	102	[1.3 ; 6.2]	1.76
DMPI TFSI	Li TFSI	480	448	249	204	0.54	140	[1.1 ; 6.0]	1.97
PYR14 TFSI	Li TFSI	421	380	92	54	0.39	165	[0.2 ; 6.8]	1.88
PP13 TFSI	Li TFSI	406	413	2108	126	0.4	463	[0.1 ; 6.9]	2.08
PYR13 TFSI	Li TFSI	414	407	2031	78	0.8	206	[0.3 ; 6.6]	1.57

In parallel, the electrolytes are tested in Li-O_2 battery cells to measure the full discharge capacity (Figure 35) and the cyclability (Figure 36). PP13 TFSI-LiTFSI, PYR13 TFSI-LiTFSI, PYR14 TFSI TFSI-LiTFSI and DMPI TFSI-LiTFSI show specific capacity lower than 200 mAh g^{-1}, which may be due to their high viscosity and low ionic conductivity. The five other electrolytes tested have higher capacity from 559 mAh g^{-1} for the BMI TFSI-LiTFSI to 4268 mAh g^{-1} for the TEGDME-LiTFSI. However, both viscosity and the ionic conductivity are not enough to explain the results obtained. Indeed, it seems that for electrolytes with viscosity in the same range, a lower coordination number will enable a better transport of the species.

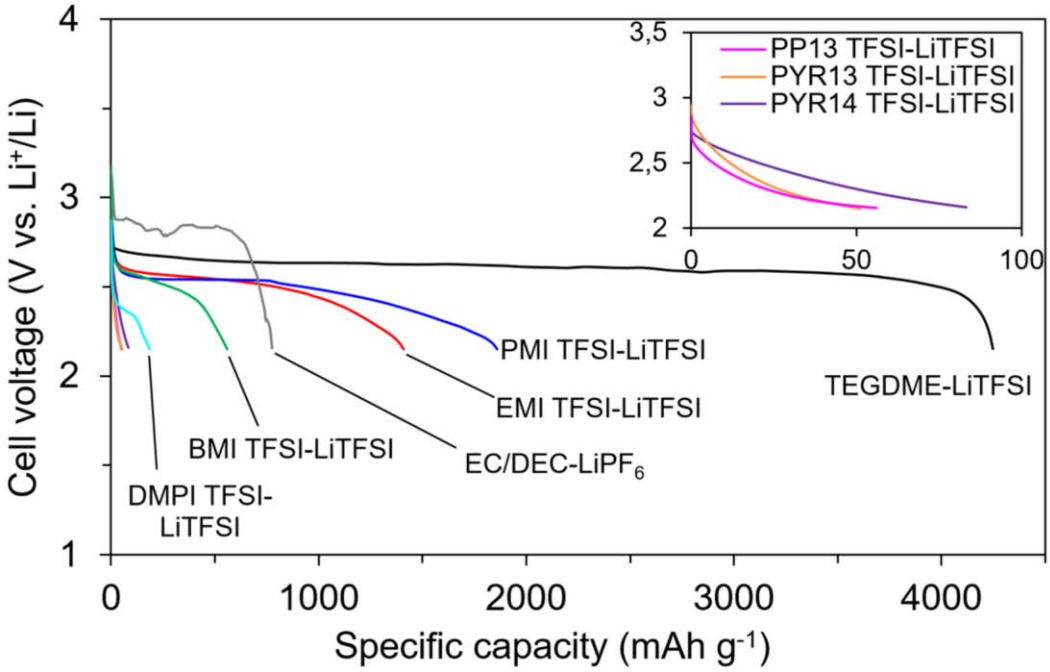

Figure 35: Initial discharge curve of Li-O_2 cells assembled with the different electrolytes studied, at a current of 100 µA cm^{-2}.

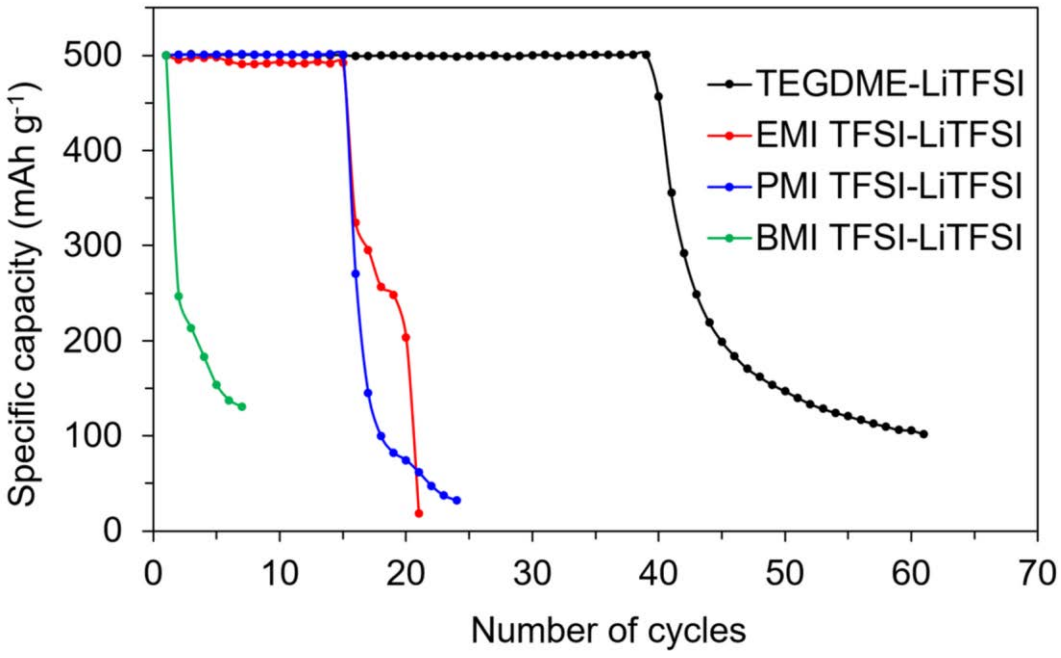

Figure 36: Galvanostatic cycling test of Li-O_2 cells at a constant current of 75 µA cm^{-2}.

Concerning the cyclability, which is measured for the five electrolytes with the highest capacity, the best result is obtained for the TEGDME-LiTFSI with 40 cycles. The EC/DEC-$LiPF_6$ do not show any reversibility as the carbonate solvent are not stable in presence of the superoxide radical. For the RTIL electrolytes, only 1, 15 and 16 cycles

are observed for BMI TFSI-LiTFSI, PMI TFSI-LiTFSI and EMI TFSI-LiTFSI respectively. This may be due to the degradation of the imidazolium cation, characterized by a reduction peak at 1.1-1.3 V vs. Li^+/Li (Figure 37), i.e. before the reduction of the lithium.

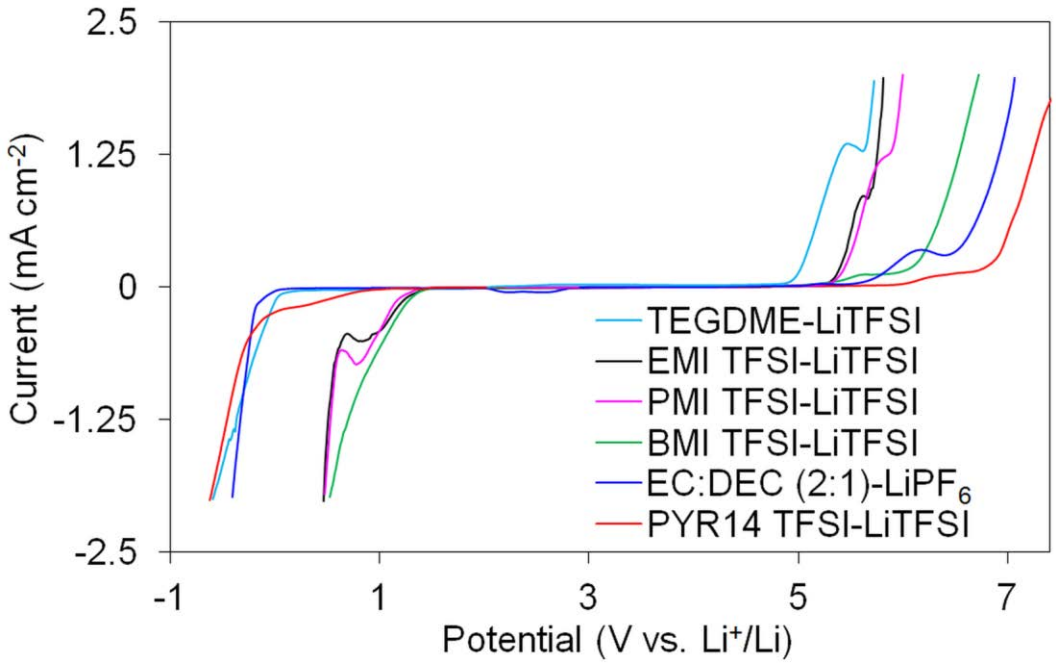

Figure 37: Linear sweep voltammograms of ionic liquids and organic electrolytes measured under argon atmosphere at 25˚C.

Based on data tables, it is suggested that viscosity and Li coordination number are the most relevant parameters (Figure 38) to select an adequate electrolyte and obtain higher capacity.

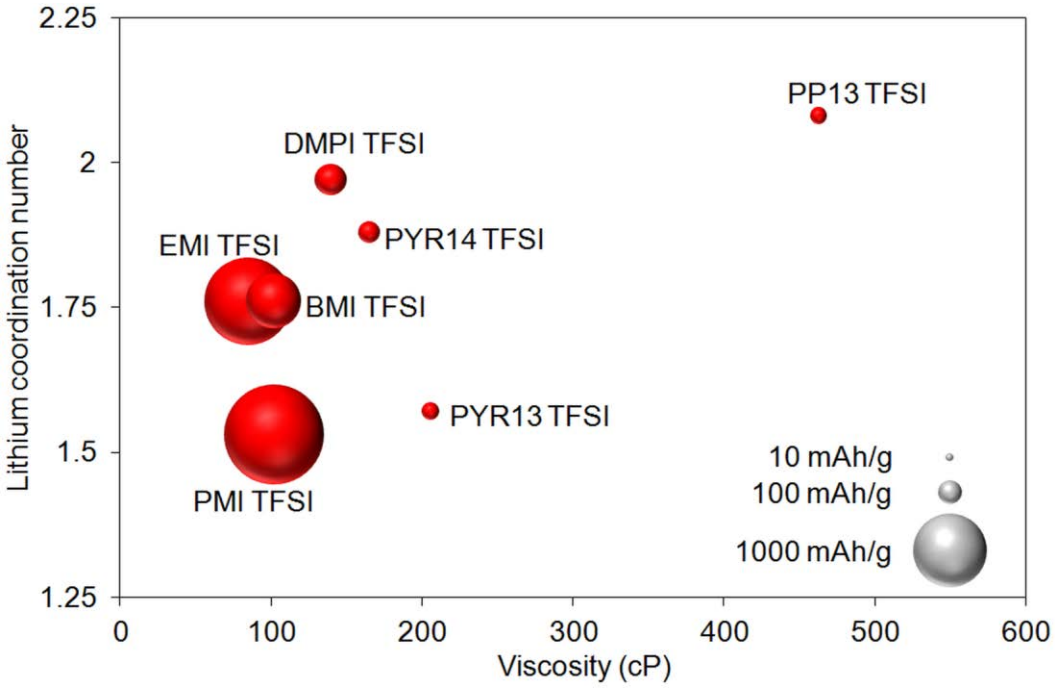

Figure 38: Representation of the specific capacity in function of the viscosity and lithium coordination number of the RTIL electrolyte.

The characterization of different RTIL and organic electrolytes enables to show some advantages of the RTILs such as their thermal stability. However, an adequate reversibility of the Li-O_2 battery reaction is not attainable probably due to their high viscosity that affects the ion diffusion and the kinetics of the battery reaction [34]. Moreover, poor battery capacity [95] and a cyclability lower than 30 cycles is generally obtained [142,145]. The compromise is then to mix RTIL and organic solvent in order to take advantage of both species and design of blended electrolyte that show enhanced performance. As explained previously, DMSO gives relatively stable electrochemical performance in Li-O_2 system and is then selected as organic solvent. Concerning the RTIL, PMI TFSI shows the highest specific capacity and cyclability but EMI TFSI, which exhibits almost equivalent performance, is cheaper and more available. That is why the RTIL chosen to be tested as co-solvent is EMI TFSI.

3.2. Suitability of blended RTIL-DMSO electrolyte for Li-O_2 battery

In this second part of the work, we study the influence of the 1-ethyl-3-methylimidazolium bis(trifluoromethylsulfonyl)imide (EMI TFSI) as co-solvent of Li-O_2 battery electrolyte in the final aim of designing an adequate solution for this technology. Thermal properties, stability with lithium metal and electrochemical performance are evaluated for DMSO-based electrolyte containing different amount of EMI TFSI, a RTIL known for its thermal resistance, high conductivity and electrochemical stability [167]. Hence, four mixed electrolytes ET-0, ET-30, ET-50 and ET-100 are prepared by adding 5w% of $LiClO_4$ to the mixed solution of DMSO and EMI TFSI, the weight ratio of EMI TFSI/DMSO being 0/100, 30/70, 50/50 and 100/0 respectively. The results are summarized in the Table 8.

Table 8: Ionic conductivity, viscosity, degradation temperature, capacity, overpotential and cycling life of the four studied electrolytes.

	ET-0	ET-30	ET-50	ET-100
Ionic conductivity (mS cm^{-1})	7.88	13.1	10.1	0.49
Viscosity (cP)	6.5	6.3	12	81
Degradation temperature (˚C)	105	182	>200	>200
Capacity full discharge (mAh g^{-1})	5651	7618	4631	3060
Overpotential 1st cycle (V)	1.43	1.06	0.90	1.16
Cycling life (cycles)	98	69	18	7

The effect of the use of ionic liquids on the thermal stability of the above-mentioned electrolytes are analyzed by performing DSC tests. Before the heating ramp, the samples are cooled and equilibrated at -90˚C to allow their crystallization. In the case of ET-0 and ET-30, the DSC profiles (Figure 39) show endothermic peaks at 13 and 2˚C respectively, corresponding to the melting point. The ET-0 shows another endothermic peak at -7˚C that may correspond to a solid-solid phase transition. For the samples with more EMI TFSI content, i.e. ET-50 and ET-100, no crystalline phase is detected, showing that for the procedure used, the electrolytes remained amorphous. Moreover, thermal stability is improved with the addition of EMI TFSI. Without RTIL, an endothermic peak occurred at 105˚C but when 30% of EMITFSI is added, the endothermic peak is postponed to 182˚C. For ET-50 and ET-100, no endothermic peak is observed, showing that the degradation of the electrolyte occurs at higher temperature. The safety of the battery can

be then improved with the addition of an RTIL, as it can enhance the thermal stability of the electrolyte.

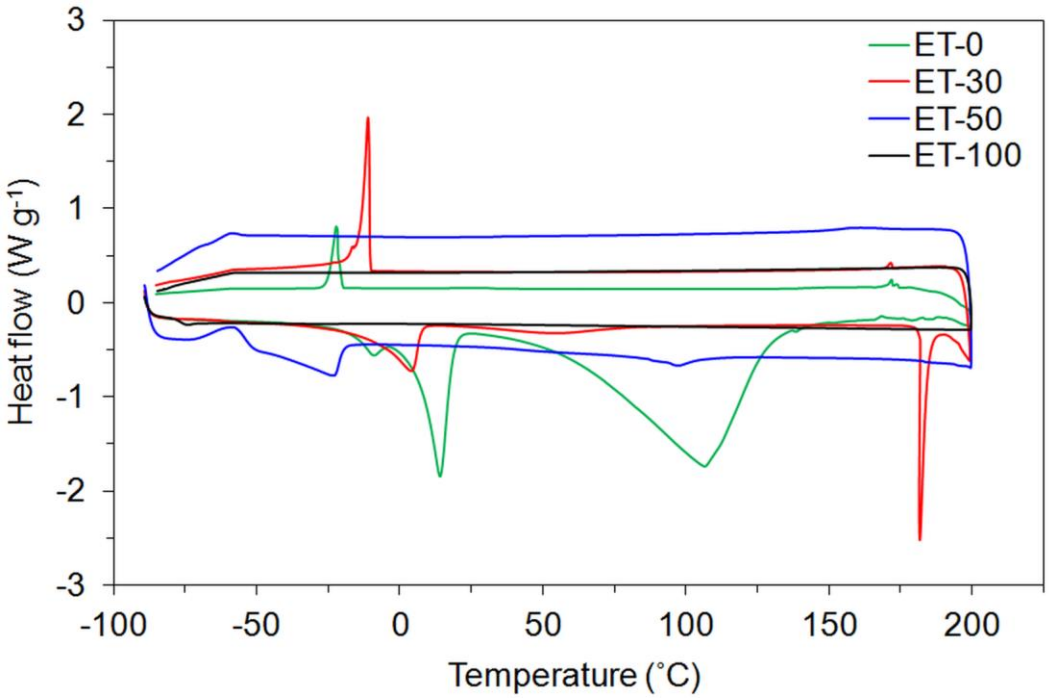

Figure 39: DSC profiles of the ET-0, ET-30, ET-50 and ET-100 electrolytes.

Ionic conductivity and viscosity of the blended electrolytes are measured and represented in function of the DMSO/EMI TFSI ratio (Figure 40). The ionic conductivity initially increases with increasing EMI TFSI content, reaching a maximum of 13.1 mS cm^{-1} at 30% by weight. Because EMI TFSI itself is a salt, the number of ions in the electrolyte increases with increasing EMI TFSI content and then the ionic conductivity too. However, adding EMI TFSI increases also the viscosity of the electrolyte from 6.5 cP for ET-0 to 81.4 for ET-100, due to the increased ion-solvent interactions and Coulombic interactions between ionic species [149]. Thus, the decrease of the ionic conductivity from 50% of EMI TFSI content can be attributed to the increase of the viscosity. It is shown then that the addition of a small amount of RTIL in the electrolyte can increase its ionic conductivity, which may be beneficial for the battery.

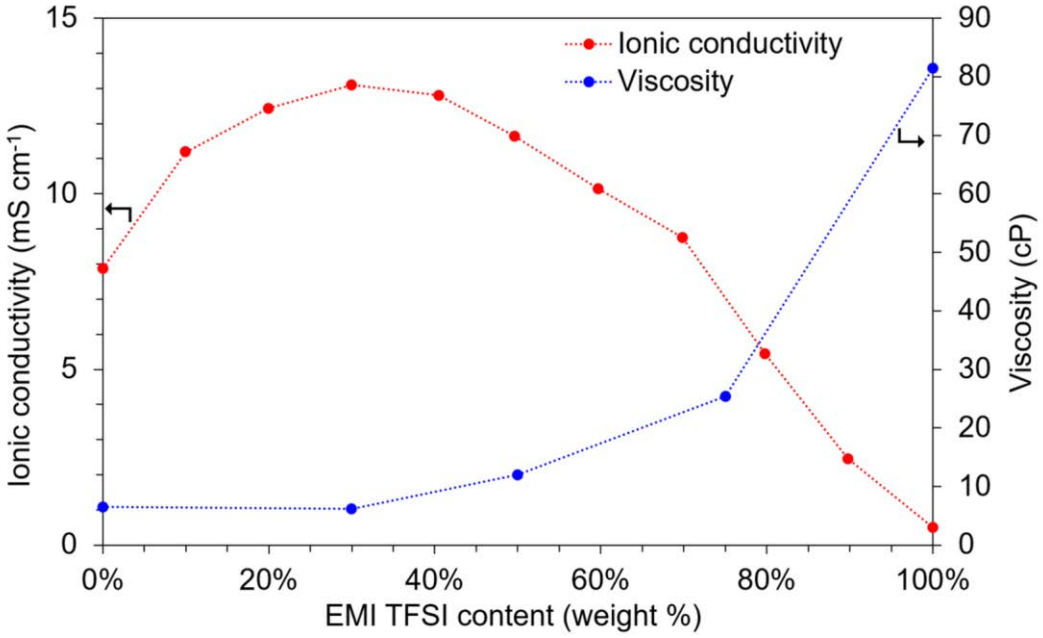

Figure 40: Ionic conductivity and viscosity of blended electrolytes as function of EMI TFSI content in the EMI TFSI/DMSO solution. All the solutions have $LiClO_4$ content of 5w%.

To verify the compatibility of these new electrolytes with the lithium anode, Li/Li stripping/plating test is realized within the different electrolyte at 10 mA cm^{-2} and 25 ˚C. The cell is charged at constant current for 1 hour at 10 mA cm^{-2} and subsequently discharge for 1 hour at -10 mA cm^{-2}. A typical voltage profile is shown in the Figure 41-A. Since the cell is symmetric, it is not affected by parasitic chemical or electrochemical reactions and the cycles are symmetrical. The evolution of the overpotential of the Li/Li cell is shown for each electrolyte (Figure 41-B). With the ET-0 as electrolyte, the cell voltage is seen to be very low, around 9 mV vs. Li^+/Li and stays constant upon cycling for at least 200 cycles. This low voltage amplitude indicates that no passivation layer is formed. Concerning both blended electrolytes (ET-30 and ET-50), the cell voltage varies between 0.2 and 0.5 V vs. Li^+/Li, which is due to the formation of a solid electrolyte interphase (SEI) layer. A cell voltage around 0.1 V vs. Li^+/Li for ET-100 is observed, showing that the lithium surface is passivated in the presence of the EMI TFSI, probably due to molecule adsorption at the surface within lower voltage amplitude with respect to blended electrolytes. In all cases, the electrolyte enables the stripping/plating of the lithium.

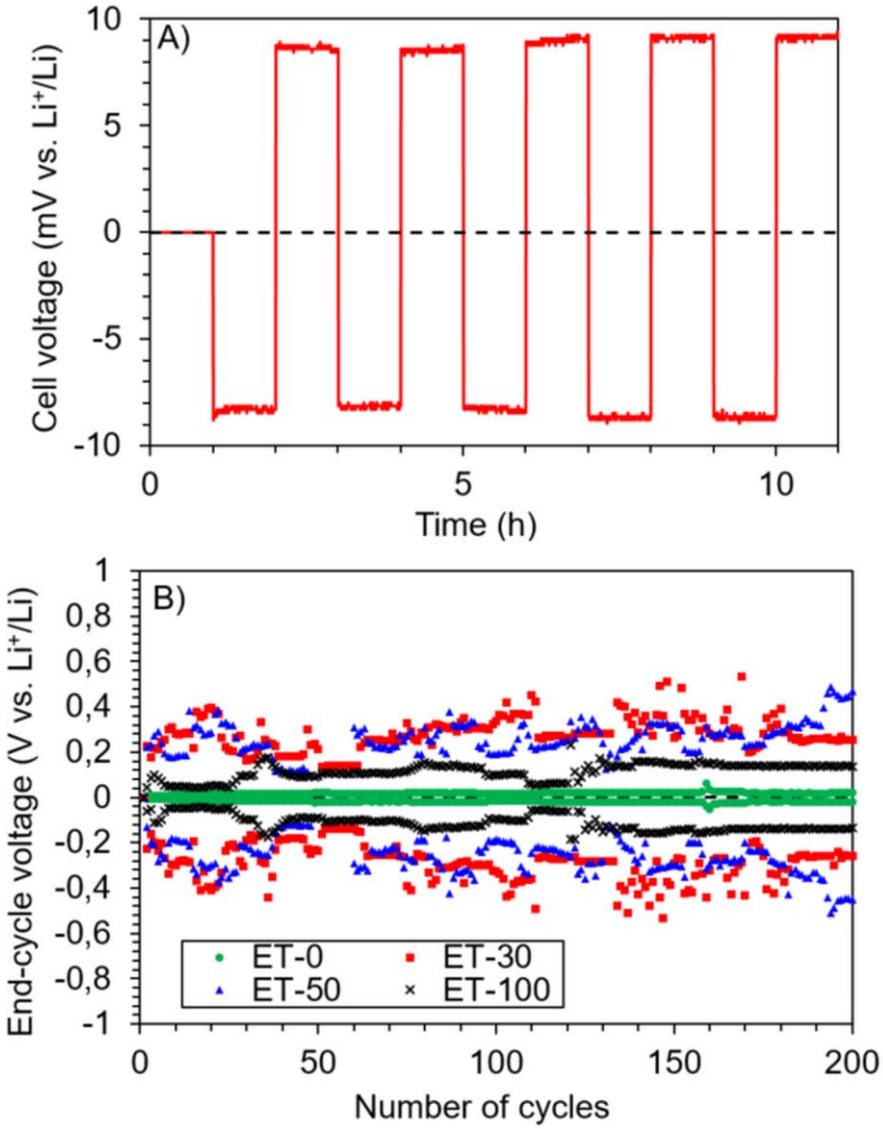

Figure 41: A) Typical voltage behavior of Li-Li cell during galvanostatic lithium stripping/plating cycle test (case of ET-0). A current of 10 mA cm^{-2} was applied for 1 hour in each direction. B) Evolution of the cell-voltage cutoff with the number of cycles for the different electrolytes studied.

The full discharge capacities of the Li-O_2 cells were measured at a constant specific current of 0.1 mA cm^{-2}. The first full discharge curves obtained with the different electrolytes are shown in the Figure 42. The cell with ET-30 presents the highest capacity with 7618 mAh g^{-1}, whereas the cell with RTIL-free electrolyte (ET-0) has a capacity of 5651 mAh g^{-1}. This improvement by adding 30% of EMI TFSI can be explained by the higher ionic conductivity and a better wettability of the ET-30. However, adding more EMI TFSI in the electrolyte increases the viscosity, which leads to lower capacity. An optimization of the electrolyte content is then needed to achieve high battery performance.

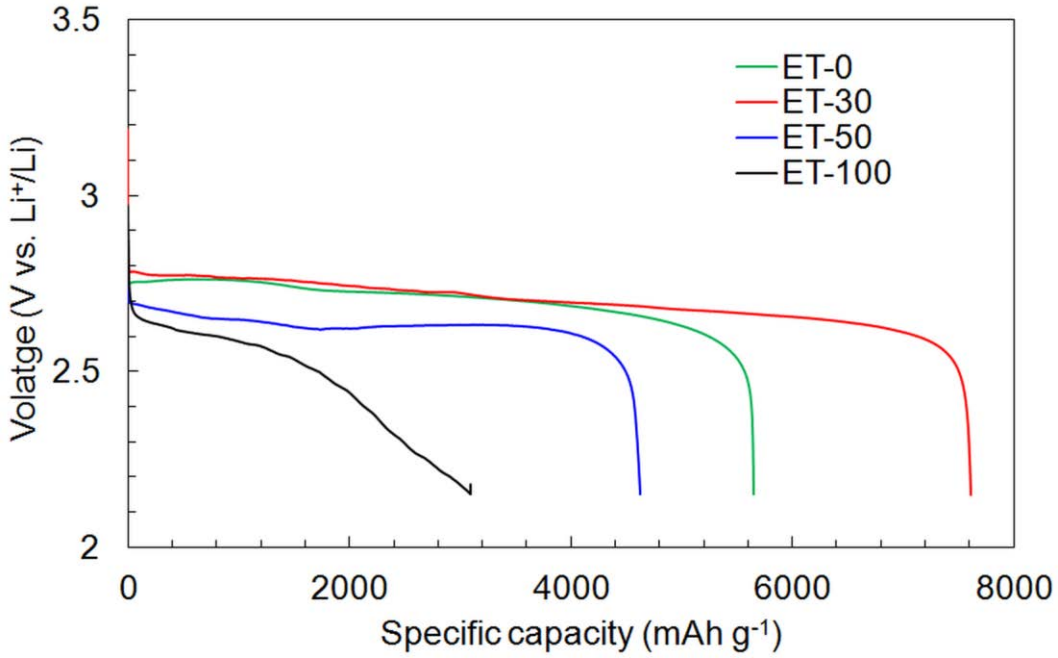

Figure 42: Initial full discharge curves of Li-O_2 cells with ET-0, ET-30, ET-50 and ET-100 electrolytes at 0.1 mA cm^{-2}.

The four electrolytes are then tested in Li-O_2 cells to obtain discharge/recharge cycles at a controlled depth of discharge of 600 mAh g^{-1} and constant current of 200 mA g^{-1}. On the first cycle (Figure 43), the oxidation potential decreases with increased content of EMI TFSI. Indeed, the higher ionic conductivity of ET-30 and ET-50 compared to ET-0 enables faster kinetics of the oxidation reactions. The difference between ET-30 and ET-50, 3.86 and 3.68 V vs. Li^+/Li respectively, may be ascribed to a better wettability of the ET-50 electrolyte [149]. The higher EMI TFSI content makes the electrolyte more hydrophobic, wetting then more effectively the hydrophobic carbon cathode. Concerning the ET-100, the discharge plateau has a lower voltage (2.66 V vs. Li^+/Li) than for the electrolytes containing DMSO (2.80 V vs. Li^+/Li). Despite its high viscosity, the ET-100 show low oxidation potential of only 3.82 V vs. Li^+/Li, which may be due its hydrophobicity [149]. However, this potential rapidly increases with the cycles (Figure 44-D).

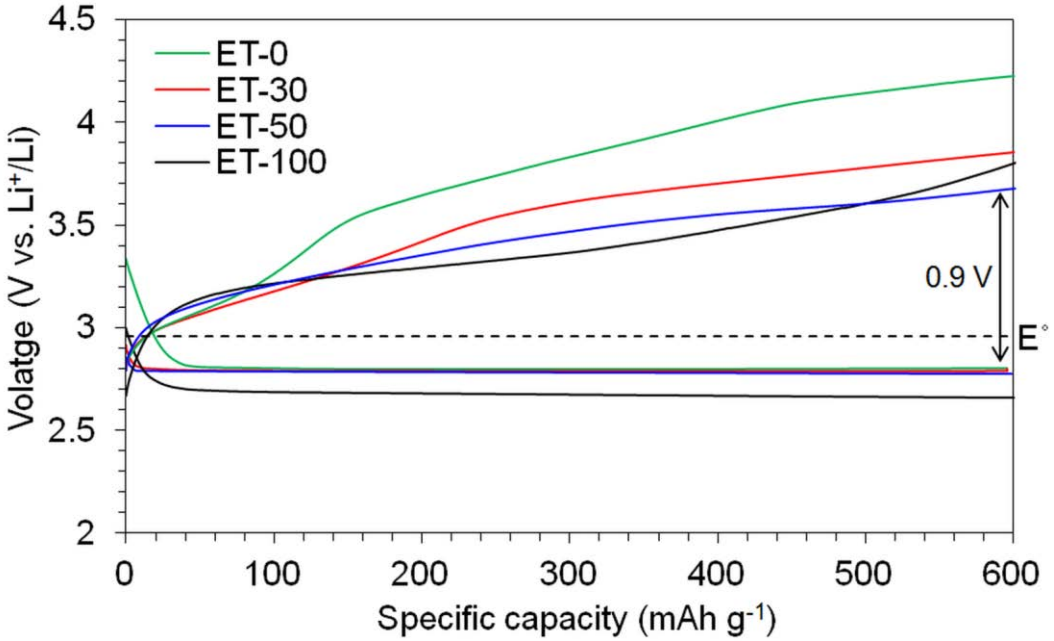

Figure 43: First cycle galvanostatic discharge and recharge of Li-O_2 cell with the different electrolytes studied, at the applied current of 200 mA g^{-1} and limited capacity of 600 mAh g^{-1}.

The evolution of the overpotential with the cell cycling is shown in the Figure 44. Although it shows the highest overpotential, ET-0 has better cycling stability with 98 cycles whereas the ET-30 and ET-50 work for 69 and 18 cycles respectively. The overpotential of ET-0 is the highest observed at the first cycle and the charge voltage increases rapidly to 4.35 V vs. Li^+/Li after only 12 cycles. On the other hand, the ET-30 shows charge voltage below 4.35 V vs. Li^+/Li until the 54th cycle. As shown previously, the addition of EMI TFSI enables to increase the ionic conductivity of the electrolyte but it may also enhance the O_2 solubility [168,169]. Thus a better reversibility is observed for the electrolytes containing the ionic liquids for the first cycles. Indeed, the charge potential increases with the number of cycles until the battery fails, which occurs earlier when the electrolyte contains EMI TFSI. This can be ascribed to the degradation products formation which was proved in previous work, that it is faster in presence of EMI TFSI than in DMSO without RTIL [161]. It was observed indeed that with cycling, LiOH concentration increases more rapidly in presence of ionic liquids, due to the high reactivity of the C2 proton of imidazolium cations, especially in presence of radical peroxide [144,170]. Concerning the DMSO, Sharon *et al.* [98] observed the formation of side products when exposed to superoxide. This would explain the battery cycling being limited at 98 cycles when using the ET-0.

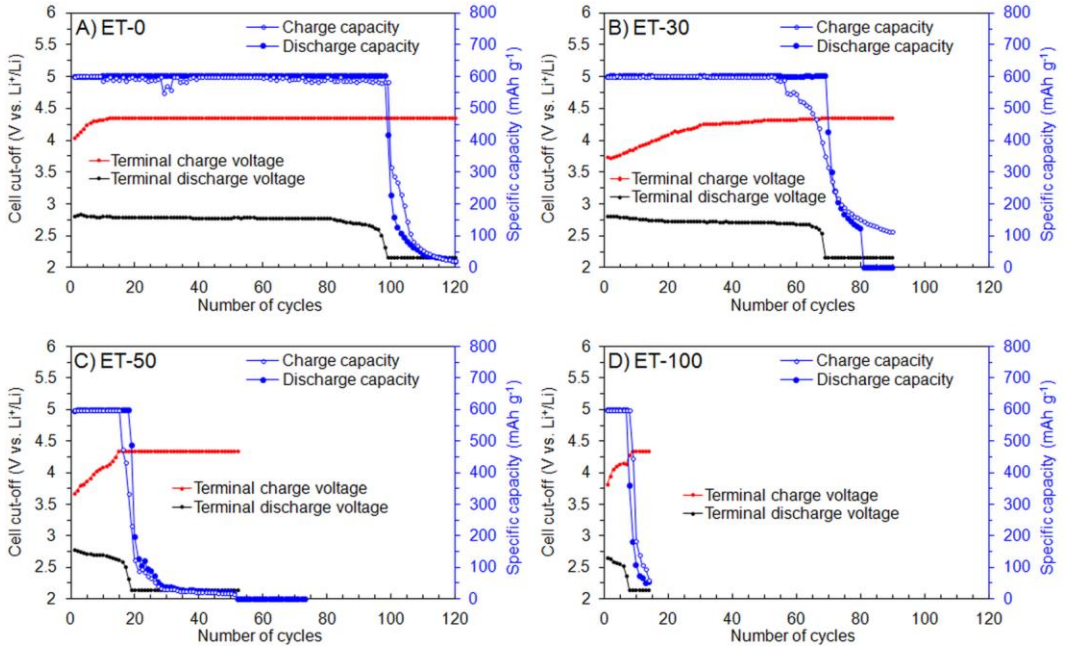

Figure 44: Cycling performance (blue curves) and corresponding cell-voltage cut-off (red and black curves) of Li-O_2 cells with A) ET-0, B) ET-30, C) ET-50 and D) ET-100 electrolytes at a constant current of 200 mA g^{-1} and 600 mAh g^{-1} capacity limit.

In summary, it is important to remark that for blended DMSO/EMI TFSI electrolytes, significant improvements are observed concerning the thermal stability with a degradation/evaporation occurring at a temperature 80° higher and the ionic conductivity increasing from 7.88 to 13.1 mS cm^{-1} by adding 30% in weight of EMI TFSI. The Li-O_2 battery performance is also improved with a 35% higher full discharge capacity and an overpotential reduced to 1.06 V versus 1.43 V for the DMSO electrolyte. Reasonable cycling performance are also obtained, although the electrolyte without RTIL shows higher cycling life (98 cycles), 69 cycles are obtained with the blended electrolyte. The use of a RTIL more stable against peroxide radical attack and in presence of lithium may enable a longer cycle life. Besides, this study shows that the bulk electrolyte parameters (ionic conductivity, viscosity) have more influence on the battery performance than the cathode surface parameters (cell overpotential, wettability) and the anode surface parameters (Li/Li overpotential).

Furthermore, in the aim of understanding better the previous observation of lower overpotential, higher capacity and lower cyclability, *in situ* synchrotron XRD analysis is carried out. This kind of analysis enables to identify the alteration of the reactions medium caused by the addition of RTIL in the electrolyte and therefore to identify the products

formed. The nature of these products and the process from which they are formed may be different in these blended electrolyte compared to DMSO electrolyte. This would explain the difference of behavior observed and the influence of RTIL on the Li-O_2 battery.

3.3. *In operando* XRD of Li-O_2 battery using RTIL as electrolyte co-solvent

The results were published in New Journal of Chemistry in the article entitled "*In operando* X-ray diffraction of lithium-oxygen battery using ionic liquid as electrolyte co-solvent" [161].

In the third and final part of the work, *in situ* XRD of the cycling Li-O_2 battery cell is carried out thanks to synchrotron light. This experiment enables to identify the species formed during the cycling of a Li-O_2 battery cell. For all the samples analyzed at each position between then anode and the cathode and at each state of charge of the battery, the only species identified is lithium hydroxide (LiOH) (Figure 45).

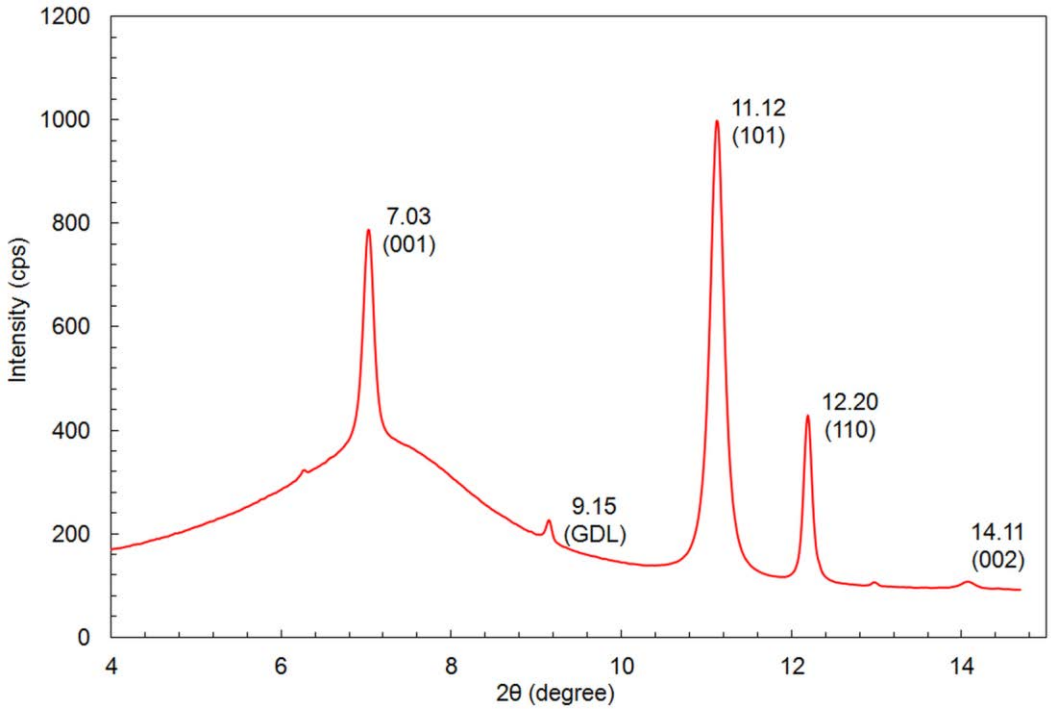

Figure 45: XRD pattern recorded on the cathode surface of an operating Li–O_2 cell after 1 discharge/recharge cycle at current density of 20 mA g^{-1}.

The lithium peroxide (Li_2O_2) formed at the cathode during the discharge is not observed as the particles may be amorphous and then not visible by XRD. The SEM analysis of the cathode (Figure 46) before cycling, after discharge and after recharge enables to evidence the presence of Li_2O_2.

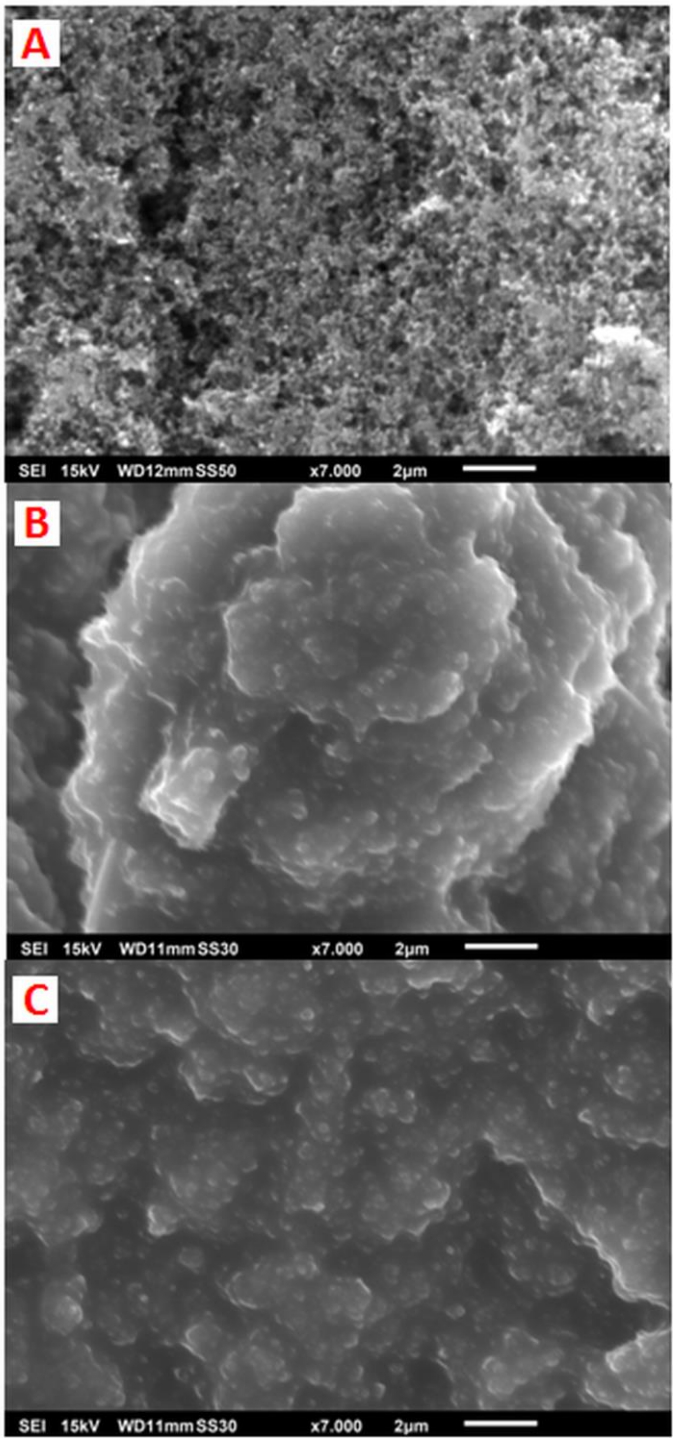

Figure 46: SEM images of the cathode in its pristine state (A), after discharge (B) and after the following charge (C) in the DET electrolyte.

The comparison of the different XRD patterns enables to see that the peaks of LiOH are more intense at the anode. This indicates that LiOH is more concentrated at this position and that it may be formed at the surface of the lithium. Moreover, as shown in the Figure 47, the increase of the peak intensity is independent of the state of charge of the battery. Then the LiOH formation is due to the reaction of the lithium with the electrolyte and/or the water coming for the degradation of the electrolyte.

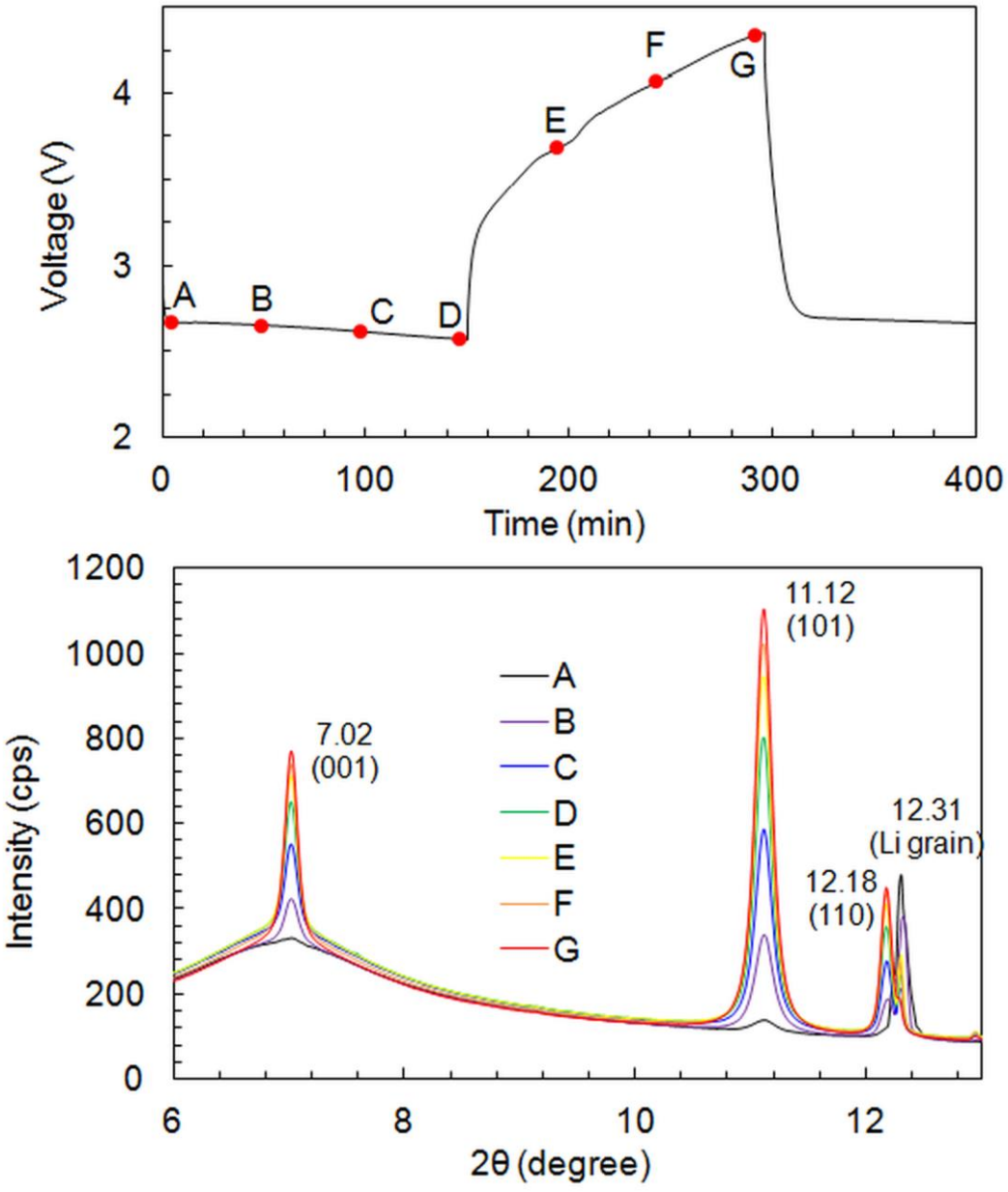

Figure 47: Discharge–recharge voltage profiles for the first cycle of a Li–O_2 cell using the DPT electrolyte at 20 mA g^{-1} (up) and XRD patterns collected from an anode position near the separator at different cycling times as marked in the up figure (down).

The evolution over time of the (101) peak intensity is studied in function of the electrolyte used the battery. The slopes of curves representing relative intensity vs. time are listed in Table 9 for each electrolyte tested.

Table 9: List of electrolytes tested, their composition and the slope of peak intensity evolution (in min^{-1}) at both the anode and cathode surface in either a cycling (with current) or resting (without current) battery cell.

Sample name	Electrolyte composition	Anode		Cathode	
		With current	Without current	With current	Without current
DMSO	DMSO:$LiClO_4$ (95:5 mol%)	0.0449	0.0482	0.021	0.036
DET	DMSO:EMIM TFSI:$LiClO_4$ (87:8:5 mol)	0.2329	0.2539	0.2450	0.2702
DPT	DMSO:PMIM TFSI:$LiClO_4$ (87:8:5 mol)	0.3334	0.2828	0.2847	0.3135
DBT	DMSO:BMIM TFSI:$LiClO_4$ (87:8:5 mol)	0.3300	0.3550	0.3302	0.3492

When comparing the evolution of the peak intensity for a battery that is cycling and another one characterized without any current applied, no difference is observed (Figure 48). The formation of LiOH is then due to a spontaneous chemical process between the lithium and the electrolyte and does not come from the electrochemical reactions of the battery.

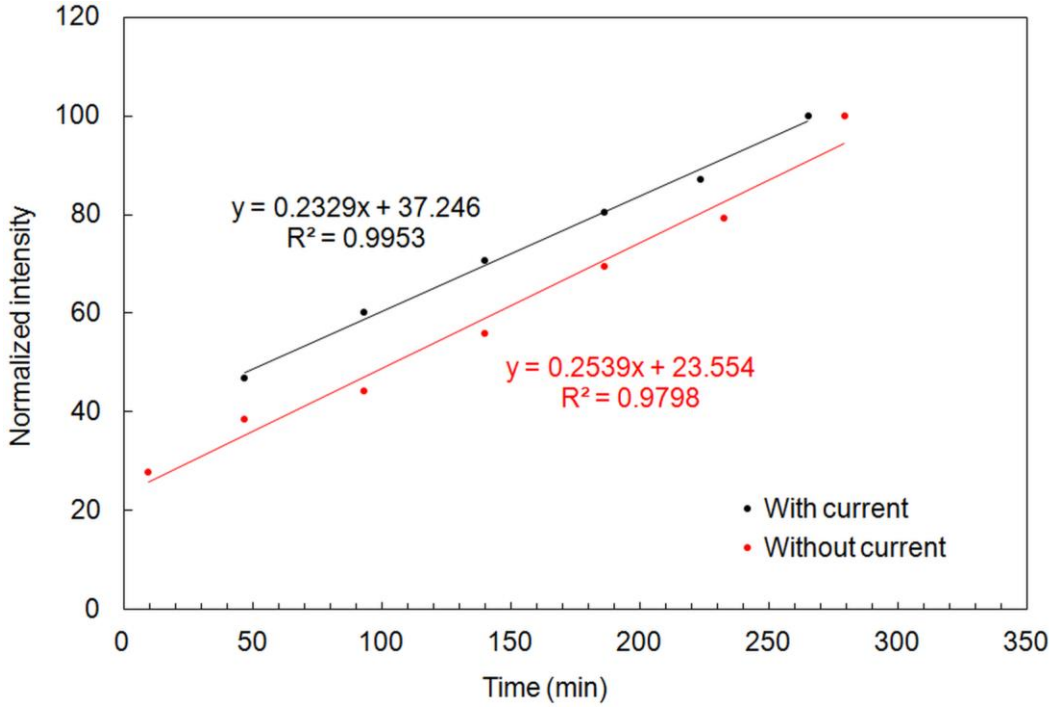

Figure 48: Comparison of the increase of the relative intensity of the (101) peak among the DET sample cell, for which a current density of 20 mA g^{-1} is applied (black), and of another without any current (red). The duration time corresponds to one discharge/recharge cycle.

The evolution of the peak intensity observed for each electrolyte is then compared. Besides the DMSO sample, three RTILs are tested as co-solvent, each cation of the RTILs having a different chain length on the imidazolium. The results show an increase of LiOH concentration 5 to 8 times higher for the electrolyte that contains a RTIL (Figure 49). This result indicates that the RTILs are more reactive with lithium than DMSO. Then, when comparing the RTILs, the imidazolium with the shortest alkyl chain seems to be less reactive than the others. This can be explained by the reactivity of the C2 proton of the imidazolium, whose pKa is 22.1 for the ethyl and 22.0 for the butyl.

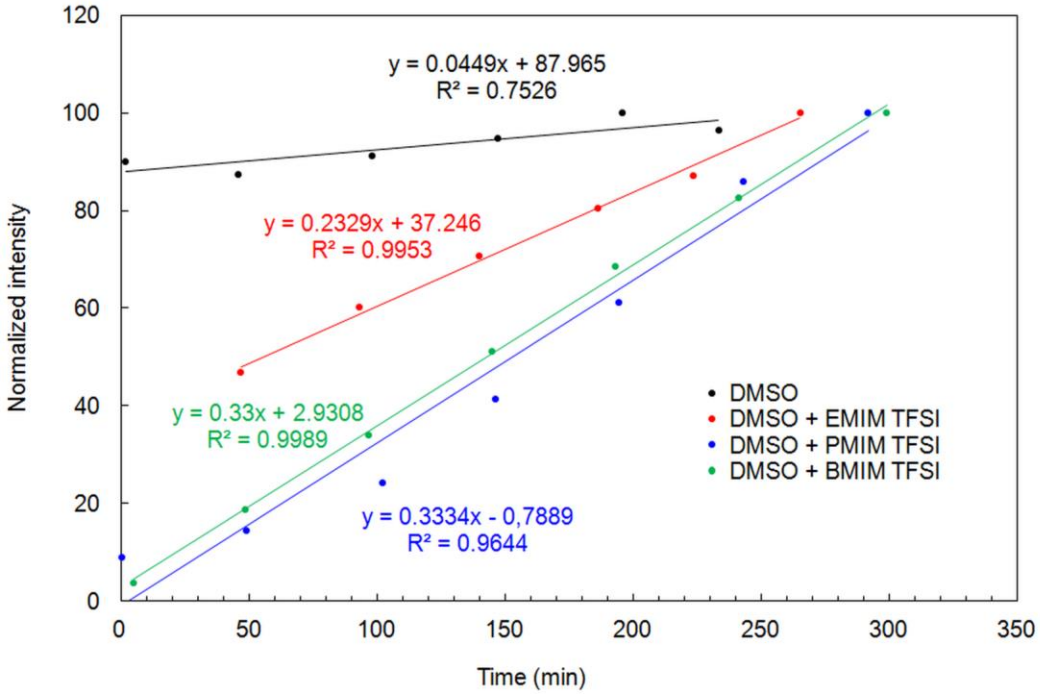

Figure 49: Relative intensity of the (101) peak at the anode position during the first discharge/recharge cycle of the battery using different electrolytes.

This work described a spontaneously reaction of ionic liquid with Li ions forming LiOH. Although the results do not show the formation/evolution of the main battery reaction products (e.g. Li_2O_2), it is meaningful in guiding the application of ionic liquid in Li-O_2 batteries.

3.4. Remarks and perspectives

RTILs are potentially suitable for Li-O_2 battery electrolyte as reasonable performance of capacity and cyclability are obtained. A combination with organic solvent seems to be needed since the viscosity must be reduced, but the interesting thermal stability properties are still preserved. Moreover, an increase of the ionic conductivity is possible if the optimum proportion of RTIL/organic solvent is reached. This can lead to reduced overpotential and better rate capability of the battery. Hence, the key challenge is to develop a RTIL that is also stable with the other species present in the cell, especially lithium and superoxide, and that presents high oxygen solubility and diffusion.

Concerning the other components of the Li-O_2 battery, many issues have also to be addressed. An optimization of the cathode structure is needed to maintain as long as possible the reaction pathways among oxygen, lithium cations and electrons. This involves an improvement of both the cathode wettability and the oxygen flow system. Besides, the problem of carbon stability has also to be resolved thanks to either a protective layer to avoid the reaction with the electrolyte or catalysts to facilitate the decomposition of carbonate species. The use of non-carbon materials is also considered but it would need more effort on their development to achieve high capacity [171]. For the anode, the main objective is to protect the lithium from degradation and reaction with electrolyte using either a protective membrane or a passivation film. The suppression of dendrite formation is also important for further research.

Furthermore, considering that the main application for Li-O_2 battery is electric vehicles, then a power comparable to Li-ion technology and an energy density close to ICE are required. Taking into account the low efficiency (15 %) of such engine, leading to an energy density of 1750 Wh kg^{-1} [10], the Li-O_2 battery used in an electric motors that presents 90 % of efficiency seems to be more advantageous. However, many other challenges will come when developing a practical cell. Indeed, the concept of the Li-O_2 battery is to work in ambient air, using the oxygen of the atmosphere. This implies the use of an oxygen-selective membrane which presents high permeability to oxygen, blocks water vapor and CO_2 and enables the electrolyte containment within the cell. Adding such membrane as well as the other inactive component of the cell (e.g. binder, current collectors), the estimation of the energy density drops to around 1000 Wh kg^{-1} [6]. This

value is still higher than current Li-ion energy density (around 250 Wh kg^{-1}) but becomes lower than ICE energy density. Moreover, the current cell are cycled using a constant gas flow, which means that practical cells will need a system to keep them under constant pressure, decreasing again the energy density. Another possibility is to design a cell including an oxygen tank [154], so that the oxygen-selective membrane is not needed. However, storing onboard oxygen gas at high pressure would implies safety concerns. In any case and despite all these issues, target values of 500 Wh kg^{-1} and 570 Wh L^{-1} are expected to be met at practical pack level [172]. This is substantially higher than the 100 Wh kg^{-1} and 150 Wh L^{-1} available from current Li-ion battery packs. The target of power is 400 W kg^{-1} and 460 W L^{-1}, with an adequate rate of C/2. But other parameters have to be taken into account for EV market penetration. The first enabler would be politics that influences the fuel cost, taxes, and laws for environment protection. Then the cost of the battery that should be below 100 €/kWh. If that value is unreachable for the Li-ion technology, it may be possible for Li-O_2 as it does not use Co or Ni. The range anxiety, related to the energy density and the time of recharge are also determinant parameters. The main barriers to consider are first the safety, the pack volume compromise (the volume is more limited in an electric car than in a bus), the performance at low temperature and the material cost.

More generally, despite 40 years in the making, with a great effort in research of development in the 2 last decades, Li-O_2 batteries are still in their infancy but interest in this promising novel battery technology keep building in the R&D field worldwide. Commonly presented as the typical post-Li-ion battery for EV applications, Li-O_2 batteries have also a great potential to open up new markets as well as applications. Indeed, the production cost will be rapidly competitive as lithium foil, electrolyte and GDL supply chain are well identified. Even RTIL are already produced at tone scale for other applications than batteries. However, this will come at a later stage, when the chemical limiting issues will be resolved.

Chapter 4. Conclusions

The work accomplished in the current PhD thesis has led to the following conclusions:

- ✓ The comparison of the physicochemical properties of RTILs with their performance in Li-O_2 battery enables to establish a correlation between the viscosity, the lithium cation solvation and the capacity of the battery. In particular, Li-O_2 battery cell using PMI TFSI and Li TFSI as electrolyte shows the best specific capacity obtained among the RTILs tested with 1856 mAh g^{-1} at 0.1 mA cm^{-2}.

- ✓ Electrolytes composed of only a RTIL and a Li salt are not suitable for Li-O_2 batteries. Indeed their relatively high viscosity affects the kinetics of the battery reactions, resulting to low cyclability, less than 20 cycles with the RTILs tested.

- ✓ A blended RTIL/organic solvent is formulated to improve the Li-O_2 battery performance. Thus, the DMSO:EMI TFSI (70:30) electrolyte shows a specific capacity of 7618 mAh g^{-1} at 100% DOD and at 0.1 mA cm^{-2}. Concerning the cyclability, 69 cycles are obtained at 200 mA g^{-1} with limited capacity of 600 mAh g^{-1}. Higher cyclability is obtained with the DMSO electrolyte with 98 cycles.

- ✓ The study of the different properties characterized enables to observe that bulk electrolyte parameters (ionic conductivity, viscosity) have more influence on the battery performance than the cathode surface parameters (cell overpotential, wettability) and the anode surface parameters (Li/Li overpotential)

- ✓ LiOH is identified as one of the main species formed during battery cycling with this electrolyte. Indeed, the EMI TFSI reacts continuously with the lithium, independently of the state-of-charge of the battery. This observation explains mainly the limited cyclability measured and confirms the low stability of imidazolium-based RTILs with lithium.

Concerning the STABLE project, the DMSO:EMI TFSI (70:30) + 5% $LiClO_4$ electrolyte shows the highest performances compared to the other electrolytes developed during the three years of the project (Figure 50).

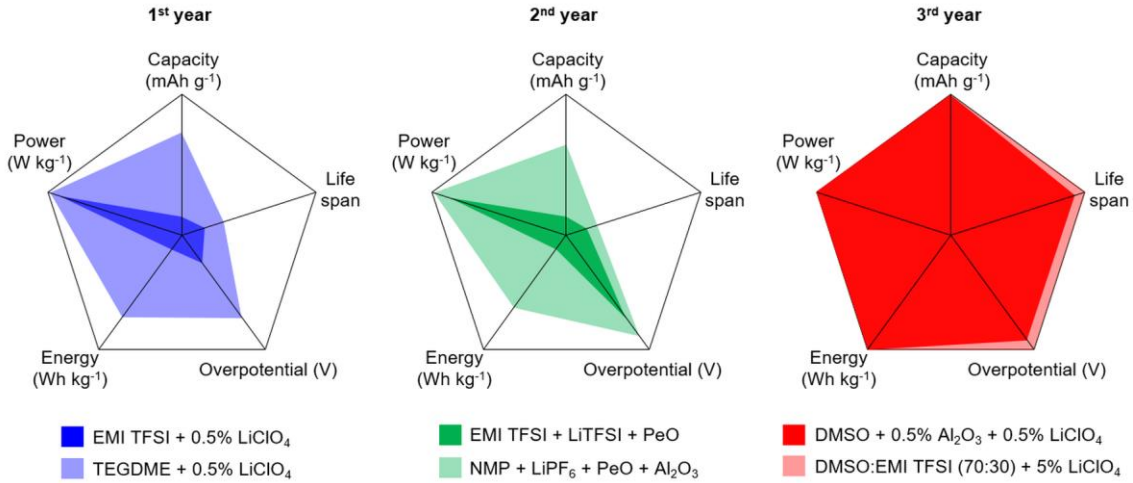

Figure 50: Li-O_2 cell performances with the electrolytes developed at the end of each year of the STABLE project (maximum for each axis: capacity: 7618 mA g^{-1}; life span: 69 cycles; overpotential: 1.06 V; energy: 21330 Wh kg^{-1}; power: 183 W kg^{-1}).

References

1. Shi, J.-L.; Xiao, D.-D.; Ge, M.; Yu, X.; Chu, Y.; Huang, X.; Zhang, X.-D.; Yin, Y.-X.; Yang, X.-Q.; Guo, Y.-G.; Gu, L.; Wan, L.-J. High-Capacity Cathode Material with High Voltage for Li-Ion Batteries. *Adv. Mater.* **2018**, *30*, 1705575, *doi:10.1002/adma.201705575*.
2. Hu, E.; Wang, X.; Yu, X.; Yang, X. Q. Probing the Complexities of Structural Changes in Layered Oxide Cathode Materials for Li-Ion Batteries during Fast Charge-Discharge Cycling and Heating. *Acc. Chem. Res.* **2018**, *51*, 290, *doi:10.1021/acs.accounts.7b00506*.
3. Zubi, G.; Dufo-López, R.; Carvalho, M.; Pasaoglu, G. The lithium-ion battery: State of the art and future perspectives. *Renew. Sustain. Energy Rev.* **2018**, *89*, 292, *doi:10.1016/j.rser.2018.03.002*.
4. Zu, C.-X.; Li, H. Thermodynamic analysis on energy densities of batteries. *Energy Environ. Sci.* **2011**, *4*, 2614, *doi:10.1039/c0ee00777c*.
5. Bruce, P. G.; Freunberger, S. A.; Hardwick, L. J.; Tarascon, J.-M. Li–O2 and Li–S batteries with high energy storage. *Nat. Mater.* **2012**, *11*, 19, *doi:10.1038/nmat3191*.
6. Christensen, J.; Albertus, P.; Sanchez-Carrera, R. S.; Lohmann, T.; Kozinsky, B.; Liedtke, R.; Ahmed, J.; Kojic, A. A Critical Review of Li/Air Batteries. *J. Electrochem. Soc.* **2012**, *159*, R1, *doi:10.1149/2.086202jes*.
7. Galbraith, A. The Lithium-Water-Air Battery for Automotive Propulsion. In *4th International Electric Vehicle Symposium, Duesseldorf, West Germany*; 1976.
8. Abraham, K. M.; Jiang, Z. A Polymer Electrolyte-Based Rechargeable lithium / Oxygen Battery. *J. Electrochem. Soc.* **1996**, *143*, 1.
9. Commission, E. Climate Action Available online: https://ec.europa.eu/clima/policies/international/negotiations/paris_en (accessed on Apr 4, 2017).
10. Girishkumar, G.; McCloskey, B. D.; Luntz, A. C.; Swanson, S.; Wilcke, W. Lithium−Air Battery: Promise and Challenges. *J. Phys. Chem. Lett.* **2010**, *1*, 2193, *doi:10.1021/jz1005384*.
11. Amine, K.; Curtiss, L. A.; Jun, L.; Kah, C. L.; Zhengcheng, Z.; Yang-Kook, S. Li-air batteries having ether-based electrolytes 2013.
12. Badding, M. E.; Cui, Y.; Lin, H.; Zhaoyin, W.; Xiangwei, W. W. Metal supported nanowire cathode catalysts for Li-air batteries 2013.
13. Barde, F.; Jeanne, J.; Bruce, P. G.; Chen, Y.; Freunberger, S. (TOYOTA Motor Europe), Stable non-aqueous electrolyte promoting ideal reaction process in rechargeable lithium-air batteries 2013.
14. Choi, J. W.; Kim, B. G.; Kim, J. S. (Korea Advanced Institute of Science and Technology), Polyurethane based membranes and/or separators for electrochemical cells 2017.
15. Kim, D. H.; Son, S. I.; Ryu, K. H.; Rhee, J. K.; Kim, S.; Lee, H. T. (Hyundai Motor Company), Li-air hybrid battery and method for manufacturing the same 2016.
16. Kim, I. D.; Jung, J. W.; Yoon, K. R.; Yoon, D. H.; Park, Y. J. (Korea Advanced Institute of Science and Technology), Li-air battery using current collector-catalysts monolithic 3 dimensional nanofiber network for Li-air battery and manufacturing method thereof 2016.

17. Kondo, M.; Okamoto, H. (Imura Zairyo Kaihatsu Kenkyusho), Li-air secondary battery and method for restoring discharge performance of the battery 2015.

18. Kweon, S. C.; Oh, I. H.; Lee, J. kee (Korea Advanced Institute of Science and Technology), Li-air battery having the function of removing irreversible lithium byproducts and method for removing irreversible lithium byproducts 2016.

19. Li, J.; Liang, J. (Guangzhou Eastpower Battery Ind. Co., Ltd.), High-energy-density Li-air battery air electrode, and battery and making method thereof 2013.

20. Sanchez-Carrera, R. S.; Kozinsky, B.; Lohmann, T.; Albertus, P.; Christensen, J. F. (BOSCH GMBH), Stable electrolyte materials for Li-air battery systems 2013.

21. Sankarasubramanian, S.; Prakash, J.; Mizuno, F.; Singh, N. (TOYOTA Motor Europe), Alloys as cathode materials for lithium-air batteries 2016.

22. Visco, S. J.; Katz, B. D.; Nimon, Y. S.; Jonghe, L. C. De (PolyPlus Battery Company), Protected active metal electrode and battery cell structures with non-aqueous interlayer architecture 2007.

23. Wen, Z.; Badding, M. E.; Lu, Y.; Cui, Y.; Wu, X. (Shanghai Institute of Ceramics, Corning Inc.), Li-air battery negative electrode, Li-air battery and Li-air battery electrode preparation method 2015.

24. Woo, S. I.; Lee, S. H.; Lee, K. R. (Korea Advanced Institute of Science and Technology), Bifunctional catalysts using bimetallic material for cathode of Li-air battery 2014.

25. Yoon, Y. S.; Lee, W. Y.; Park, Y. J.; Lee, S. H.; Jee, S. H. (Office of Research Affairs IACF, Yonsei University), Cathode for Li-air cell and Li-air cell including the same 2013.

26. Zhian, Z.; Yanqing, L.; Geng, Z.; Jie, L.; Ming, J. (Central South University), Composite electrocatalyst material used for Li-air batteries and preparation method thereof 2012.

27. Grande, L.; Paillard, E.; Hassoun, J.; Park, J.-B. B.; Lee, Y.-J. J.; Sun, Y.-K. K.; Passerini, S.; Scrosati, B. The lithium/air battery: Still an emerging system or a practical reality? *Adv. Mater.* **2014**, *27*, 784, *doi:10.1002/adma.201403064*.

28. Jin, Y.; Guo, S.; He, P.; Zhou, H. Status and prospects in polymer electrolyte for solid-state Li-O2 (air) battery. *Energy Environ. Sci.* **2017**, *10*, 860, *doi:10.1039/C6EE03499C*.

29. Lou, P.; Li, C.; Cui, Z.; Guo, X. Job-sharing cathode design for Li–O2 batteries with high energy efficiency enabled by in situ ionic liquid bonding to cover carbon surface defects. *J. Mater. Chem. A* **2016**, *4*, 241, *doi:10.1039/C5TA07886E*.

30. Bhatt, M. D.; Geaney, H.; Nolan, M.; O'Dwyer, C. Key scientific challenges in current rechargeable non-aqueous Li-O2 batteries: experiment and theory. *Phys. Chem. Chem. Phys.* **2014**, *16*, 12093, *doi:10.1039/c4cp01309c*.

31. Li, Q.; Cao, R.; Cho, J.; Wu, G. Nanostructured carbon-based cathode catalysts for nonaqueous lithium-oxygen batteries. *Phys. Chem. Chem. Phys.* **2014**, *16*, 13568, *doi:10.1039/c4cp00225c*.

32. Shimonishi, Y.; Zhang, T.; Imanishi, N.; Im, D.; Lee, D. J.; Hirano, A.; Takeda, Y.; Yamamoto, O.; Sammes, N. A study on lithium/air secondary batteries - Stability of the NASICON-type lithium ion conducting solid electrolyte in alkaline aqueous solutions. *J. Power Sources* **2011**, *196*, 5128, *doi:10.1016/j.jpowsour.2011.02.023*.

33. Kumar, B.; Kumar, J.; Leese, R.; Fellner, J. P.; Rodrigues, S. J.; Abraham, K. M. A Solid-State, Rechargeable, Long Cycle Life Lithium–Air Battery. *J. Electrochem. Soc.* **2010**, *157*, A50, *doi:10.1149/1.3256129*.

34. Laoire, C. O.; Mukerjee, S.; Abraham, K. M.; Plichta, E. J.; Hendrickson, M. a. Elucidating the Mechanism of Oxygen Reduction for Lithium-Air Battery Applications. *J. Phys. Chem. C* **2009**, *113*, 20127, *doi:10.1021/jp908090s*.

35. Laoire, C. O.; Mukerjee, S.; Abraham, K. M.; Plichta, E. J.; Hendrickson, M. A. Influence of Nonaqueous Solvents on the Electrochemistry of Oxygen in the Rechargeable Lithium-Air Battery. *J. Phys. Chem. C* **2010**, *114*, 9178, *doi: 10.1021/jp102019y*.

36. Zhai, D.; Lau, K. C.; Wang, H. H.; Wen, J.; Miller, D. J.; Lu, J.; Kang, F.; Li, B.; Yang, W.; Gao, J.; Indacochea, E.; Curtiss, L. A.; Amine, K. Interfacial effects on lithium superoxide disproportionation in Li-O2 batteries. *Nano Lett.* **2015**, *15*, 1041, *doi:10.1021/nl503943z*.

37. Younesi, R.; Veith, G. M.; Johansson, P.; Edstrom, K.; Vegge, T. Lithium salts for advanced lithium batteries: Li-metal, Li-O2, and Li-S. *Energy Environ. Sci.* **2015**, *8*, 1905, *doi:10.1039/C5EE01215E*.

38. Luntz, A. C.; Mccloskey, B. D. Nonaqueous Li − Air Batteries : A Status Report. *Chem. Rev.* **2014**, *114*, 11721, *doi:10.1021/cr500054y*.

39. Zhao, Z.; Huang, J.; Peng, Z. Achilles' Heel of Li-Air Batteries: Li2CO3. *Angew. Chemie Int. Ed.* **2018**, *57*, 3874, *doi:10.1002/anie.201710156*.

40. Chawla, N.; Chamaani, A.; Safa, M.; El-Zahab, B. Palladium-Filled Carbon Nanotubes Cathode for Improved Electrolyte Stability and Cyclability Performance of Li-O 2 Batteries. *J. Electrochem. Soc.* **2017**, *164*, A6303, *doi:10.1149/2.0491701jes*.

41. Cui, Y.; Wen, Z.; Liu, Y. A free-standing-type design for cathodes of rechargeable Li–O2 batteries. *Energy Environ. Sci.* **2011**, *4*, 4727, doi:10.1039/c1ee02365a.

42. Cui, Y.; Wen, Z.; Lu, Y.; Wu, M.; Liang, X.; Jin, J. Functional binder for high-performance Li–O2 batteries. *J. Power Sources* **2013**, *244*, 614, *doi:10.1016/j.jpowsour.2012.12.117*.

43. Geaney, H.; O'Dwyer, C. Electrochemical investigation of the role of MnO2 nanorod catalysts in water containing and anhydrous electrolytes for Li–O2 battery applications. *Phys. Chem. Chem. Phys.* **2015**, *17*, 6748, *doi:10.1039/C4CP05785F*.

44. Guo, Z.; Zhou, D.; Dong, X.; Qiu, Z.; Wang, Y.; Xia, Y. Ordered hierarchical mesoporous/macroporous carbon: A high-performance catalyst for rechargeable li-o2 batteries. *Adv. Mater.* **2013**, *25*, 5668, *doi:10.1002/adma.201302459*.

45. Hou, J.; Yang, M.; Ellis, M. W.; Moore, R. B.; Yi, B. Lithium oxides precipitation in nonaqueous Li–air batteries. *Phys. Chem. Chem. Phys.* **2012**, *14*, 13487, *doi:10.1039/c2cp42768k*.

46. Jung, C. Y.; Zhao, T. S.; Zeng, L.; Tan, P. Vertically aligned carbon nanotube-ruthenium dioxide core-shell cathode for non-aqueous lithium-oxygen batteries. *J. Power Sources* **2016**, *331*, 82, *doi:10.1016/j.jpowsour.2016.09.020*.

47. Jung, J.-W.; Jang, J.-S.; Yun, T. G.; Yoon, K. R.; Kim, I.-D. 3D Nanofibrous Air Electrode Assembled With Carbon Nanotubes Bridged Hollow Fe2O3 Nanoparticles for High Performance Lithium-Oxygen Batteries. *ACS Appl. Mater. Interfaces* **2018**, 10, 6531, *doi:10.1021/acsami.7b15421*.

48. Kim, S. H.; Lee, Y. J. Y. J.; Kim, D. H.; Lee, Y. J. Y. J. Bimetallic Metal-Organic-Frameworks as Efficient Cathode Catalysts for Li-O2 Batteries. *ACS Appl. Mater. Interfaces* **2018**, *10*, 660, *doi:10.1021/acsami.7b15499*.

49. Kuboki, T.; Okuyama, T.; Ohsaki, T.; Takami, N. Lithium-air batteries using hydrophobic room temperature ionic liquid electrolyte. *J. Power Sources* **2005**, *146*, 766, *doi:10.1016/j.jpowsour.2005.03.082*.

50. Laoire, C. O.; Mukerjee, S.; Plichta, E. J.; Hendrickson, M. A.; Abraham, K. M. Rechargeable Lithium/TEGDME-LiPF[sub 6]/O[sub 2] Battery. *J. Electrochem. Soc.* **2011**, *158*, A302, *doi:10.1149/1.3531981*.

51. Leng, L.; Li, J.; Zeng, X.; Song, H.; Shu, T.; Wang, H.; Liao, S. Enhancing the cyclability of Li–O2 batteries using PdM alloy nanoparticles anchored on nitrogen-doped reduced graphene as the cathode catalyst. *J. Power Sources* **2016**, *337*, 173, *doi:10.1016/j.jpowsour.2016.10.089*.

52. Lim, H. D.; Park, K. Y.; Song, H.; Jang, E. Y.; Gwon, H.; Kim, J.; Kim, Y. H.; Lima, M. D.; Robles, R. O.; Leprõ, X.; Baughman, R. H.; Kang, K. Enhanced power and rechargeability of a Li-O2 battery based on a hierarchical-fibril CNT electrode. *Adv. Mater.* **2013**, *25*, 1348, *doi:10.1002/adma.201204018*.

53. Lu, J.; Lei, Y.; Lau, K. C.; Luo, X.; Du, P.; Wen, J.; Assary, R. S.; Das, U.; Miller, D. J.; Elam, J. W.; Albishri, H. M.; El-Hady, D. A.; Sun, Y.-K. K.; Curtiss, L. A.; Amine, K. A nanostructured cathode architecture for low charge overpotential in lithium-oxygen batteries. *Nat. Commun.* **2013**, *4*, 2383, *doi:10.1038/ncomms3383*.

54. Ma, S.; Liu, Q.; Lei, D.; Guo, X.; Li, S.; Li, Z. A powerful Li-O 2 battery based on an efficient hollow Cu 2 O cathode catalyst with tailored crystal plane. *Electrochim. Acta* **2017**, *260*, 31, *doi:10.1016/j.electacta.2017.11.065*.

55. Mei, D.; Yuan, X.; Ma, Z. Z.-F. Z.; Wei, P.; Yu, X.; Yang, J.; Ma, Z. Z.-F. Z. A SnO2-based cathode catalyst for lithium air batteries. *ACS Appl. Mater. Interfaces* **2016**, *8*, 12804, *doi:10.1021/acsami.6b02402*.

56. Meini, S.; Piana, M.; Beyer, H.; Schwammlein, J.; Gasteiger, H. a. Effect of Carbon Surface Area on First Discharge Capacity of Li-O2 Cathodes and Cycle-Life Behavior in Ether-Based Electrolytes. *J. Electrochem. Soc.* **2012**, *159*, A2135, *doi:10.1149/2.011301jes*.

57. Mitchell, R. R.; Gallant, B. M.; Thompson, C. V.; Shao-Horn, Y. All-carbon-nanofiber electrodes for high-energy rechargeable Li–O2 batteries. *Energy Environ. Sci.* **2011**, *4*, 2952, *doi:10.1039/c1ee01496j*.

58. Mo, Y.; Ong, S. P.; Ceder, G. First-principles study of the oxygen evolution reaction of lithium peroxide in the lithium-air battery. *Phys. Rev. B - Condens. Matter Mater. Phys.* **2011**, *84*, 205446, *doi:10.1103/PhysRevB.84.205446*.

59. Nasybulin, E.; Xu, W.; Engelhard, M. H.; Nie, Z.; Burton, S. D.; Cosimbescu, L.; Gross, M. E.; Zhang, J. Effects of Electrolyte Salts on the Performance of Li−O2 Batteries. *J. Phys. Chem. C* **2013**, *117*, 2635, *doi:10.1021/jp311114u*.

60. Oh, S. H.; Black, R.; Pomerantseva, E.; Lee, J.-H.; Nazar, L. F. Synthesis of a metallic mesoporous pyrochlore as a catalyst for lithium–O2 batteries. *Nat. Chem.* **2012**, *4*, 1004, *doi:10.1038/nchem.1499*.

61. Ren, X.; Liao, B.; Li, Y.; Zhang, P.; Deng, L.; Gao, Y. Facile synthesis of PdSnCo/nitrogen-doped reduced graphene as a highly active catalyst for lithium-air batteries. *Electrochim. Acta* **2017**, *228*, 36, *doi:10.1016/j.electacta.2017.01.032*.

62. Ryu, W.; Yoon, T.; Song, S. H.; Jeon, S.; Park, Y.; Kim, I. Bifunctional Composite Catalysts Using Co3O4 Nano fi bers Immobilized on Nonoxidized Graphene Nano fl akes for High- Capacity and Long-Cycle Li−O2 Batteries. *Nano Lett.* **2013**, 13, 4190, *doi:10.1021/nl401868q*.

63. Shen, Y.; Sun, D.; Yu, L.; Zhang, W.; Shang, Y.; Tang, H.; Wu, J.; Cao, A.; Huang, Y. A high-capacity lithium-air battery with Pd modified carbon nanotube sponge cathode working in regular air. *Carbon N. Y.* **2013**, *62*, 288, *doi:10.1016/j.carbon.2013.05.066*.

64. Su, D.; Kim, H.-S.; Kim, W.-S.; Wang, G. A study of PtxCoy alloy nanoparticles as cathode catalysts for lithium-air batteries with improved catalytic activity. *J. Power Sources* **2013**, *244*, 488, *doi:10.1016/j.jpowsour.2012.11.024*.

65. Sun, B.; Huang, X.; Chen, S.; Munroe, P.; Wang, G. Porous Graphene Nanoarchitectures: An Efficient Catalyst for Low Charge-Overpotential, Long Life, and High Capacity Lithium−Oxygen Batteries. *Nano Lett.* **2014**, *14*, 3145, *doi: 10.1021/nl500397y*.

66. Trahan, M. J.; Mukerjee, S.; Plichta, E. J.; Hendrickson, M. a.; Abraham, K. M. Studies of Li-Air Cells Utilizing Dimethyl Sulfoxide-Based Electrolyte. *J. Electrochem. Soc.* **2012**, *160*, A259, *doi:10.1149/2.048302jes*.

67. Wang, Z. L.; Xu, D.; Xu, J. J.; Zhang, L. L.; Zhang, X. B. Graphene oxide gel-derived, free-standing, hierarchically porous carbon for high-capacity and high-rate rechargeable Li-O2 batteries. *Adv. Funct. Mater.* **2012**, *22*, 3699, *doi:10.1002/adfm.201200403*.

68. Williford, R. E.; Zhang, J.-G. Air electrode design for sustained high power operation of Li/air batteries. *J. Power Sources* **2009**, *194*, 1164, *doi:10.1016/j.jpowsour.2009.06.005*.

69. Wu, F.; Xing, Y.; Li, L.; Qian, J.; Qu, W.; Wen, J.; Miller, D. J.; Ye, Y.; Chen, R.; Amine, K.; Lu, J. Facile Synthesis of Boron-Doped RGO as Cathode Material for High Energy Li-O2 Batteries. *ACS Appl. Mater. Interfaces* **2016**, *8*, 23635, *doi:10.1021/acsami.6b05403*.

70. Xiao, J.; Mei, D.; Li, X.; Xu, W.; Wang, D.; Graff, G. L.; Bennett, W. D.; Nie, Z.; Saraf, L. V.; Aksay, I. a.; Liu, J.; Zhang, J. G. Hierarchically porous graphene as a lithium-air battery electrode. *Nano Lett.* **2011**, *11*, 5071, *doi:10.1021/nl203332e*.

71. Zhang, R. H.; Zhao, T. S.; Wu, M. C.; Jiang, H. R.; Zeng, L. Mesoporous ultrafine Ta2O5nanoparticle with abundant oxygen vacancies as a novel and efficient catalyst for non-aqueous Li-O2batteries. *Electrochim. Acta* **2018**, *271*, 232, *doi:10.1016/j.electacta.2018.03.164*.

72. Shui, J.-L.; Okasinski, J. S.; Kenesei, P.; Dobbs, H. a; Zhao, D.; Almer, J. D.; Liu, D.-J. Reversibility of anodic lithium in rechargeable lithium-oxygen batteries. *Nat. Commun.* **2013**, *4*, 2255, *doi:10.1038/ncomms3255*.

73. Gong, H.; Xue, H.; Wang, T.; Guo, H.; Fan, X.; Song, L.; Xia, W.; He, J. High-Loading Nickel Cobaltate Nanoparticles Anchored on Three-Dimensional N-Doped Graphene as an Efficient Bifunctional Catalyst for Lithium–Oxygen Batteries. *ACS Appl. Mater. Interfaces* **2016**, *8*, 18060, *doi:10.1021/acsami.6b04810*.

74. Kim, G. P.; Lim, D.; Park, I.; Park, H.; Shim, S. E.; Baeck, S. H. RuO2 nanoparticles decorated MnOOH/C as effective bifunctional electrocatalysts for lithium-air battery cathodes with long-cycling stability. *J. Power Sources* **2016**, *324*, 687, *doi:10.1016/j.jpowsour.2016.05.131*.

75. Park, J.-B.; Luo, X.; Lu, J.; Shin, C. D.; Yoon, C. S.; Amine, K.; Sun, Y.-K. Improvement of Electrochemical Properties of Lithium-Oxygen Batteries Using a Silver Electrode. *J. Phys. Chem. C* **2015**, *119*, 15036, *doi:10.1021/acs.jpcc.5b04653*.

76. Martinez Crespiera, S.; Amantia, D.; Knipping, E.; Aucher, C.; Aubouy, L.; Amici, J.; Zeng, J.; Rancia, C.; Bodoardo, S. Electrospun Pd-doped mesoporous Carbon Nano Fibres as catalysts for rechargeable Li-O2 Batteries. *RSC Adv.* **2016**, *6*, 57335, *doi:10.1039/b000000x*.

77. Chen, Y.; Freunberger, S. a; Peng, Z.; Fontaine, O.; Bruce, P. G. Charging a Li-O2 battery using a redox mediator. *Nat. Chem.* **2013**, *5*, 489, *doi:10.1038/nchem.1646*.

78. Liu, T.; Leskes, M.; Yu, W.; Moore, A. J.; Zhou, L.; Bayley, P. M.; Kim, G.; Grey, C. P. Cycling Li-O2 batteries via LiOH formation and decomposition. *Science.* **2015**, *350*, 530, *doi:10.1126/science.aac7730*.

79. Kwak, W.-J.; Hirshberg, D.; Sharon, D.; Shin, H.-J.; Afri, M.; Park, J.-B.; Garsuch, A.; Chesneau, F. F.; Frimer, A. a.; Aurbach, D.; Sun, Y.-K. Understanding the behavior of Li–oxygen cells containing LiI. *J. Mater. Chem. A* **2015**, *3*, 8855, *doi:10.1039/C5TA01399B*.

80. Lee, C. K.; Park, Y. J. CsI as multi-functional redox mediator for enhanced Li-air batteries. *ACS Appl. Mater. Interfaces* **2016**, *8*, 8561, *doi:10.1021/acsami.6b01775*.

81. Bergner, B. J.; Schürmann, A.; Peppler, K.; Garsuch, A.; Janek, J. TEMPO: A Mobile Catalyst for Rechargeable Li-O2 Batteries. *J. Am. Chem. Soc.* **2014**, *136*, 15054, *doi:10.1002/anie.201307976*.

82. Feng, N.; Mu, X.; Zhang, X.; He, P.; Zhou, H. Intensive Study on the Catalytical Behavior of N -Methylphenothiazine as a Soluble Mediator to Oxidize the Li2O2 Cathode of the Li–O2 Battery. *ACS Appl. Mater. Interfaces* **2017**, *9*, 3733, *doi:10.1021/acsami.6b14889*.

83. Gutmann, V. Solvent effects on the reactivities of organometallic compounds. *Coord. Chem. Rev.* **1976**, *18*, 225, *doi:10.1016/S0010-8545(00)82045-7*.

84. Aetukuri, N. B.; McCloskey, B. D.; Garciá, J. M.; Krupp, L. E.; Viswanathan, V.; Luntz, A. C. Solvating additives drive solution-mediated electrochemistry and enhance toroid growth in non-aqueous Li–O2 batteries. *Nat. Chem.* **2015**, *7*, 50, *doi:10.1038/nchem.2132*.

85. Johnson, L.; Li, C.; Liu, Z.; Chen, Y.; Freunberger, S. a; Ashok, P. C.; Praveen, B. B.; Dholakia, K.; Tarascon, J.-M.; Bruce, P. G. The role of LiO2 solubility in O2 reduction in aprotic solvents and its consequences for Li-O2 batteries. *Nat. Chem.* **2014**, *6*, 1091, *doi:10.1038/nchem.2101*.

86. Cho, S. H. M. H. M.; Yom, J. H.; Hwang, S. W.; Seong, I. W.; Kim, J.; Cho, S. H. M. H. M.; Yoon, W. Y. Morphology control of lithium peroxide using Pd3Co as an additive in aprotic Li-O2 batteries. *J. Power Sources* **2017**, *342*, 427, *doi:10.1016/j.jpowsour.2016.12.076*.

87. Matsuda, S.; Uosaki, K.; Nakanishi, S. Enhanced energy capacity of lithium-oxygen batteries with ionic liquid electrolytes by addition of ammonium ions. *J. Power Sources* **2017**, *356*, 12, *doi:10.1016/j.jpowsour.2017.04.069*.

88. Yao, X.; Dong, Q.; Cheng, Q.; Wang, D. Why Do Lithium-Oxygen Batteries Fail: Parasitic Chemical Reactions and Their Synergistic Effect. *Angew. Chemie - Int. Ed.* **2016**, *55*, 11344, *doi:10.1002/anie.201601783*.

89. Liu, Q. C.; Xu, J. J.; Yuan, S.; Chang, Z. W.; Xu, D.; Yin, Y. Bin; Li, L.; Zhong, H. X.; Jiang, Y. S.; Yan, J. M.; Zhang, X. B. Artificial Protection Film on Lithium Metal Anode toward Long-Cycle-Life Lithium-Oxygen Batteries. *Adv. Mater.* **2015**, *27*, 5241, *doi:10.1002/adma.201501490*.

90. Guo, Z.; Dong, X.; Wang, Y.; Xia, Y. A lithium air battery with a lithiated Al-carbon anode. *Chem. Commun. (Camb).* **2014**, *51*, 676, *doi:10.1039/c4cc07315k*.

91. Wu, S.; Zhu, K.; Tang, J.; Liao, K.; Bai, S.; Yi, J.; Yamauchi, Y.; Ishida, M.; Zhou, H. A Long-Life Lithium Ion Oxygen Battery Based on Commercial Silicon Particles as the Anode. *Energy Environ. Sci.* **2016**, *9*, 3262, *doi:10.1039/C6EE01512C*.

92. Lee, D. J.; Lee, H.; Kim, Y. J.; Park, J. K.; Kim, H. T. Sustainable Redox Mediation for Lithium-Oxygen Batteries by a Composite Protective Layer on the Lithium-Metal Anode. *Adv. Mater.* **2016**, *28*, 857, *doi:10.1002/adma.201503169*.

93. Luo, Z. K.; Liang, C. S.; Wang, F.; Xu, Y. H.; Chen, J.; Liu, D.; Sun, H. Y.; Yang, H.; Fan, X. P. Optimizing main materials for a lithium-air battery of high cycle life. *Adv. Funct. Mater.* **2014**, *24*, 2101, *doi:10.1002/adfm.201303076*.

94. Sharon, D.; Hirshberg, D.; Afri, M.; Garsuch, A.; Frimer, A. A.; Aurbach, D. Lithium-oxygen electrochemistry in non-aqueous solutions. *Isr. J. Chem.* **2015**, *55*, 508, *doi:10.1002/ijch.201400135*.

95. Nakamoto, H.; Suzuki, Y.; Shiotsuki, T.; Mizuno, F.; Higashi, S.; Takechi, K.; Asaoka, T.; Nishikoori, H.; Iba, H. Ether-functionalized ionic liquid electrolytes for lithium-air batteries. *J. Power Sources* **2013**, *243*, 19, *doi:10.1016/j.jpowsour.2013.05.147*.

96. Peng, Z.; Freunberger, S. A.; Chen, Y.; Bruce, P. G. A reversible and higher-rate Li-O2 battery. *Science (80-.).* **2012**, *337*, 563, *doi:10.1126/science.1223985*.

97. Ottakam Thotiyl, M. M.; Freunberger, S. a; Peng, Z.; Chen, Y.; Liu, Z.; Bruce, P. G. A stable cathode for the aprotic Li-O2 battery. *Nat. Mater.* **2013**, *12*, 1050, *doi:10.1038/nmat3737*.

98. Sharon, D.; Afri, M.; Noked, M.; Garsuch, A.; Frimer, A. a; Aurbach, D. Oxidation of Dimethyl Sulfoxide Solutions by Electrochemical Reduction of Oxygen. *J. Phys. Chem. Lett.* **2013**, *4*, 3115, *doi: 10.1021/jz4017188*.

99. Elia, G. A.; Park, J.-B.; Sun, Y.-K.; Scrosati, B.; Hassoun, J. Role of the Lithium Salt in the Performance of Lithium-Oxygen Batteries: A Comparative Study. *ChemElectroChem* **2014**, *1*, 47, *doi:10.1002/celc.201300160*.

100. Veith, G. M.; Nanda, J.; Delmau, L. H.; Dudney, N. J. Influence of Lithium Salts on the Discharge Chemistry of Li − Air Cells. *J. Phys. Chem. Lett.* **2012**, *3*, 1242, *doi: 10.1021/jz300430s*.

101. Wilkes, J. S. A Short History of Ionic Liquids - From Molten Salts to Neoteric Solvents. *Green Chem.* **2002**, *4*, 73, *doi:10.1039/b110838g*.

102. Walden, P. Molecular weights and electrical conductivity of several fused salts. *Bull. l'Academie Imp. des Sci. St.-petersbg.* **1914**, 405, *doi:citeulike-article-id:12856962*.

103. Sugden, S.; Wilkins, H. CLXVI1.-The Parachor and Chemical Constitution. Part X I I . Fused Metals and Salts. *J. Chem. Soc.* **1929**, 1291, *doi:10.1039/JR9290001291*.

104. Armand, M.; Endres, F.; MacFarlane, D. R.; Ohno, H.; Scrosati, B. Ionic-liquid materials for the electrochemical challenges of the future. *Nat. Mater.* **2009**, *8*, 621, *doi:10.1038/nmat2448*.

105. Hurley, F. H. U.S. Patent 2446331 - Electrodepositon of Aluminium 1948.

106. Hurley, F. H.; WIer, T. P. The Electrodeposition of Aluminum from Nonaqueous Solutions at Room Temperature. *J. Electrochem. Soc.* **1951**, *98*, 207, *doi:10.1149/1.2778133*.

107. Chum, H. L.; Koch, V. R.; Miller, L. L.; Osteryoung, R. a An Electrochemical Scrutiny of Organometallic Iron Complexes and Hexamethylbenzene in a Room-Temperature Molten-Salt. *J. Am. Chem. Soc.* **1975**, *97*, 3264, *doi:10.1021/ja00844a081*.

108. Wilkes, J. S.; Levisky, J. A.; Wilson, R. A.; Hussey, C. L. Dialkylimidazolium chloroaluminate melts: a new class of room-temperature ionic liquids for electrochemistry, spectroscopy and synthesis. *Inorg. Chem.* **1982**, *21*, 1263, *doi:10.1021/ic00133a078*.

109. Welton, T. Room-Temperature Ionic Liquids . Solvents for Synthesis and Catalysis. *Chem. Rev.* **1999**, *99*, 2071, *doi:10.1021/cr980032t*.

110. Fukaya, Y.; Hayashi, K.; Wada, M.; Ohno, H. Cellulose dissolution with polar ionic liquids under mild conditions: required factors for anions. *Green Chem.* **2008**, *10*, 44, *doi:10.1039/b713289a*.

111. Salminen, J.; Papaiconomou, N.; Kumar, R. A.; Lee, J.-M.; Kerr, J.; Newman, J.; Prausnitz, J. M. Physicochemical properties and toxicities of hydrophobic piperidinium and pyrrolidinium ILs. *Fluid Phase Equilib.* **2007**, *261*, 421, *doi: 10.1016/j.fluid.2007.06.031*.

112. Earle, M. J.; Seddon, K. R. Ionic liquids. Green solvents for the future. *Pure Appl. Chem.* **2000**, *72*, 1391, *doi:10.1351/pac200072071391*.

113. Park, J.; Jung, Y.; Kusumah, P.; Lee, J.; Kwon, K.; Lee, C. K. Application of ionic liquids in hydrometallurgy. *Int. J. Mol. Sci.* **2014**, *15*, 15320, *doi:10.3390/ijms150915320*.

114. Plechkova, N. V; Seddon, K. R. Applications of ionic liquids in the chemical industry. *Chem. Soc. Rev.* **2008**, *37*, 123, *doi:10.1039/b006677j*.

115. Zhou, Y.; Antonietti, M. Synthesis of Very Small TiO2 Nanocrystals in a Room-Temperature Ionic Liquid and Their Self-Assembly Towards Mesoporous Spherical Aggregates. *J. Am. Chem. Soc.* **2003**, *125*, 14960, *doi: 10.1021/nl025861f*.

116. Zhu, H.; Huang, J. F.; Pan, Z.; Dai, S.; Sciences, C.; Di, V.; Ridge, O.; Ridge, O.; February, R. V; Re, V.; Recei, M.; July, V. Ionothermal synthesis of hierarchical ZnO nanostructures from ionic-liquid precursors. *Chem. Mater.* **2006**, *18*, 4473, *doi:10.1021/cm060472y*.

117. Wei, D.; Ivaska, A. Applications of ionic liquids in electrochemical sensors. *Anal. Chim. Acta* **2008**, *607*, 126, *doi:10.1016/j.aca.2007.12.011*.

118. Shiddiky, M. J. A.; Torriero, A. A. J. Application of ionic liquids in electrochemical sensing systems. *Biosens. Bioelectron.* **2011**, *26*, 1775, *doi:10.1016/j.bios.2010.08.064*.

119. Nakashima, T.; Kawai, T. Quantum dots-ionic liquid hybrids: efficient extraction of cationic CdTe nanocrystals into an ionic liquid. *Chem. Commun.* **2005**, 1643, *doi:10.1039/b418001a*.

120. Huddleston, J. G.; Willauer, H. D.; Swatloski, R. P.; Visser, A. E.; Rogers, R. D. Room temperature ionic liquids as novel media for "clean" liquid–liquid extraction. *Chem. Commun.* **1998**, *16*, 1765, *doi: 10.1039/A803999B*.

121. Yu, B.; Liu, Z.; Zhou, F.; Liu, W.; Liang, Y. A novel lubricant additive based on carbon nanotubes for ionic liquids. *Mater. Lett.* **2008**, *62*, 2967, *doi:10.1016/j.matlet.2008.01.128*.

122. Ye, C.; Liu, W.; Chen, Y.; Yu, L. Room-temperature ionic liquids: a novel versatile lubricant. *Chem. Commun. (Camb).* **2001**, *0*, 2244, *doi:10.1039/B106935G*.

123. Liu, H.; He, P.; Li, Z.; Liu, Y.; Li, J. A novel nickel-based mixed rare-earth oxide/activated carbon supercapacitor using room temperature ionic liquid electrolyte. *Electrochim. Acta* **2006**, *51*, 1925, *doi:10.1016/j.electacta.2005.06.034*.

124. Su, Y. Z.; Fu, Y. C.; Wei, Y. M.; Yan, J. W.; Mao, B. W. The electrode/ionic liquid interface: Electric double layer and metal electrodeposition. *ChemPhysChem* **2010**, *11*, 2764, *doi:10.1002/cphc.201000278*.

125. Matsumoto, H.; Matsuda, T.; Tsuda, T.; Hagiwara, R.; Ito, Y.; Miyazaki, Y. The Application of Room Temperature Molten Salt with Low Viscosity to the Electrolyte for Dye-Sensitized Solar Cell. *Chem. Lett.* **2001**, *30*, 26, *doi:10.1246/cl.2001.26*.

126. Ue, M.; Takeda, M.; Toriumi, A.; Kominato, A.; Hagiwara, R.; Ito, Y. Application of low-viscosity ionic liquid to the electrolyte of double-layer capacitors. *J. Electrochem. Soc.* **2003**, *150*, A499, *doi: 10.1149/1.1559069*.

127. De Souza, R. F.; Padilha, J. C.; Gonçalves, R. S.; Dupont, J. Room temperature dialkylimidazolium ionic liquid-based fuel cells. *Electrochem. commun.* **2003**, *5*, 728, *doi:10.1016/S1388-2481(03)00173-5*.

128. Kim, H.-T.; Kang, J.; Mun, J.; Oh, S. M.; Yim, T.; Kim, Y. G. Pyrrolinium-based Ionic Liquid as a Flame Retardant for Binary Electrolytes of Lithium Ion Batteries. *ACS Sustain. Chem. Eng.* **2016**, *4*, 497, *doi:10.1021/acssuschemeng.5b00981*.

129. Hess, S.; Wohlfahrt-Mehrens, M.; Wachtler, M. Flammability of Li-Ion Battery Electrolytes: Flash Point and Self-Extinguishing Time Measurements. *J. Electrochem. Soc.* **2015**, *162*, A3084, *doi:10.1149/2.0121502jes*.

130. Park, J.; Ueno, K.; Tachikawa, N.; Dokko, K.; Watanabe, M. Ionic Liquid Electrolytes for Lithium − Sulfur Batteries. **2013**.

131. Wang, J.; Chew, S. Y.; Zhao, Z. W.; Ashraf, S.; Wexler, D.; Chen, J.; Ng, S. H.; Chou, S. L.; Liu, H. K. Sulfur-mesoporous carbon composites in conjunction with a novel ionic liquid electrolyte for lithium rechargeable batteries. *Carbon N. Y.* **2008**, *46*, 229, *doi:10.1016/j.carbon.2007.11.007*.

132. Park, J.; Yamauchi, K.; Takashima, E.; Tachikawa, N.; Ueno, K.; Dokko, K.; Watanabe, M. Solvent Effect of Room Temperature Ionic Liquids on Electrochemical Reactions in Lithium−Sulfur Batteries. **2013**, 2, *doi: 10.1021/jp400153m*.

133. Xia, S.; Zhang, X. M.; Huang, K.; Chen, Y.-L. Le; Wu, Y. T. Ionic liquid electrolytes for aluminium secondary battery: Influence of organic solvents. *J. Electroanal. Chem.* **2015**, *757*, 167, *doi:10.1016/j.jelechem.2015.09.022*.

134. Angell, M.; Pan, C.; Rong, Y.; Yuan, C.; Lin, M.-C.; Hwang, B.-J.; Dai, H. High Coulombic efficiency aluminum-ion battery using an AlCl 3 -urea ionic liquid analog electrolyte. *PNAS* **2017**, *114*, 834, *doi:10.1073/pnas.1619795114*.

135. Gao, T.; Li, X.; Wang, X.; Hu, J.; Han, F.; Fan, X.; Suo, L.; Pearse, A. J.; Lee, S. B.; Rubloff, G. W.; Gaskell, K. J.; Noked, M.; Wang, C. A Rechargeable Al/S Battery with an Ionic-Liquid Electrolyte. *Angew. Chemie Int. Ed.* **2016**, 55, 9898, *doi:10.1002/anie.201603531*.

136. Mainar, A. R.; Iruin, E.; Colmenares, L. C.; Kvasha, A.; de Meatza, I.; Bengoechea, M.; Leonet, O.; Boyano, I.; Zhang, Z.; Blazquez, J. A. An overview of progress in electrolytes for secondary zinc-air batteries and other storage systems based on zinc. *J. Energy Storage* **2018**, *15*, 304, *doi:10.1016/j.est.2017.12.004*.

137. Xu, M.; Ivey, D. G.; Xie, Z.; Qu, W. Rechargeable Zn-air batteries: Progress in electrolyte development and cell configuration advancement. *J. Power Sources* **2015**, *283*, 358, *doi:10.1016/j.jpowsour.2015.02.114*.

138. Allen, C. J.; Hwang, J.; Kautz, R.; Mukerjee, S.; Plichta, E. J.; Hendrickson, M. a.; Abraham, K. M. Oxygen Reduction Reactions in Ionic Liquids and the Formulation of a General ORR Mechanism for Li–Air Batteries. *J. Phys. Chem. C* **2012**, *116*, 20755, *doi:10.1021/jp306718v*.

139. Allen, C. J.; Mukerjee, S.; Plichta, E. J.; Hendrickson, M. A.; Abraham, K. M. Oxygen Electrode Rechargeability in an Ionic Liquid for the Li-Air Battery. *J. Phys. Chem. Lett.* **2011**, *2*, 2420, *doi: 10.1021/jz201070t*.

140. Asadi, M.; Sayahpour, B.; Abbasi, P.; Ngo, A. T.; Karis, K.; Jokisaari, J. R.; Liu, C.; Narayanan, B.; Gerard, M.; Yasaei, P.; Hu, X.; Mukherjee, A.; Lau, K. C.; Assary, R. S.; Khalili-Araghi, F.; Klie, R. F.; Curtiss, L. A.; Salehi-Khojin, A. A lithium–oxygen battery with a long cycle life in an air-like atmosphere. *Nat. Publ. Gr.* **2018**, *555*, 502, *doi:10.1038/nature25984*.

141. Bresser, D.; Paillard, E.; Passerini, S. Ionic Liquid-based Electrolytes for Li Metal/Air Batteries: A Review of Materials and the New "LABOHR" Flow Cell Concept. *J. Electrochem. Sci. Technol.* **2014**, *5*, 37, *doi: 10.5229/JECST.2014.5.2.37*.

142. Cai, K.; Jiang, H.; Pu, W. Comparative Investigation of Organic Solution and Ionic Liquid as Electrolyte under Lithium-Air Battery. *Int. J. Electrochem. Sci.* **2014**, *9*, 390.

143. Cecchetto, L.; Salomon, M.; Scrosati, B.; Croce, F. Study of a Li–air battery having an electrolyte solution formed by a mixture of an ether-based aprotic solvent and an ionic liquid. *J. Power Sources* **2012**, *213*, 233, *doi:10.1016/j.jpowsour.2012.04.038*.

144. Das, S.; Højberg, J.; Knudsen, K. B.; Younesi, R.; Johansson, P.; Norby, P.; Vegge, T. Instability of Ionic Liquid Based Electrolytes in Li-O2 Batteries. *J. Phys. Chem. C* **2015**, *119*, 18084, *doi:10.1021/acs.jpcc.5b04950*.

145. Elia, G. A.; Hassoun, J.; Scrosati, B.; Mueller, F.; Bresser, D.; Passerini, S.; Oberhumer, P.; Tsiouvaras, N.; Reiter, J. An Advanced Lithium−Air Battery Exploiting an Ionic Liquid-Based Electrolyte. *Nano Lett.* **2014**, *14*, 6572, *doi: 10.1021/nl5031985*.

146. Ferrari, S.; Quartarone, E.; Tomasi, C.; Bini, M.; Galinetto, P.; Fagnoni, M.; Mustarelli, P. Investigation of Ether-Based Ionic Liquid Electrolytes for Lithium-O2 Batteries. *J. Electrochem. Soc.* **2014**, *162*, A3001, *doi:10.1149/2.0011502jes*.

147. Giordani, V.; Tozier, D.; Tan, H.; Burke, C. M.; Gallant, B. M.; Uddin, J.; Greer, J. R.; McCloskey, B. D.; Chase, G. V; Addison, D. A Molten Salt Lithium-Oxygen Battery. *J. Am. Chem. Soc.* **2016**, 138, 2656, *doi:10.1021/jacs.5b11744*.

148. Grande, L.; Paillard, E.; Kim, G. T.; Monaco, S.; Passerini, S. Ionic liquid electrolytes for Li-air batteries: Lithium metal cycling. *Int. J. Mol. Sci.* **2014**, *15*, 8122, *doi:10.3390/ijms15058122*.

149. Han, S.-M.; Kim, J.-H.; Kim, D.-W. Cycling Performances of Lithium-Air Cells Assembled with Mixed Electrolytes of Ionic Liquid and Diethylene Glycol Diethyl Ether. *J. Electrochem. Soc.* **2015**, *162*, A3103, *doi:10.1149/2.0161502jes*.

150. Li, Y.; Zhang, Z.; Duan, D.; Sun, Y.; Wei, G.; Hao, X.; Liu, S.; Han, Y.; Meng, W. The correlation of the properties of pyrrolidinium-based ionic liquid electrolytes with the discharge–charge performances of rechargeable Li–O2 batteries. *J. Power Sources* **2016**, *329*, 207, *doi:10.1016/j.jpowsour.2016.08.077*.

151. Ni, W.; Liu, S.; Fei, Y.; He, Y.; Ma, X.; Lu, L.; Deng, Y. Preparation of Carbon Nanotubes/Manganese Dioxide Composite Catalyst with Fewer Oxygen-Containing Groups for Li-O2 Batteries Using Polymerized Ionic Liquids as Sacrifice Agent. *ACS Appl. Mater. Interfaces* **2017**, *9*, 14749, *doi:10.1021/acsami.6b16531*.

152. Olivares-marín, M.; Sorrentino, A.; Pereiro, E.; Tonti, D. Discharge products of ionic liquid-based Li-O2 batteries observed by energy dependent soft x-ray transmission microscopy. *J. Power Sources* **2017**, *359*, 234, *doi:10.1016/j.jpowsour.2017.05.039*.

153. Ulissi, U.; Elia, G. A.; Jeong, S.; Reiter, J.; Tsiouvaras, N.; Passerini, S.; Hassoun, J. New Electrode and Electrolyte Configurations for Lithium-Oxygen Battery. *Chem. - A Eur. J.* **2018**, 24, 3178, *doi:10.1002/chem.201704293*.

154. Watanabe, M.; Thomas, M. L.; Zhang, S.; Ueno, K.; Yasuda, T.; Dokko, K. Application of Ionic Liquids to Energy Storage and Conversion Materials and Devices. *Chem. Rev.* **2017**, *117*, 7190, *doi:10.1021/acs.chemrev.6b00504*.

155. Yamagata, M.; Nishigaki, N.; Nishishita, S.; Matsui, Y.; Sugimoto, T.; Kikuta, M.; Higashizaki, T.; Kono, M.; Ishikawa, M. Charge–discharge behavior of graphite negative electrodes in bis(fluorosulfonyl)imide-based ionic liquid and structural aspects of their electrode/electrolyte interfaces. *Electrochim. Acta* **2013**, *110*, 181, *doi:10.1016/j.electacta.2013.03.018*.

156. Capsoni, D.; Bini, M.; Ferrari, S.; Quartarone, E.; Mustarelli, P. Recent advances in the development of Li–air batteries. *J. Power Sources* **2012**, *220*, 253, *doi:10.1016/j.jpowsour.2012.07.123*.

157. Liu, H.; Liu, Y.; Li, J. Ionic liquids in surface electrochemistry. *Phys. Chem. Chem. Phys.* **2010**, *12*, 1685, *doi:10.1039/c001176m*.

158. Anthony, J. L.; Anderson, J. L.; Maginn, E. J.; Brennecke, J. F. Anion effects on gas solubility in ionic liquids. *J. Phys. Chem. B* **2005**, *109*, 6366, *doi:10.1021/jp046404l*.

159. Buzzeo, M. C.; Evans, R. G.; Compton, R. G. Non-haloaluminate room-temperature ionic liquids in electrochemistry-A review. *Chemphyschem* **2004**, *5*, 1106, *doi:10.1002/cphc.200301017*.

160. Knipping, E.; Aucher, C.; Guirado, G.; Aubouy, L. Room Temperature Ionic Liquids versus organic solvents as lithium-oxygen battery electrolytes. *New J. Chem.* **2018**, *42*, 4693, *doi:10.1039/C8NJ00449H*.

161. Knipping, E.; Aucher, C.; Guirado, G.; Fauth, F. F.; Aubouy, L. In operando X-ray diffraction of lithium-oxygen battery using ionic liquid as electrolyte co-solvent. *New J. Chem.* **2017**, *41*, 7267, *doi:10.1039/c7nj01027c*.

162. Brousse, T.; Taberna, P.-L.; Crosnier, O.; Dugas, R.; Guillemet, P.; Scudeller, Y.; Zhou, Y.; Favier, F.; Bélanger, D.; Simon, P. Long-term cycling behavior of asymmetric activated carbon/MnO2 aqueous electrochemical supercapacitor. *J. Power Sources* **2007**, *173*, 633, *doi:10.1016/j.jpowsour.2007.04.074*.

163. Zeng, J.; Nair, J. R.; Francia, C.; Bodoardo, S.; Penazzi, N. Aprotic Li–O2 cells: Gas diffusion layer (GDL) as catalyst free cathode and tetraglyme/LiClO4 as electrolyte. *Solid State Ionics* **2014**, *262*, 160, *doi:10.1016/j.ssi.2013.09.032*.

164. Ramis, G.; Busca, G.; Lorenzelli, V. Low-temperature CO2 adsorption on metal oxides: spectroscopic characterization of some weakly adsorbed species. *Mater. Chem. Phys.* **1991**, *29*, 425, *doi:10.1016/0254-0584(91)90037-U*.

165. Lassègues, J.-C.; Grondin, J.; Aupetit, C.; Johansson, P. Spectroscopic Identification of the Lithium Ion Transporting Species in LiTFSI-Doped Ionic Liquids. *J. Phys. Chem. A* **2009**, *113*, 305, *doi: 10.1021/jp806124w*.

166. Fauth, F.; Boer, R.; Gil-Ortiz, F.; Popescu, C.; Vallcorba, O.; Peral, I.; Fullà, D.; Benach, J.; Juanhuix, J. The crystallography stations at the Alba synchrotron. *Eur. Phys. J. Plus* **2015**, *130*, 160, *doi:10.1140/epjp/i2015-15160-y*.

167. Bonhôte, P.; Dias, A.-P.; Papageorgiou, N.; Kalyanasundaram, K.; Grätzel, M. Hydrophobic, Highly Conductive Ambient-Temperature Molten Salts †. *Inorg. Chem.* **1996**, *35*, 1168, *doi:10.1021/ic951325x*.

168. Hu, Y.-F.; Liu, Z.-C.; Xu, C.-M.; Zhang, X.-M. The molecular characteristics dominating the solubility of gases in ionic liquids. *Chem. Soc. Rev.* **2011**, *40*, 3802, *doi:10.1039/c0cs00006j*.

169. Monaco, S.; Arangio, A. M.; Soavi, F.; Mastragostino, M.; Paillard, E.; Passerini, S. An electrochemical study of oxygen reduction in pyrrolidinium-based ionic liquids for lithium/oxygen batteries. *Electrochim. Acta* **2012**, *83*, 94, *doi:10.1016/j.electacta.2012.08.001*.

170. Hayyan, M.; Mjalli, F. S.; Hashim, M. A.; Alnashef, I. M. An investigation of the reaction between 1-butyl-3-methylimidazolium trifluoromethanesulfonate and superoxide ion. *J. Mol. Liq.* **2013**, *181*, 44, *doi:10.1016/j.molliq.2013.02.001*.

171. Tan, P.; Jiang, H. R.; Zhu, X. B.; An, L.; Jung, C. Y.; Wu, M. C.; Shi, L.; Shyy, W.; Zhao, T. S. Advances and challenges in lithium-air batteries. *Appl. Energy* **2017**, *204*, 780, *doi:10.1016/j.apenergy.2017.07.054*.

172. Imanishi, N.; Luntz, A. C.; Bruce, P. G. *The Lithium Air Battery: Fundamentals*; Springer.; New York, 2014; ISBN 9781489980618.

Appendices

Appendix I

Published articles validated to present the thesis as a compendium of publications.

"Room Temperature Ionic Liquids versus organic solvents as lithium-oxygen battery electrolytes"

E. Knipping, C. Aucher, G. Guirado, L. Aubouy

New Journal of Chemistry **42** (2018) 4693–4699 (doi:10.1039/C8NJ00449H)

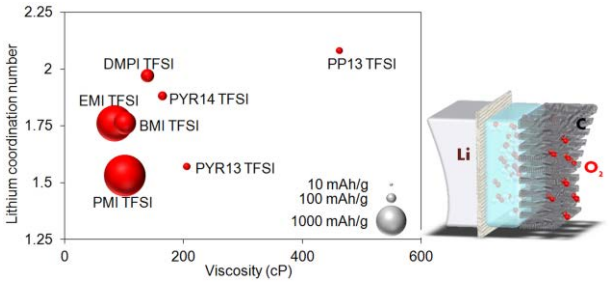

NJC

PAPER

View Article Online
View Journal | View Issue

Cite this: *New J. Chem.*, 2018, 42, 4693

Room temperature ionic liquids *versus* organic solvents as lithium–oxygen battery electrolytes

E. Knipping,*[ab] C. Aucher,[a] G. Guirado[b] and L. Aubouy[a]

Received 25th January 2018,
Accepted 11th February 2018

DOI: 10.1039/c8nj00449h

rsc.li/njc

Imidazolium, pyrrolidinium and piperidinium room temperature ionic liquids (RTILs) are characterized to evaluate their thermal stability, ionic conductivity, viscosity, potential window and lithium solvation, which are key parameters for lithium–oxygen ($Li–O_2$) battery electrolytes. The electrochemical tests of these RTILs are also carried out in $Li–O_2$ cells and show reasonable values of specific capacity, up to 1659 mA h per gram of carbon in the case of 1-propyl-3-methylimidazolium bis(trifluoromethylsulfonyl)imide (PMI TFSI) with a molar fraction of 0.2 of LiTFSI. RTILs are compared with conventional organic electrolytes like ethylene carbonate (EC)/diethyl carbonate (DEC) solution or tetraethylene glycol dimethyl ether (TEGDME), which enables us to provide a further insight into ways of improving the electrolyte properties of $Li–O_2$ batteries. In particular, a viscosity lower than 100 cP combined with a lithium coordination number lower than 1.5 tends to enhance the battery performance.

Introduction

$Li–O_2$ batteries have received much interest in the last few years as global energy demand is growing and availability of fossil energies becomes limited. At present, Li-ion batteries are limited to 250–300 W h kg^{-1} at the cell level whereas the new approach of $Li–O_2$ batteries offers a theoretical specific energy superior to 1000 W h kg^{-1}.[1,1–5] This value is comparable to the actual internal combustion engine technology (ICE). Moreover, the population growth and the European policy that targets to reduce the CO_2 emissions by 40% by 2030[6] pushes to transportation electrification. From this context and regarding the potential of this new technology, the main application for $Li–O_2$ batteries is electric vehicles (EVs), with the possibility in the next few years to develop an electric car with the same distance range as a gasoline powered car but cheaper and more environmentally friendly. However, this new technology will remain a research topic for at least the next 20 following years, due to the low cyclability, the limited electrical efficiency, the low rate capability and the difficulty of assembling a safe practical cell working in an ambient atmosphere better than on the laboratory scale under well-controlled conditions. Indeed, since the battery reaction is not fully reversible, the capacity drastically decreases after 20 cycles in most cases.[7] The main cause of this irreversibility is the formation of Li_xO_y ($x, y = 1, 2$) discharge products, since they are insoluble in the electrolyte and lead to the degradation of the battery components.[8] In particular, the cathode's pores hosting the reaction between the lithium ions and the oxygen become obstructed[3] and besides, the anodic lithium, which is a very reactive metal, forms a hydroxide layer preventing the diffusion of lithium ions.[7]

One of the biggest challenges to progress in $Li–O_2$ batteries is the development of an electrolyte that requires the following characteristics: (i) compatibility with the anode, (ii) low volatility to avoid the evaporation of the solvent in open cell systems, (iii) high oxygen solubility and diffusivity, (iv) a low viscosity to ensure fast kinetics of mass transport and a high ionic conductivity and (v) a wide electrochemical stability window.[9] Usual carbonate solvents, such as ethylene carbonate (EC), propylene carbonate (PC) and diethyl carbonate (DEC) from the lithium-ion technology, would be good candidates with their stability at high potentials, their ability to form a stable solid electrolyte interphase (SEI) on lithium and their high polarity that enables transporting lithium cations effectively. The main drawback associated with those solvents is their reactivity towards a nucleophilic attack of the superoxide ($O_2^{-\bullet}$) coming from the ORR.[10,11] Then the decomposition of the carbonate, forming mostly lithium carbonate, will result in the passivation of the cathode and a very poor cycle life of the batteries.[10,12] On the other hand, ether solvents are more stable to the superoxide and the discharge products and show the advantages of cathodic stability and low volatility.[13] Both 1,2-dimethoxyethane (DME) and tetraethylene glycol dimethyl ether (TEGDME) are the most-used ether solvents as they form the most of Li_2O_2 during discharge and evolved the most oxygen during charge.[14] However, the degradation of these electrolytes has been observed with the formation of side

[a] *Leitat Technological Center, Carrer de la Innovació, 2 08225 Terrassa, Spain. E-mail: eknipping@leitat.org*
[b] *Departament de Química, Universitat Autònoma de Barcelona, E-08193 Bellaterra, Barcelona, Spain*

products like acetates, formates and carbonates,[10] which makes them unsuitable for a practical commercial battery.

Recently, Room Temperature Ionic Liquids (RTILs) attracted much attention. 1,3-Dialkylimidazolium bis(trifluoromethylsulfonyl)imide ionic liquids are known for their thermal and electrochemical stability and high conductivity.[15] Ammonium and phosphonium cations with long alkyl chains showed a large cathodic potential window and high oxygen solubility.[16] Pyrrolidinium ionic liquids exhibited a reasonable ionic conductivity (>1 mS cm^{-1}) and a cathodic stability limit exceeding the lithium plating/stripping potential.[17] Hence, the high thermal stability, non-flammability, low vapour pressure and a wide potential window of RTILs can offer an interesting alternative to the traditional organic solvents for Li–O_2 battery electrolytes.[12,18–22] Nakamoto *et al.*[11] showed the advantage of the RTIL stability against electrochemical oxidation *vs.* Li^+/Li and O_2 redox reversibility. Cai *et al.*[23] proved that ionic liquids could show a higher specific capacity compared to a carbonate solvent electrolyte and Cechetto *et al.*[24] observed a decrease of 0.4 V of the overpotential by mixing ionic liquids with an ether-based electrolyte.

In this paper, we report on the study of the properties of several organic and ionic liquid-based electrolytes and their performance in Li–O_2 battery cells. The main chemical and physical properties of 9 different electrolytes are characterized before testing them in Li–O_2 battery cells in order to compare their electrochemical performance with respect to the electrolyte intrinsic properties. Both glyme and carbonate-based organic solvents used in lithium batteries are also studied and compared with the most performing RTILs for the Li–O_2 battery technology.

Experimental

Sample preparation

All ionic liquids, 99% pure, were purchased from IoLiTec (Ionic Liquids Technologies GmbH). The molecular structure of the RTIL ions studied is shown in Fig. 1. TEGDME, EC and DEC were purchased from Sigma Aldrich with purity higher than 99% as well as the salts of lithium bis(trifluoromethanesulphonyl)imide (LiTFSI – 99.95%) and lithium hexafluorophosphate ($LiPF_6$ – 99.99%). Nine electrolytes are prepared by direct mixing of an appropriate amount of salt with either a RTIL or a solvent to reach the molar fraction of $x = 0.2$. The water content of all samples is measured using Karl Fischer (Coulometer KF 831) titration, before and after drying the electrolyte with 4 Å molecular sieves (Aldrich) for two days and stored in an argon filled glove box (H_2O < 1 ppm, O_2 < 1 ppm). To exclude the influence of water contamination in the electrolyte, which could affect its stability and the cyclability of the batteries,[23] the water content of the ionic liquids is lowered until it reaches values between 43 and 322 ppm (Table 1). The same range as for the organic solvents is then obtained.

Ionic conductivity, viscosity, thermal stability

The ionic conductivity is measured with a titanium tip (Ref. 50 and 73) on an EC Meter Basic 30+ conductimeter (Crison Instrument) in a range of temperature from −10 °C to 80 °C. The viscosities are measured using a Malvern Bohlin CVO 100-901 rheometer in air, at room temperature. Shear rates are varied between 0.1 s^{-1} and 10 s^{-1}. No shear thinning behavior due to the variation of the shear rate is observed. Hence, the viscosities are determined from the plateau value at all shear rates. Thermo gravimetric analysis is done using a TA Instrument Q500 apparatus, applying a ramp of 10 °C min^{-1} until 800 °C in O_2 and N_2 atmospheres.

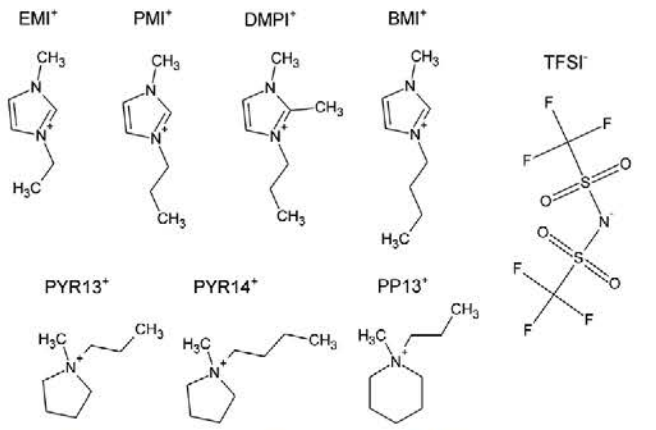

Fig. 1 Molecular structure of the RTIL ions used. EMI: 1-ethyl-3-methylimidazolium; PMI: 1-methyl-3-propylimidazolium; DMPI: 1,2-dimethyl-3-propylimidazolium; BMI: 1-butyl-3-methylimidazolium; PYR13: 1-methyl-1-propylpyrrolidinium; PYR14: 1-butyl-1-methylpyrrolidinium; PP13: 1-methyl-1-propylpiperidinium; TFSI: bis(trifluoromethylsulfonyl)imide.

Raman spectroscopy

The Raman spectra are recorded using a Bruker RFS/100 FT-Raman spectrometer with a Nd–YAG laser (wavelength of 1064 nm). The collected spectra are the average of 512 scans at an optical resolution of 2 cm^{-1}. The samples are sealed in glass ampoules under argon and measured at room temperature. For a detailed analysis of the region 730–770 cm^{-1}, the RTIL spectra are fit with the multipeak fitting package in IGOR PRO 6.37 using a Voigt function with a fixed Lorentzian/Gaussian ratio, following the procedure of Lassègues *et al.*[25] The lithium coordination numbers are calculated for each RTIL electrolyte from the deconvoluted spectra, dividing the area of the band corresponding to Li^+ coordinated anions with the total band area (including also the contributions from "free" anions) and the molar fraction of Li salt x.

Electrochemical characterization

The electrochemical stability window of the electrolytes is determined with linear sweep voltammetry measured on a 3 mm-diameter platinum working electrode with a lithium metal counter and reference electrodes at a scanning rate of 1 mV s^{-1}. The potential is scanned from the open circuit voltage toward positive and negative potentials to evaluate the anodic and cathodic limit respectively.

Li–O_2 batteries are assembled inside an Ar-filled glove box using an ECC-air cell (EL-Cell). The cathode for the Li–O_2

Table 1 Composition, degradation temperature, H_2O content, ionic conductivity, potential window and Li coordination number of the studied electrolytes

Solvent/RTIL	Salt (x = 0.2)	Degradation temperature (°C) Under N_2	Under O_2	H_2O content (ppm) Before drying	After drying	Ionic conductivity at 25 °C (mS cm^{-1})	Viscosity at 25 °C (cP)	Potential window (V *vs.* Li^+/Li)	Lithium coordination number
TEGDME	Li TFSI	118	115	851	156	1.79	14.2	[0.1; 4.9]	—
PMI TFSI	Li TFSI	411	406	1062	33.1	2.3	102	[1.1; 5.4]	1.53
EMI TFSI	Li TFSI	407	369	3800	46	3.22	85.2	[1.3; 5.4]	1.76
EC : DEC (2 : 1 vol)	Li PF_6	88	75	22	—	8.87	5.1	[0.0; 5.7]	—
BMI TFSI	Li TFSI	405	362	110	43	1.42	102	[1.3; 6.2]	1.76
DMPI TFSI	Li TFSI	480	448	249	204	0.54	140	[1.1; 6.0]	1.97
PYR14 TFSI	Li TFSI	421	380	92	54	0.39	165	[0.2; 6.8]	1.88
PP13 TFSI	Li TFSI	406	413	2108	126	0.4	463	[0.1; 6.9]	2.08
PYR13 TFSI	Li TFSI	414	407	2031	78	0.8	206	[0.3; 6.6]	1.57

battery is prepared from a mixture of 90 wt% PICAtif (PICA) and 10 wt% polyvinylidene fluoride (PVdF Kynar ADX 161, Arkema) in *N*-methyl-2-pyrrolidone (NMP, 99.5%, Sigma-Aldrich). PICAtif is an activated carbon with a mesoporous volume of 0.68 cm^3 g^{-1}, suitable for Li–O_2 battery cathodes.[8] A full description of this material is given by Brousse *et al.*[26] The slurry is tape casted on a Gas Diffusion Layer (GDL SIGRACET 24BC – SGL Company) using the doctor blade technique up to an active loading of 1.5 mg cm^{-2}. Although this GDL may participate in the overall capacity of the battery,[27] only the mass of PICA is taken into account to normalize the specific capacity calculated. A circular lithium chip (Ref: EQ-Lib-LiC25, MTI Corp.) is used as the anode. The separator is a glass fiber membrane (Whatman GF/A) soaked with the tested electrolyte. A thickness of 260 μm ensures that the electrolyte is in excess with at least 100 μL. Prior to applying any current, the cell is maintained under O_2 flow (8 mL min^{-1}) to stabilize the open circuit voltage after 10 hours. Galvanostatic tests are performed using a VMP3 biologic instrument with a current of 100 μA cm^{-2} applied between 2.15 V and 4.35 V with an oxygen flow rate of 8 mL min^{-1} for the full initial discharge measurement. For the cycling test, discharge and recharge curves are recorded at a constant specific current of 75 μA cm^{-2} within a limited capacity of 500 mA h g^{-1}.

Results and discussion

The properties of the 9 studied electrolytes, including 7 RTILs and 2 organic solvents, are gathered in Table 1. All the RTIL electrolyte formulations contain the same anion (TFSI) and a 0.2 molar fraction of LiTFSI. The use of TFSI guarantees the hydrophobic character of the electrolyte as well as a good electrochemical performance. The use of different anions would allow tuning the physico-chemical properties of the solvent, such as viscosity or conductivity. Two of the most common organic electrolyte formulations are also studied for comparison.

Thermal stability

TGA experiments show two different trends as a function of the electrolyte composition (Fig. 2). For organic electrolytes, such as EC : DEC (2 : 1)-LiPF_6 and TEGDME-LiTFSI, a weight loss is observed either as soon as the measurement begins in the case of EC/DEC-LiPF_6 or at about 150 °C in the case of TEGDME-LiTFSI,

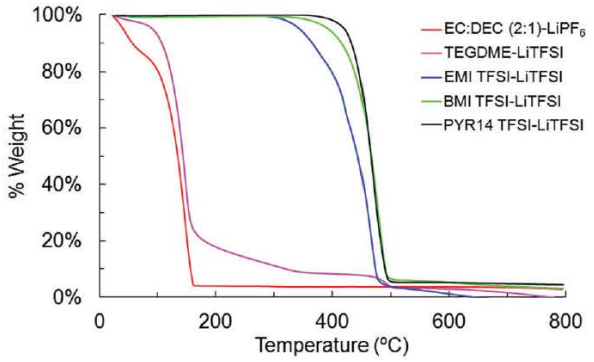

Fig. 2 TGA spectra of ionic liquids and organic electrolytes measured under a nitrogen atmosphere.

which corresponds to the EC/DEC or TEGDME evaporation.[28–30] However, when RTILs are used as electrolytes the degradation temperature, with or without salt, is considerably higher (between 350 and 450 °C). Hence, those TGA profiles indicate that RTILs can be safely used in a wider range of temperatures than the organic electrolytes, which may enable increasing the safety of current batteries using organic solvents.[31] This would be one of the major advantages of ionic liquids as battery electrolytes.

The influence of oxygen on the thermal stability of the electrolytes is also evaluated in order to be in conditions as similar as possible to the operating conditions of Li–O_2 technology. In the presence of oxygen the degradation temperature is obtained up to 20 °C lower with respect to the same test run under a nitrogen atmosphere (Table 1). Indeed, degradation reactions occur at lower temperature in a more oxidizing environment, which is why the actual temperature range of ionic liquid stability is lower than the one measured under inert conditions using TGA.[32] However, this slight decrease is not an issue considering the important gap between thermal stability of both RTILs and organic solvents.

Ionic conductivity

A higher ionic conductivity of the electrolyte enables reducing the resistance of the system, to lower the overpotential and then improving the reversibility of the system for a higher current density applied.[33] The dependence of the ionic conductivity of different electrolytes on the temperature is shown in Fig. 3.

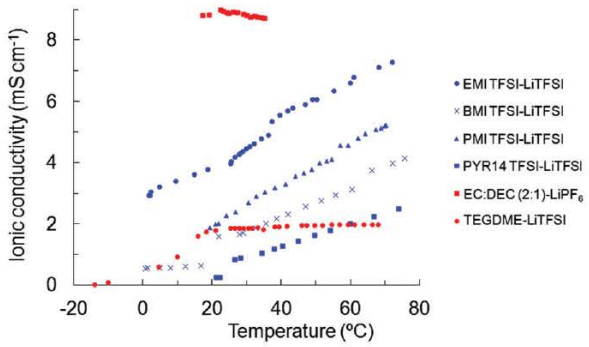

Fig. 3 Ionic conductivity *versus* temperature for different families of electrolytes: in blue the RTILs and in red the organic solvents.

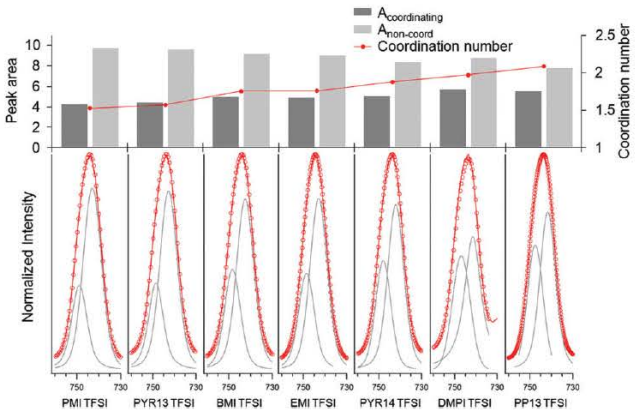

Fig. 4 Raman spectra of solutions containing LiTFSI (molar fraction 0.2) and RTILs in the range between 760 and 730 cm^{-1}. The red lines represent the measured data, the circles represent the fitted curve and the grey lines represent the two individual fitted peaks for coordinated and non-coordinated $[TFSI]^-$ anions.

Again two different behaviors are observed, for organic electrolytes the conductivity with the temperature reveals that TEGDME-LiTFSI reaches a maximum conductivity of 1.9 mS cm^{-1} from 25 to at least 70 °C, whereas the ionic liquids have an increasing conductivity with the temperature.

Focusing on ionic liquid electrolytes, it clearly appears that EMI TFSI-LiTFSI has the best ionic conductivity (from 3 to 7.5 mS cm^{-1} at temperature between 0 and 80 °C). Then, BMI TFSI-LiTFSI and PYR14 TFSI-LiTFSI are in the same range as TEGDME-LiTFSI with an ionic conductivity between 1 and 4 mS cm^{-1}. These results can be easily rationalized taking into account the viscosity of the different RTILs electrolytes depicted in Table 1. A low viscosity value of the RTIL solvent, which in fact is related to a larger asymmetry in the cation structure, helps the mobility of the charge carriers[34] leading to a higher conductivity value of the electrolyte. Finally, it is worthy of note that the electrolytes based on organic solvents follow the same general trend.

Lithium coordination

The ion–ion interactions taking place in the electrolytes studied are investigated using Raman spectroscopy. As reported by several authors,[25,35–37] in TFSI-based RTILs the coordination of the anion $[TFSI]^-$ can be evaluated considering the peak at a wavenumber of ≈742 cm^{-1}. Such a peak is associated with the anion expansion and contraction. In the presence of Li^+ cations, the $TFSI^-$ anions coordinating with Li^+ generate an additional signal, which is shifted to higher wavenumbers in the Raman spectra (Fig. 4). As shown, the areas $A_{coordinating}$ of this peak and $A_{non\text{-}coord}$ of the non-coordinating $TFSI^-$ peak are strongly dependent on the cation–anion interaction occurring in the RTIL. The comparison of both areas is used to determine the lithium coordination number of the electrolyte (Table 1 and Fig. 4). The stronger is the anion–cation interaction occurring in the RTIL, the lower is the lithium coordination number. Among the RTILs studied, the values vary between 1.53 for the PMI TFSI and 2.08 for the PP13 TFSI. These results are in line with previous works on BMI TFSI,[38] EMI TFSI,[37] PYR14 TFSI[35] and PYR13 TFSI[39] where coordination numbers close to two are obtained. This means that most of the lithium cations are involved in $[Li(TFSI)_2]^-$ clusters. However, it seems that for a LiTFSI molar fraction of 0.2 or higher, the coordination number decreases due to the formation of more complex ionic associations between Li^+ and $TFSI^-$.[38] Thus the values obtained increase in the following order PMI TFSI-LiTFSI < PYR13 TFSI-LiTFSI < BMI TFSI-LiTFSI < EMI TFSI-LiTFSI < PYR14 TFSI-LiTFSI < DMPI TFSI-LiTFSI < PP13 TFSI-LiTFSI. These results show that the cation chemistry such as the number of protons and the ring size has a strong influence on the lithium coordination number.[35,39,40] In particular, Kunze *et al.*[39] observed that the lithium coordination increases with increasing alkyl chain length of 1-alkyl-1-methyl-pyrrolidiniums. The same observation can be done here with PYR13 TFSI and PYR14 TFSI.

Electrochemical characterization

The different electrolytes are further investigated in aprotic Li–O_2 batteries (Fig. 5A), for which the full discharge capacity is measured. EC : DEC (2 : 1)-$LiPF_6$, typically used for Li-ion batteries, presents a reasonable capacity of 775 mA h g^{-1}. Concerning the RTILs with lithium salt, PP13 TFSI-LiTFSI, PYR13 TFSI-LiTFSI, PYR14 TFSI-LiTFSI and DMPI TFSI-LiTFSI have a specific capacity below 200 mA h g^{-1}. This may be due to their high viscosity, leading to poor kinetics of the battery reaction.[41] These electrolytes have actually the lowest ionic conductivity, which indicates that a minimum is required for the Li–O_2 battery to work. However, this parameter is not directly correlated with the capacity neither the cyclability of the battery.[42] TEGDME-LiTFSI shows clearly a higher capacity (4268 mA h g^{-1}) than other electrolytes but not the highest ionic conductivity (1.79 mS cm^{-1}). On the other hand, the viscosity of the electrolyte seems to be correlated with the capacity as TEGDME-LiTFSI (14.2 cP) has a much lower value than the RTILs (> 85 cP). Concerning PMI TFSI, EMI TFSI and BMI TFSI, they present a specific capacity of 559, 1408 and 1856 mA h g^{-1} respectively. Although EMI TFSI has the lowest viscosity (85.2 cP), it seems that the lower lithium coordination number of PMI TFSI (1.53 *vs.* 1.76 for the EMI TFSI) compensates the unfavorable transport properties of this RTIL. BMI TFSI has

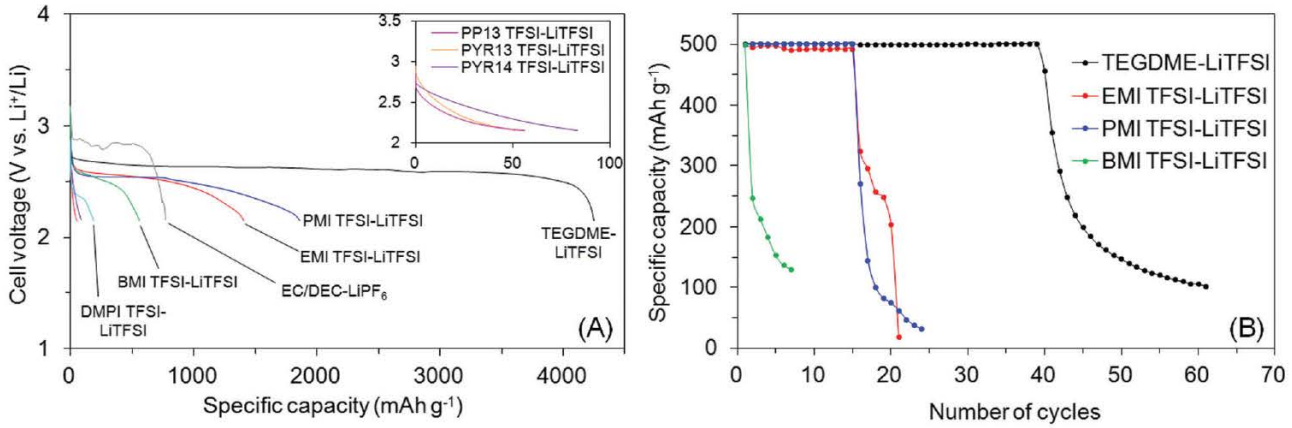

Fig. 5 (A) Initial discharge curve of Li–O_2 cells assembled with the different electrolytes studied, at a current of 100 μA cm^{-2}. (B) The Galvanostatic cycling test of Li–O_2 cells at a constant current of 75 μA cm^{-2}.

both a high viscosity and a high lithium coordination number, and has a lower specific capacity. Taking these results into account, the viscosity and the lithium solvation number are two determinant parameters influencing the mobility of the lithium cation and then the performance of the Li–O_2 battery.

The five electrolytes with the highest full capacity, *i.e.* TEGDME-LiTFSI, PMI TFSI-LiTFSI, EMI TFSI-LiTFSI, EC/DEC-$LiPF_6$ and BMI TFSI-LiTFSI, are then tested in Li–O_2 cells cycled with a controlled depth of discharge of 500 mA h g^{-1}. The discharge and charge curves are shown in Fig. 5B. Among these electrolytes, TEGDME-LiTFSI has the best cyclability with 40 cycles. On the other hand, EC/DEC-$LiPF_6$ shows no rechargeability. As has been shown previously,[43,44] the carbonate electrolytes are not stable to nucleophilic attack by the superoxide radical ($O_2^{-\bullet}$). Concerning the RTIL electrolytes, only 15 and 16 cycles are observed for PMI TFSI-LiTFSI and EMI TFSI-LiTFSI respectively. The degradation of the electrolyte, observed during the electrochemical window measurement (Fig. 6), may contribute to the consumption of solution components and the fast clogging of the cathode.

Indeed, observing the voltammetry curves shown in Fig. 6, all the imidazolium-based solutions, *i.e.* EMI TFSI-LiTFSI, PMI TFSI-LiTFSI, BMI TFSI-LiTFSI and DMPI TFSI-LiTFSI, present a reduction peak at 1.1–1.3 V *vs.* Li^+/Li. This peak, which may be related to the deprotonation of the cation,[45,46] corresponds to the cathodic stability of the imidazolium RTILs. As this reaction occurs before the lithium plating (*i.e.* at 0 V *vs.* Li^+/Li), there is degradation of the electrolyte during the cycling of the battery, explaining its low cyclability. The RTILs with non-aromatic cations such as PYR13 TFSI, PYR14 TFSI and PP13 TFSI, present a wider electrochemical stability window. The large reductive current observed around 0 V *vs.* Li^+/Li corresponds to the reductive deposition of lithium onto the electrode. At the anodic potentials, the RTILs with the lowest limits are EMI TFSI and PMI TFSI with 5.4 V *vs.* Li^+/Li, which can be attributed to the oxidative decomposition of the $TFSI^-$ anion. For both organic solvent electrolytes, the anodic currents starting at 4.9 V *vs.* Li^+/Li for TEGDME and 5.7 V *vs.* Li^+/Li for EC/DEC can be attributed to the oxidative decomposition of the electrolyte. In conclusion, RTILs have a wide potential window, up to 6.6 V in the case of PYR14 TFSI-LiTFSI. Their electrochemical stability is directly related to the oxidation and reduction potential values of the anions and cations respectively. That is why the medium is stable in the 2.15–4.35 V *vs.* Li^+/Li operating voltage window of the battery for all the electrolytes except for those containing imidazolium RTILs.

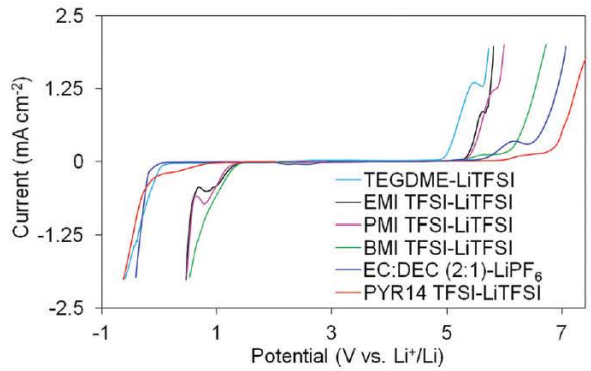

Fig. 6 Linear sweep voltammograms of ionic liquids and organic electrolytes measured under an argon atmosphere at 25 °C.

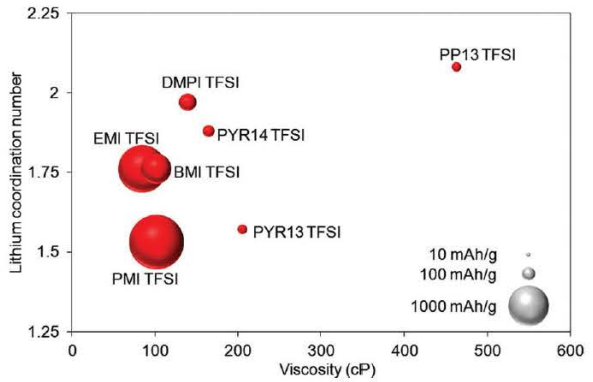

Fig. 7 Representation of the specific capacity as a function of the viscosity and lithium coordination number of the RTIL electrolyte.

To summarize, the selection of an adequate electrolyte for a Li–O_2 battery depends especially on the viscosity and the lithium coordination number of the solution. The viscosity has a direct influence on the kinetics of the battery reaction whereas the solvation of the lithium cation in the electrolyte may have an effect on its thermodynamics. As represented in Fig. 7, the highest capacities are situated at the low viscosity values. Then, for the electrolytes for which the viscosities are in the same range, a low lithium coordination number indicates a higher capacity. Nonetheless, the electrolyte has to be stable in the battery operating voltages, which is why the electrochemical stability window is a determinant parameter too.

Conclusions

The properties of different electrolytes based on organic solvents and RTILs were studied and tested in Li–O_2 batteries. The main advantage of ionic liquids over organic solvents is their high thermal stability, with a degradation temperature of up to 480 °C in N_2, whereas organic solvents evaporate completely above 150 °C. The ionic conductivity increases constantly with temperature, reaching almost 8 mS cm^{-1} for EMI TFSI at 70 °C, which gives them interesting potential for application at medium and high temperatures.[47–49] At room temperature, most of the ionic liquids are in the same range as organic solvents with 3.33 mS cm^{-1} for EMI TFSI-LiTFSI. This value is equivalent to that of TEGDME-LiTFSI, which is widely used for Li–O_2 batteries. The ionic liquids with an ionic conductivity below 1 mS cm^{-1} show a very low specific capacity, below 200 mA h g^{-1}. There is then a minimum needed but other parameters such as the viscosity and the lithium solvation number are more critical for the battery capacity. Indeed, the highest specific capacity is obtained with TEGDME-LiTFSI (1.79 mS cm^{-1}) with 4268 mA h per gram of carbon from the cathode for a full discharge. Imidazolium RTILs (EMI, PMI, BMI and DMPI) show capacities up to 1659 mA h g^{-1}, higher than pyrrolidinium and piperidinium, which are attributed to a lower viscosity. However, the degradation of the imidazolium cation leads to low cyclability of the Li–O_2 cells.

Conflicts of interest

There are no conflicts to declare.

Acknowledgements

The STABLE project has received funding from the European Union's FP7 research and innovation program under grant agreement No. 314508. The authors thank Mr Jerónimo Juan Juan from the University of Alicante (Spain) for the Raman measurements. G. G. thanks financial support from project CTQ2015-65439-R from the MINECO.

References

1 K. M. Abraham and Z. Jiang, *J. Electrochem. Soc.*, 1996, **143**, 1–5.
2 P. G. Bruce, S. A. Freunberger, L. J. Hardwick and J.-M. Tarascon, *Nat. Mater.*, 2012, **11**, 19–29.
3 J. Christensen, P. Albertus, R. S. Sanchez-Carrera, T. Lohmann, B. Kozinsky, R. Liedtke, J. Ahmed and A. Kojic, *J. Electrochem. Soc.*, 2012, **159**, R1.
4 G. Girishkumar, B. D. McCloskey, A. C. Luntz, S. Swanson and W. Wilcke, *J. Phys. Chem. Lett.*, 2010, **1**, 2193–2203.
5 R. Padbury and X. Zhang, *J. Power Sources*, 2011, **196**, 4436–4444.
6 E. Commission and C. Action, https://ec.europa.eu/clima/policies/international/negotiations/paris_en, accessed 04-04-2017, 2015, Climate Action.
7 J.-L. Shui, J. S. Okasinski, P. Kenesei, H. A. Dobbs, D. Zhao, J. D. Almer and D.-J. Liu, *Nat. Commun.*, 2013, **4**, 2255.
8 J. Hou, M. Yang, M. W. Ellis, R. B. Moore and B. Yi, *Phys. Chem. Chem. Phys.*, 2012, **14**, 13487–13501.
9 S. Das, J. Højberg, K. B. Knudsen, R. Younesi, P. Johansson, P. Norby and T. Vegge, *J. Phys. Chem. C*, 2015, **119**, 18084–18090.
10 D. Sharon, D. Hirshberg, M. Afri, A. Garsuch, A. A. Frimer and D. Aurbach, *Isr. J. Chem.*, 2015, **55**, 508–520.
11 H. Nakamoto, Y. Suzuki, T. Shiotsuki, F. Mizuno, S. Higashi, K. Takechi, T. Asaoka, H. Nishikoori and H. Iba, *J. Power Sources*, 2013, **243**, 19–23.
12 J. Zeng, J. R. Nair, C. Francia, S. Bodoardo and N. Penazzi, *Int. J. Electrochem. Sci.*, 2013, **8**, 3912–3927.
13 C. O. Laoire, S. Mukerjee, K. M. Abraham, E. J. Plichta and M. A. Hendrickson, *J. Phys. Chem. C*, 2010, **114**, 9178–9186.
14 A. C. Luntz and B. D. Mccloskey, *Chem. Rev.*, 2014, **114**, 11721–11750.
15 P. Bonhôte, A. Dias, N. Papageorgiou, K. Kalyanasundaram, M. Grätzel, P. Bonho, A. Dias, N. Papageorgiou, K. Kalyanasundaram, M. Gra, P. Bonhôte, A. Dias, M. Armand, N. Papageorgiou, K. Kalyanasundaram, M. Grätzel, P. Bonho, A. Dias, N. Papageorgiou, K. Kalyanasundaram, M. Gra, P. Bonhôte, A. Dias, N. Papageorgiou, K. Kalyanasundaram and M. Grätzel, *Inorg. Chem.*, 1996, **35**, 1168–1178.
16 M. C. Buzzeo, O. V. Klymenko, J. D. Wadhawan, C. Hardacre, K. R. Seddon and R. G. Compton, *J. Phys. Chem. A*, 2003, **107**, 8872–8878.
17 G. B. Appetecchi, M. Montanino, A. Balducci, S. F. Lux, M. Winterb and S. Passerini, *J. Power Sources*, 2009, **192**, 599–605.
18 C. J. Allen, J. Hwang, R. Kautz, S. Mukerjee, E. J. Plichta, M. A. Hendrickson and K. M. Abraham, *J. Phys. Chem. C*, 2012, **116**, 20755–20764.
19 D. Bresser, E. Paillard and S. Passerini, *J. Electrochem. Sci. Technol.*, 2014, **5**, 37–44.
20 S. Ferrari, E. Quartarone, C. Tomasi, M. Bini, P. Galinetto, M. Fagnoni and P. Mustarelli, *J. Electrochem. Soc.*, 2014, **162**, A3001–A3006.
21 S.-M. Han, J.-H. Kim and D.-W. Kim, *J. Electrochem. Soc.*, 2015, **162**, A3103–A3109.

22 J. Kim, E. Ahn and Y. Tak, *Int. J. Electrochem. Sci.*, 2015, **10**, 2921–2930.
23 K. Cai, H. Jiang and W. Pu, *Int. J. Electrochem. Sci.*, 2014, **9**, 390–397.
24 L. Cecchetto, M. Salomon, B. Scrosati and F. Croce, *J. Power Sources*, 2012, **213**, 233–238.
25 J.-C. Lassègues, J. Grondin, C. Aupetit and P. Johansson, *J. Phys. Chem. A*, 2009, **113**, 305–314.
26 T. Brousse, P.-L. Taberna, O. Crosnier, R. Dugas, P. Guillemet, Y. Scudeller, Y. Zhou, F. Favier, D. Bélanger and P. Simon, *J. Power Sources*, 2007, **173**, 633–641.
27 J. Zeng, J. R. Nair, C. Francia, S. Bodoardo and N. Penazzi, *Solid State Ionics*, 2014, **262**, 160–164.
28 D. J. Lee, J. Hassoun, S. Panero, Y. K. Sun and B. Scrosati, *Electrochem. Commun.*, 2012, **14**, 43–46.
29 D.-J. Lee, J.-W. Park, I. Hasa, Y.-K. Sun, B. Scrosati and J. Hassoun, *J. Mater. Chem. A*, 2013, **1**, 5256.
30 J. H. Shin and E. J. Cairns, *J. Electrochem. Soc.*, 2008, **155**, A368.
31 B. Garcia, S. Lavallée, G. Perron, C. Michot and M. Armand, *Electrochim. Acta*, 2004, **49**, 4583–4588.
32 T. J. Wooster, K. M. Johanson, K. J. Fraser, D. R. MacFarlane and J. L. Scott, *Green Chem.*, 2006, **8**, 691.
33 D. Capsoni, M. Bini, S. Ferrari, E. Quartarone and P. Mustarelli, *J. Power Sources*, 2012, **220**, 253–263.
34 Y. Litaiem and M. Dhahbi, *J. Mol. Liq.*, 2012, **169**, 54–62.
35 T. Vogl, P. Goodrich, J. Jacquemin, S. Passerini and A. Balducci, *J. Phys. Chem. C*, 2016, **120**, 8525–8533.
36 S. Menne, T. Vogl and A. Balducci, *Phys. Chem. Chem. Phys.*, 2014, **16**, 5485.
37 M. Kerner, N. Plylahan, J. Scheers and P. Johansson, *Phys. Chem. Chem. Phys.*, 2015, **17**, 19569–19581.
38 S. Duluard, J. Grondin, J.-L. Bruneel, I. Pianet, A. Grélard, G. Campet, M.-H. Delville and J.-C. Lassègues, *J. Raman Spectrosc.*, 2008, **39**, 627–632.
39 M. Kunze, S. Jeong, E. Paillard, M. Schönhoff, M. Winter and S. Passerini, *Adv. Energy Mater.*, 2011, **1**, 274–281.
40 P. Ray, T. Vogl, A. Balducci and B. Kirchner, *J. Phys. Chem. B*, 2017, **121**, 5279–5292.
41 C. O. Laoire, S. Mukerjee, K. M. Abraham, E. J. Plichta and M. A. Hendrickson, *J. Phys. Chem. C*, 2009, **113**, 20127–20134.
42 G. A. Giffin, A. Moretti, S. Jeong and S. Passerini, *J. Power Sources*, 2017, **342**, 335–341.
43 F. Mizuno, S. Nakanishi, Y. Kotani, S. Yokoishi and H. Iba, *Electrochem. Commun.*, 2010, **78**, 403–405.
44 B. D. McCloskey, D. S. Bethune, R. M. Shelby, G. Girishkumar and A. C. Luntz, *J. Phys. Chem. Lett.*, 2011, **2**, 1161–1166.
45 J. Dupont and P. A. Suarez, *Phys. Chem. Chem. Phys.*, 2006, **8**, 2441–2452.
46 P. A. Z. Suarez, C. S. Consorti, R. F. De Souza, J. Dupont and R. S. Gonçalves, *J. Braz. Chem. Soc.*, 2002, **13**, 106–109.
47 R. Lin, P.-L. Taberna, S. Fantini, V. Presser, C. R. Pérez, F. Malbosc, N. L. Rupesinghe, K. B. K. Teo, Y. Gogotsi and P. Simon, *J. Phys. Chem. Lett.*, 2011, **2**, 2396–2401.
48 N. Plylahan, M. Kerner, D. H. Lim, A. Matic and P. Johansson, *Electrochim. Acta*, 2016, **216**, 24–34.
49 A. Balducci, R. Dugas, P. L. Taberna, P. Simon, D. Plée, M. Mastragostino and S. Passerini, *J. Power Sources*, 2007, **165**, 922–927.

"In operando X-ray diffraction of lithium-oxygen battery using ionic liquid as electrolyte co-solvent"

E. Knipping, C. Aucher, G. Guirado, F.F. Fauth, L. Aubouy

New Journal of Chemistry **41** (2017) 7267–7272 (doi:10.1039/c7nj01027c)

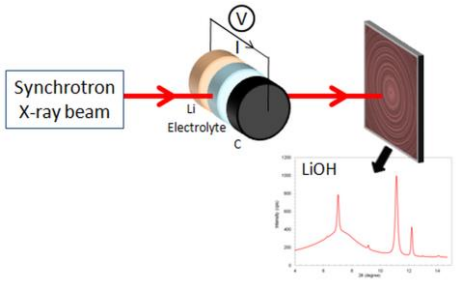

NJC

PAPER

View Article Online
View Journal | View Issue

Cite this: *New J. Chem.*, 2017, 41, 7267

In operando X-ray diffraction of lithium–oxygen batteries using an ionic liquid as an electrolyte co-solvent

E. Knipping, *[ab] C. Aucher,[a] G. Guirado,[b] F. Fauth[c] and L. Aubouy[a]

Received 28th March 2017,
Accepted 13th June 2017

DOI: 10.1039/c7nj01027c

rsc.li/njc

A real-time synchrotron X-ray diffraction technique is applied to study the oxidation/reduction of lithium oxide derivatives in an operating lithium–air battery cell containing a Room Temperature Ionic Liquid (RTIL) in its electrolyte. Four different electrolytes are tested, composed of dimethylsulfoxide (DMSO), a RTIL and lithium perchlorate salt ($LiClO_4$). This study proves that lithium as an anode material reacts with the RTIL, forming lithium hydroxide (LiOH) spontaneously, independently of the cycling stage. Comparisons between different electrolytes provide insights for future investigation of the improvement of electrolyte design of this technology.

Introduction

$Li–O_2$ batteries have received much interest in the last few years, as their theoretical capacity reaches 5–10 times the current Li-ion battery capacity.[1] The main electrochemical process in an aprotic $Li–O_2$ battery is the formation and decomposition of Li_2O_2, during discharge and recharge, respectively. However, this reaction suffers from low reversibility leading to a low cyclability of the battery. Recently, Room Temperature Ionic Liquids (RTILs) attracted much attention for $Li–O_2$ battery electrolytes.[2–9] Namely, Nakamoto *et al.*[10] demonstrated the advantage of the stability of RTILs against electrochemical oxidation *vs.* Li^+/Li and O_2 redox reversibility. Cai *et al.*[11] proved that ionic liquid electrolytes could show higher specific capacity compared to carbonate solvent electrolytes. Moreover, Cechetto *et al.*[12] observed a decrease of 0.4 V of the overpotential by mixing ionic liquids with an ether-based electrolyte. This could be explained by a higher ionic conductivity of the electrolyte containing an ionic liquid, a less insulating Li_2O_2 particle interface and a better Li_2O_2 solubility resulting in improved kinetics of Li_2O_2 oxidation. However, the authors presented the difficulty in characterizing, using electrochemical impedance spectroscopy, the thin solid films at the cathode/air/electrolyte interface. Further investigation is needed for a deeper understanding of the reactions occurring.

In situ studies of $Li–O_2$ batteries have been proposed by several groups,[13–18] in order to improve the understanding of the electrochemical process of the discharge/recharge cycle and its relationship with the structural transformations of electrode materials. The real-time acquisition of Li_2O_2 X-Ray Diffraction (XRD) patterns allowed Lim *et al.*[13] to estimate the rates of formation and decomposition of this discharge product during cycling. Shui and coworkers[17] accurately mapped the temporal and spatial distribution of Li_2O_2 at different cathode depths and discharge capacities in an operating battery. Nevertheless, all of these *in situ* studies were effectuated with $Li–O_2$ batteries using organic solvents, generally ethers. The measurements are not yet presented, either in pure ionic liquids or with an electrolyte containing a RTIL. Pure RTIL electrolytes were tested in previous experiments, although an adequate reversibility of the $Li–O_2$ battery reaction is not attainable probably due to their high viscosity that affects the ion diffusion and the kinetics of the battery reaction.[19] Moreover, poor battery capacity[10,20] and cyclability lower than 30 cycles are generally obtained.[9,11] Our most significant $Li–O_2$ battery performance ensues from the optimized blended electrolyte based on imidazolium RTILs. A decrease of 0.5 V of the overpotential and a cycling life of 80 cycles are reached *versus* 50 cycles for a tetraethylene glycol dimethyl ether electrolyte. The initial conjecture was that a better reversibility is obtained by using a blended electrolyte containing a RTIL. Thence, to explain the aforementioned observed improvement, an *in situ* synchrotron X-ray diffraction study of a $Li–O_2$ battery using such an electrolyte is proposed. This study aims to provide a fruitful insight into the chemical species involved in the electrochemical process of the battery, which is essential towards the identification process of the issues that impede the attainment of high performance. In this scope, another objective is to analyse the influence of the chemical compounds of the electrolyte on the battery behavior.

[a] *Leitat Technological Center, Carrer de la Innovació, 2 08225 Terrassa, Spain. E-mail: eknipping@leitat.org*
[b] *Departament de Química, Universitat Autònoma de Barcelona, E-08193 Bellaterra, Barcelona, Spain*
[c] *CELLS – ALBA Synchrotron, E-08290 Cerdanyola del Vallès, Barcelona, Spain*

A real-time synchrotron X-ray diffraction technique is applied to examine the oxidation/reduction of lithium oxide derivatives in an operating Li–O_2 battery cell containing a RTIL in its electrolyte. Four different electrolytes are tested, one without RTIL and the others composed of DMSO, a RTIL and lithium perchlorate salt ($LiClO_4$). The three RTILs tested are 1-ethyl-3-methylimidazolium bis(trifluoromethylsulfonyl)imide (EMIM TFSI), 1-methyl-3-propyl-imidazolium bis(trifluoromethylsulfonyl)imide (PMIM TFSI) and 1-butyl-3-methylimidazolium bis(trifluoromethylsulfonyl)imide (BMIM TFSI). In the following sections the experimental setup is described, followed by the presentation of the empirical results and their assessment.

Experimental

Li–O_2 batteries are assembled in an Ar-filled glove box by sandwiching a 200 μm-thick carbon-coated Gas Diffusion Layer cathode (GDL Sigracet 24BA from SGL Group), a 260 μm-thick glass fiber separator (Whatman GF/A) soaked with the studied electrolyte and a 250 μm-thick Li foil (MTI Corp.) in a polyimide tube (diameter: 3 mm) as shown in Fig. 1A and B. The electrolyte is in excess in the cell to compensate for degradation by parasitic reactions. The cathode current collector is a stainless steel tube filled with pure O_2 and a stainless steel rod was used at the anode side. Both the rod and tube fit exactly in the polyimide tube, although a Teflon tape was used to wrap the junctions for a better impermeability. The chemical aging has been carried out as well as electrochemical studies with the following setup. The discharge/recharge cycling of the cell is controlled using a VSP potentiostat (Bio-Logic) under a current density of 20 mA g^{-1} between 2.15 and 4.35 V *vs.* Li^+/Li as a cut-off voltage for discharge and recharge, respectively, with a discharge/recharge cycle duration of 5 h each, while registering diffraction scans continuously every minute. *Operando* micro-diffraction measurements are performed at the synchrotron MSPD beamline,[21] using transmission geometry with the beam going through the battery cell from its side. A set of several XRD data points at different cathode layer depths is collected by moving the battery for every selected state-of-charge. As the cathode–electrolyte–anode stack has a thickness of 760 μm, the number of scans per set is 8 data points taken along the cell's stack from the anode to the cathode. To achieve such data points, the measurements are performed on the HP/MD station of the BL04_MSPD beamline able to deliver a 15 × 15 μm FWHM beam size matching the size of the probed sample. The operating energy selected is 23.22 keV (Rh K-edge, the choice of a specific absorption edge is for calibration purpose). The corresponding wavelength is long enough to minimize Bragg peak overlap and has interesting peaks in the optimum detector range (2θ angle between 6 and 14 degrees). Data are collected using a 2D Rayonix CCD detector positioned within a distance range of 200–300 mm. A suitable support is built to mount in the horizontal position the electrochemical cell on the HP/MD stages in compliance with the beamline staff (Fig. 1C). Four different electrolytes (DMSO, DET, DPT and DBT) are tested, (Table 1). The morphology of the cathodes was examined using a scanning electron microscope (SEM, JEOL JSM-6010LV).

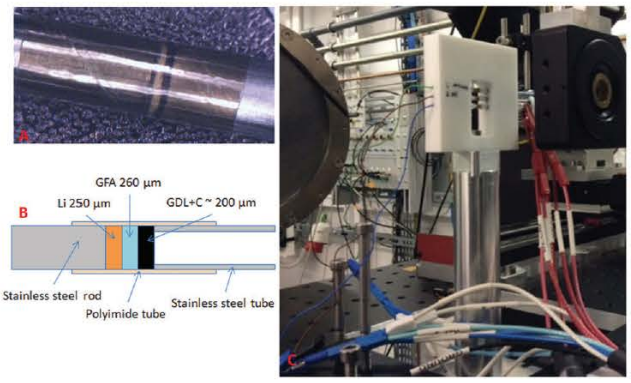

Fig. 1 (A) Photograph (×24) of the anode/separator/cathode stack between the stainless steel tube and the rod in the polyimide tube. (B) Schematic representation of the cell. (C) Picture of the cell support placed in the beam line.

Results and discussion

For all the analysed samples and at every position between the lithium surface and the cathode, lithium hydroxide is identified in view of the peaks at $2\theta = 7.03^\circ$, 11.15° and 12.21° corresponding to the (001), (101) and (110) lattice planes respectively (Fig. 2). The GDL ($2\theta = 9.15^\circ$) that is used as a cathode current collector is also identified.

The lithium peroxide (Li_2O_2) formed at the cathode during the discharge is not observed as the particles may be amorphous and hence not visible in XRD patterns. That is why the Li–O_2 cells were also investigated using SEM, collecting the cathode at the pristine (Fig. 3A), discharged (Fig. 3B) and recharged state (Fig. 3C), here for the DET sample. The typical morphology of the carbon electrode changes upon discharge revealing bright

Table 1 List of electrolytes tested, their composition and the slope of peak intensity evolution (in min^{-1}) at both the anode and cathode surface in a cycling (with current) or resting (without current) battery cell

		Anode		Cathode	
Sample name	Electrolyte composition	With current	Without current	With current	Without current
DMSO	DMSO : $LiClO_4$ (95 : 5 mol%)	0.0449	0.0482	0.021	0.036
DET	DMSO : EMIM TFSI : $LiClO_4$ (87 : 8 : 5 mol)	0.2329	0.2539	0.2450	0.2702
DPT	DMSO : PMIM TFSI : $LiClO_4$ (87 : 8 : 5 mol)	0.3334	0.2828	0.2847	0.3135
DBT	DMSO : BMIM TFSI : $LiClO_4$ (87 : 8 : 5 mol)	0.3300	0.3550	0.3302	0.3492

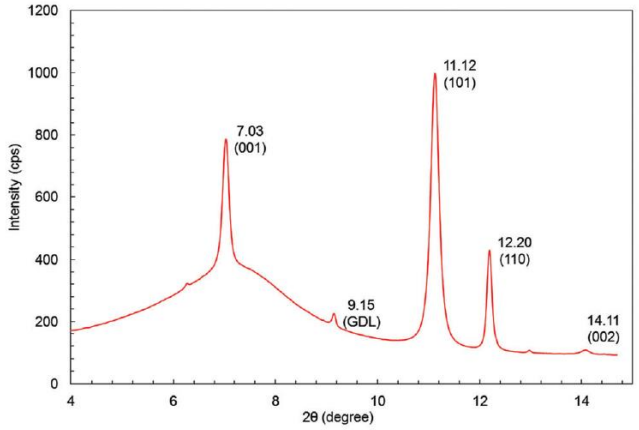

Fig. 2 XRD patterns recorded on the cathode surface of an operating Li–O_2 cell after 1 discharge/recharge cycle at a current density of 20 mA g^{-1}.

particles emerging from the main glassy component. These particles can suggest the presence of Li_2O_2 as reported in previous works.[4,5,22] After recharge, the less compact surface of the electrode may come from the reversibility of the electrochemical process of the Li–O_2 batteries. The electrode does not completely return back to the initial state upon recharge due to the remaining LiOH, formed by another process.

Indeed, the LiOH peaks depicted in Fig. 2 are more intense at the anode and at the separator positions, suggesting that they are formed at the lithium anode surface. Moreover, for each electrolyte tested, the peak intensity progressively increases over time, independently of the state-of-charge. Fig. 4 represents the case of the DPT electrolyte. The XRD patterns A, B, C and D at minutes 0, 50, 100 and 150 are collected during the discharge whereas patterns E, F and G at minutes 200, 250 and 300 are collected during the recharge. This increase of the LiOH peaks, hence its concentration, indicates that the metallic lithium anode may react with the solvent, the ionic liquid and/or with the water coming from the degradation of the electrolyte.[16] Sharon *et al.*[23] proposed indeed the degradation mechanism of the DMSO solvent in Li–O_2 batteries that can result in the formation of LiOH. This implies also that LiOH is not soluble in any electrolyte used, although it does not seem to cause the clogging of the separator.

In order to compare the impact of each electrolyte composition on LiOH formation, the XRD patterns collected at the surface of the lithium anode are assessed. A linear increase of the LiOH concentration is observed at different speeds, depending on the electrolyte used. Then, for each sample, the relative intensity of the (101) peak is computed at different time instances between the start and the end of the first cycle (1 discharge, 1 charge). The results ensue by dividing the actual peak intensity at a given time by the maximum peak intensity measured for the sample in question. The slopes of the curves representing relative intensity *vs.* time are listed in Table 1 for each electrolyte tested.

The increase of the LiOH concentration is in the same range for both the cycling battery and the resting battery. Fig. 5 shows the evolution of relative intensity as a function of time for the

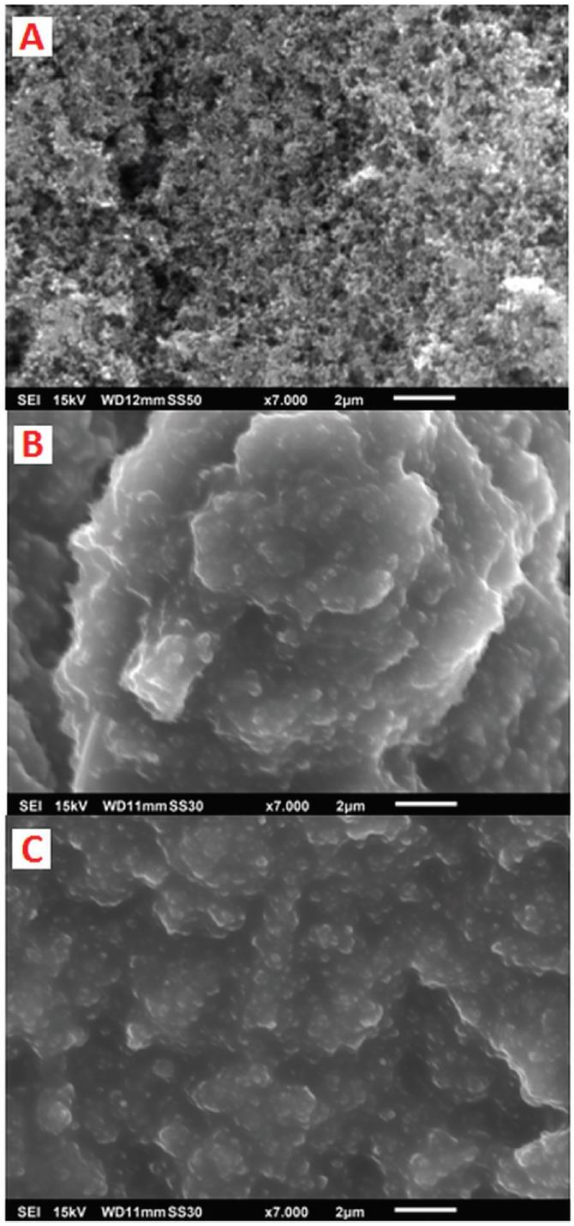

Fig. 3 SEM images of the cathode in its pristine state (A), after discharge (B) and after the following charge (C) in the DET electrolyte.

DET sample. One curve corresponds to the battery cycling and the other to a "blank" battery cell, which is characterized without applying any current, in order to follow the chemical aging of the cell component over time. No difference ensues by the comparison of the slopes of the peak intensity evolution of both blank and real batteries. The LiOH concentration increases linearly over time, regardless of the application of current, and this observation is valid for all the tested samples. Therefore, the reactions between lithium and the different electrolytes are not related to an electrochemical reaction but to a spontaneous chemical process between lithium and the electrolyte. As the formation rate of LiOH is constant, this chemical process may be a pseudo-zero-order reaction. Only a small fraction of lithium may react at the interface with the

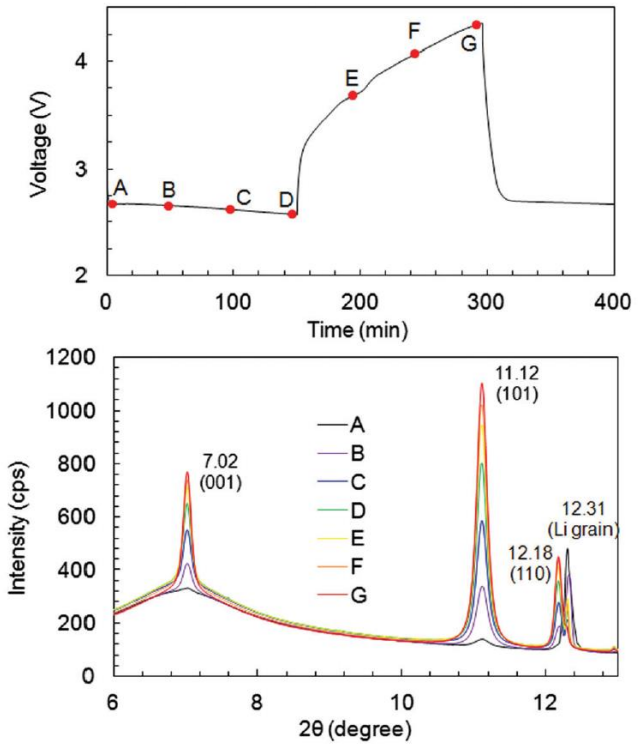

Fig. 4 Discharge–recharge voltage profiles for the first cycle of a Li–O_2 cell using the DPT electrolyte at 20 mA g^{-1} (up) and XRD patterns collected from an anode position near the separator at different cycling times as marked in the up figure (down).

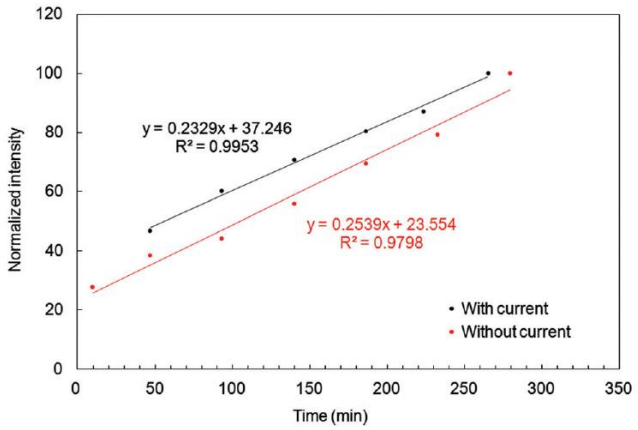

Fig. 5 Comparison of the increase of the relative intensity of the (101) peak among the DET sample cell, for which a current density of 20 mA g^{-1} is applied (black), and of another without any current (red). The duration time corresponds to one discharge/recharge cycle.

electrolyte then the bulk lithium continually replenishes this fraction so its theoretical concentration remains constant.

Besides the DMSO sample, three RTILs with different cations have been tested as co-solvents, each cation having a different chain length on imidazolium (Fig. 6).

The corresponding peak intensity evolution, which is proportional to the LiOH formation rate, is represented in Fig. 7. As it depicts, this evolution is linear for all but not with the same slope. Indeed, the increase of the peak intensity is 5 to 8 times higher for the electrolyte that contains an ionic liquid.

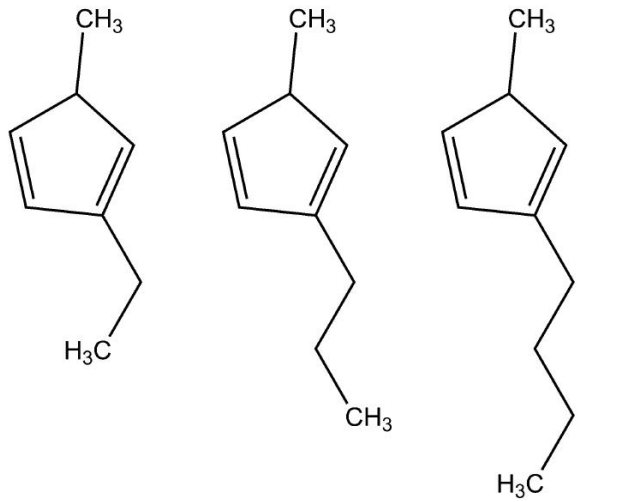

Fig. 6 Molecular structure of the 3 ionic liquid cations used. From the left to the right: 1-ethyl-3-methylimidazolium, 1-propyl-3-methylimidazolium and 1-butyl-3-methylimidazolium.

As the concentration of LiOH is proportional to the peak intensity, this result implies that a reaction occurs between the metallic lithium anode and the ionic liquid contained in the electrolyte. LiOH measured initially in each electrolyte is assumed to be entailed by the reaction of the lithium with the few ppm of water present in the solvent. The slight increase of the DMSO ionic liquid free electrolyte may be ensued by the DMSO decomposition in the presence of electroactive lithium oxygen species.[24] The difference between the propyl and butyl chain is marginal. However, the shortest chain (ethyl) cation suggests that it is less reactive, as the slope of the peak intensity evolution is lower than the one of the propyl and the butyl. It is noteworthy that imidazolium ionic liquids were widely studied in organic chemistry as solvent alternatives, particularly in the chemistry of carbenes.[25–31] The presence of an acidic proton at the C2 position of the cation enables its reactivity towards

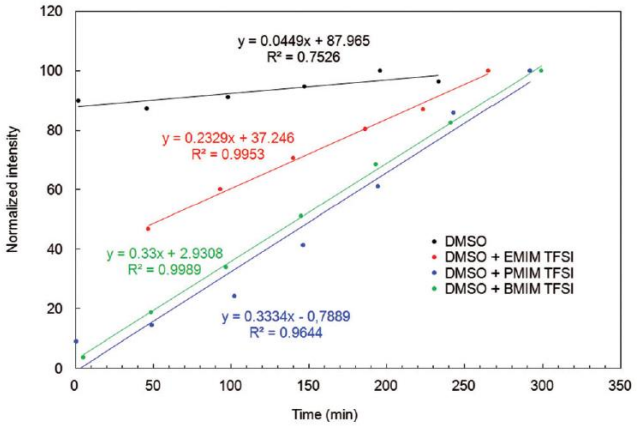

Fig. 7 Relative intensity of the (101) peak at the anode position during the first discharge/recharge cycle of the battery using different electrolytes.

relatively weak bases or electron-rich transition metal complexes.[27] In the studied case, the degradation of the $TFSI^-$ anion in the presence of oxygen and lithium metal leads to the formation of lithium monoxide, namely a strong base.[32] This base will then react with the C2 proton of the imidazolium to form LiOH. The pK_a value of the 1,3-dialkylimidazolium is approximately 22.1 for the one with ethyl and 22.0 for the one with butyl,[25] which is in agreement with the observed LiOH formation rates, although the difference of the pK_a values is insignificant. The kinetics of the reaction may then be the main factor controlling this reaction.

Conclusions

A lithium–oxygen battery using RTIL as an electrolyte co-solvent is characterized using *in situ* XRD during discharge/recharge cycling and without applying any current. The formation of lithium hydroxide is observed for all the different electrolytes tested but at different formation rates. In the DMSO electrolyte, a very small increase of the LiOH concentration is observed whereas it is increasing 5 to 7 times higher during the entirety of the discharge/recharge cycles of the batteries using a RTIL in the electrolyte. Moreover, upon LiOH formation no difference is detected for the same cell for which no current was applied. Therefore, the formation of LiOH occurs mainly due to the reaction between the lithium anode and the RTIL present in the electrolyte. These side reactions may be related to the reduced overpotential observed with electrolytes containing RTILs. The use of the specific RTILs selected for this study is not suitable for practical Li–O_2 batteries as they increase significantly their aging. The previously established hypothesis for the improvement of reversibility based on the blended electrolyte containing an RTIL is not confirmed. The use of RTILs leads to an increase of LiOH formation leading to higher electrolyte consumption. A more stable electrolyte containing for instance a C2-substituted imidazolium or a pyrrolidinium RTIL is required for the development of this technology on a higher scale.

Acknowledgements

The STABLE project received funding from the European Union's FP7/2007–2013 research and innovation program under grant agreement no. 314508. G. G. thanks financial support from project CTQ2015-65439-R from the MINECO. These experiments are performed at the BL04_MSPD beamline at ALBA Synchrotron with the collaboration of ALBA staff. E. K. gratefully acknowledges helpful discussions with Dr A. M. Valdivielso.

References

1 G. Girishkumar, B. D. McCloskey, A. C. Luntz, S. Swanson and W. Wilcke, *J. Phys. Chem. Lett.*, 2010, **1**, 2193–2203.
2 C. J. Allen, J. Hwang, R. Kautz, S. Mukerjee, E. J. Plichta, M. a. Hendrickson and K. M. Abraham, *J. Phys. Chem. C*, 2012, **116**, 20755–20764.
3 D. Bresser, E. Paillard and S. Passerini, *J. Electrochem. Sci. Technol.*, 2014, **5**, 37–44.
4 J. Zeng, J. R. Nair, C. Francia, S. Bodoardo and N. Penazzi, *Int. J. Electrochem. Sci.*, 2013, **8**, 3912–3927.
5 S. Ferrari, E. Quartarone, C. Tomasi, M. Bini, P. Galinetto, M. Fagnoni and P. Mustarelli, *J. Electrochem. Soc.*, 2014, **162**, A3001–A3006.
6 S.-M. Han, J.-H. Kim and D.-W. Kim, *J. Electrochem. Soc.*, 2015, **162**, A3103–A3109.
7 J. Kim, E. Ahn and Y. Tak, *Int. J. Electrochem. Sci.*, 2015, **10**, 2921–2930.
8 S. Das, J. Højberg, K. B. Knudsen, R. Younesi, P. Johansson, P. Norby and T. Vegge, *J. Phys. Chem. C*, 2015, **119**, 18084–18090.
9 G. A. Elia, J. Hassoun, B. Scrosati, F. Mueller, D. Bresser, S. Passerini, P. Oberhumer, N. Tsiouvaras and J. Reiter, *Nano Lett.*, 2014, **14**, 6572–6577.
10 H. Nakamoto, Y. Suzuki, T. Shiotsuki, F. Mizuno, S. Higashi, K. Takechi, T. Asaoka, H. Nishikoori and H. Iba, *J. Power Sources*, 2013, **243**, 19–23.
11 K. Cai, H. Jiang and W. Pu, *Int. J. Electrochem. Sci.*, 2014, **9**, 390–397.
12 L. Cecchetto, M. Salomon, B. Scrosati and F. Croce, *J. Power Sources*, 2012, **213**, 233–238.
13 H. Lim, E. Yilmaz and H. R. Byon, *J. Phys. Chem. Lett.*, 2012, **3**, 3210–3215.
14 J. Liu, M. Roberts, R. Younesi, M. Dahbi and J. Zhu, *J. Phys. Chem. Lett.*, 2013, **4**, 4045–4050.
15 K. R. Ryan, L. Trahey, J. S. Okasinski, A. K. Burrell and B. J. Ingram, *J. Mater. Chem. A*, 2013, **1**, 6915–6919.
16 J.-L. Shui, J. S. Okasinski, P. Kenesei, H. a Dobbs, D. Zhao, J. D. Almer and D.-J. Liu, *Nat. Commun.*, 2013, **4**, 2255.
17 J. L. Shui, J. S. Okasinski, C. Chen, J. D. Almer and D. J. Liu, *ChemSusChem*, 2014, **7**, 543–548.
18 M. M. Storm, R. E. Johnsen, R. Younesi and P. Norby, *J. Mater. Chem. A*, 2015, **3**, 3113–3119.
19 C. O. Laoire, S. Mukerjee, K. M. Abraham, E. J. Plichta and M. a. Hendrickson, *J. Phys. Chem. C*, 2009, **113**, 20127–20134.
20 T. Vogl, P. Goodrich, J. Jacquemin, S. Passerini and A. Balducci, *J. Phys. Chem. C*, 2016, **120**, 8525–8533.
21 F. Fauth, R. Boer, F. Gil-Ortiz, C. Popescu, O. Vallcorba, I. Peral, D. Fullà, J. Benach and J. Juanhuix, *Eur. Phys. J. Plus*, 2015, **130**, 160.
22 F. Soavi, S. Monaco and M. Mastragostino, *J. Power Sources*, 2013, **224**, 115–119.
23 D. Sharon, D. Hirshberg, M. Afri, A. Garsuch, A. A. Frimer and D. Aurbach, *Isr. J. Chem.*, 2015, **55**, 508–520.
24 D. Sharon, M. Afri, M. Noked, A. Garsuch, A. a Frimer and D. Aurbach, *J. Phys. Chem. Lett.*, 2013, **4**, 3115–3119.
25 D. J. Nelson and S. P. Nolan, *Chem. Soc. Rev.*, 2013, **42**, 6723–6753.
26 S. Sowmiah, V. Srinivasadesikan, M. C. Tseng and Y. H. Chu, *Molecules*, 2009, **14**, 3780–3813.
27 J. Dupont and P. A. Suarez, *Phys. Chem. Chem. Phys.*, 2006, **8**, 2441–2452.

28 T. L. Amyes, S. T. Diver, J. P. Richard, F. M. Rivas and K. Toth, *J. Am. Chem. Soc.*, 2004, **126**, 4366–4374.
29 H. Chen, D. R. Justes and R. G. Cooks, *Org. Lett.*, 2005, **7**, 3949–3952.
30 P. A. Z. Suarez, C. S. Consorti, R. F. De Souza, J. Dupont and R. S. Gonçalves, *J. Braz. Chem. Soc.*, 2002, **13**, 106–109.
31 F. F. C. Bazito, Y. Kawano and R. M. Torresi, *Electrochim. Acta*, 2007, **52**, 6427–6437.
32 A. Budi, A. Basile, G. Opletal, A. F. Hollenkamp, A. S. Best, R. J. Rees, A. I. Bhatt, A. P. O'Mullane and S. P. Russo, *J. Phys. Chem. C*, 2012, **116**, 19789–19797.

Appendix II

Non-published article

"Suitability of blended ionic liquid-dimethylsulfoxide electrolyte for lithium-oxygen battery"

E. Knipping, C. Aucher, G. Guirado, L. Aubouy

Non-published manuscript

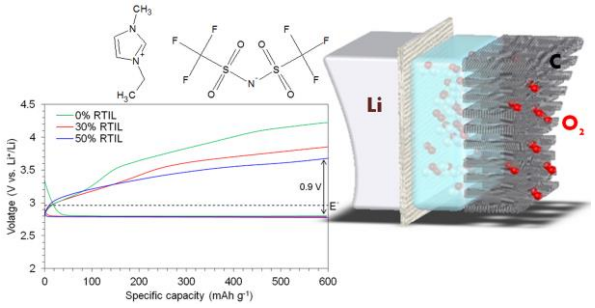

Journal Name

COMMUNICATION

Suitability of blended ionic liquid-dimethylsulfoxide electrolyte for lithium-oxygen battery

Received 00th January 20xx,
Accepted 00th January 20xx

DOI: 10.1039/x0xx00000x

www.rsc.org/

E. Knipping,[a,b] C. Aucher,[a] G. Guirado[b] and L. Aubouy[a]

Electrolytes composed of dimethylsulfoxide (DMSO), 1-ethyl-3-methylimidazolium bis(trifluoromethylsulfonyl)imide (EMI TFSI) and $LiClO_4$ are characterized for lithium-oxygen battery. The optimum addition of EMI TFSI enables to reduce the overpotential from 1.43 V to 1.06 V, with a cyclability of 69 cycles with 200 mAh g^{-1} of limited capacity.

The Li-O_2 battery has received much interest in the last few years, as its theoretical capacity reaches 5-10 times the current Li-ion battery capacity.[1] The main electrochemical process in an aprotic Li-O_2 battery is the formation and decomposition of the Li_2O_2, during discharge and recharge respectively. However, this reaction suffers from low reversibility leading to a low cyclability of the battery. Recently, Room Temperature Ionic Liquids (RTILs) attracted much attention for Li-O_2 battery electrolyte.[2–12] Namely, Nakamoto et al.[13] demonstrated the advantage of the RTILs stability against electrochemical oxidation vs. Li^+/Li and O_2 redox reversibility. Cai et al.[14] proved that ionic liquid could show higher specific capacity compared to carbonate solvent electrolytes. Moreover, Cechetto et al.[15] observed a decrease of 0.4 V of the overpotential by mixing ionic liquids with an ether-based electrolyte. This could be explained by a higher ionic conductivity of the electrolyte containing the ionic liquid, a less insulating Li_2O_2 particle interface and a better Li_2O_2 solubility resulting to improved kinetics of the Li_2O_2 oxidation. On the other hand, pure RTIL electrolytes were tested in previous experiments, but an adequate reversibility of the Li-O_2 battery reaction is not attainable probably due to their high viscosity that affects the ion diffusion and the kinetics of the battery reaction.[16] Moreover, poor battery capacity[13] and a cyclability lower than 30 cycles is generally obtained.[4,14] In the present work, we study the influence of the 1-ethyl-3-methylimidazolium bis(trifluoromethylsulfonyl)imide (EMI TFSI) as co-solvent of Li-O_2 battery electrolyte in the final aim of designing an adequate solution for this technology. Thermal properties, stability with lithium metal and electrochemical performance are evaluated for DMSO-based electrolyte containing different amount of EMI TFSI, a RTIL known for its thermal resistance, high conductivity and electrochemical stability.[17] Hence, four mixed electrolytes ET-0, ET-30, ET-50 and ET-100 are prepared by adding 5w% of $LiClO_4$ to the mixed solution of DMSO and EMI TFSI, the weight ratio of EMI TFSI/DMSO being 0/100, 30/70, 50/50 and 100/0 respectively. The results are summarized in the Table 1.

Table 1. Ionic conductivity, viscosity, degradation temperature, capacity, overpotential and cycling life of the four studied electrolytes.

	ET-0	ET-30	ET-50	ET-100
Ionic conductivity (mS cm^{-1})	7.88	13.1	10.1	0.49
Viscosity (cP)	6.5	6.3	12	81
Degradation temperature (°C)	105	182	>200	>200
Capacity full discharge (mAh g^{-1})	5651	7618	4631	3060
Overpotential 1st cycle (V)	1.43	1.06	0.90	1.16
Cycling life (cycles)	98	69	18	7

The effect of the use of ionic liquids on the thermal stability of the above-mentioned electrolytes are analysed by performing DSC tests. Before the heating ramp, the samples are cooled and equilibrated at -90°C to allow their crystallization. In the case of ET-0 and ET-30, the DSC profiles (Figure 1) show endothermic peaks at

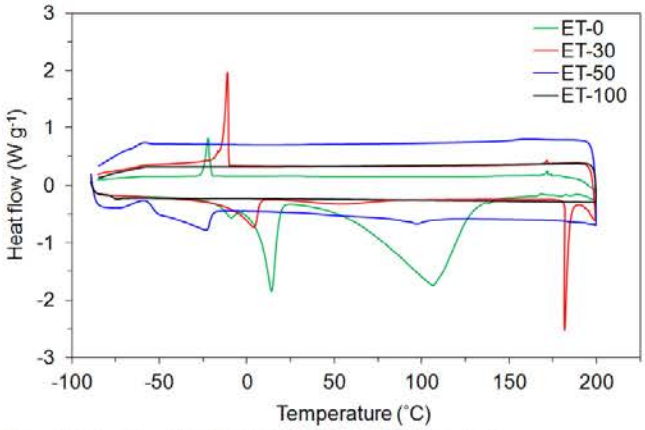

Figure 1. DSC profiles of the ET-0, ET-30, ET-50 and ET-100 electrolytes.

[a] Leitat Technological Center, Carrer de la Innovació, 2 08225 Terrassa, Spain.
[b] Departament de Química, Universitat Autònoma de Barcelona, E-08193 Bellaterra, Barcelona, Spain.

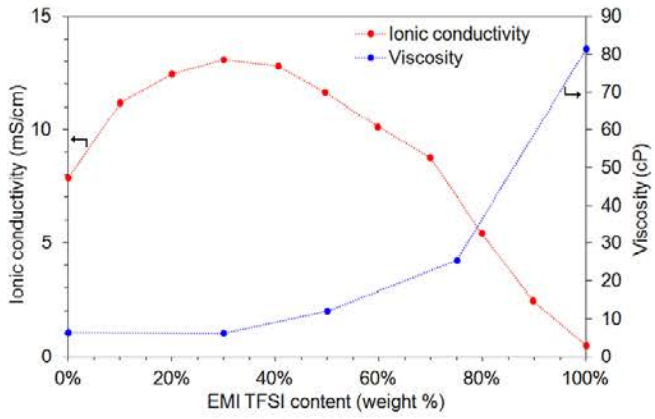

Figure 2. Ionic conductivity and viscosity of blended electrolytes as function of EMI TFSI content in the EMI TFSI/DMSO solution. All the solutions have $LiClO_4$ content of 5w%.

13 and 2°C respectively, corresponding to the melting point. The ET-0 shows another endothermic peak at -7°C that may correspond to a solid-solid phase transition. For the samples with more EMI TFSI content, i.e. ET-50 and ET-100, no crystalline phase is detected, showing that for the procedure used, the electrolytes remained amorphous. Moreover, thermal stability is improved with the addition of EMI TFSI. Without RTIL, an endothermic peak occurred at 105°C but when 30% of EMITFSI is added, the endothermic peak is postponed to 182°C. For ET-50 and ET-100, no endothermic peak is observed, showing that the degradation of the electrolyte occurs at higher temperature. The safety of the battery can be then improved with the addition of an RTIL, as it can enhance the thermal stability of the electrolyte.

Ionic conductivity and viscosity of the blended electrolytes are measured and represented in function of the DMSO/EMI TFSI ratio (Figure 2). The ionic conductivity initially increases with increasing EMI TFSI content, reaching a maximum of 13.1 mS cm^{-1} at 30% by weight. Because EMI TFSI itself is a salt, the number of ions in the electrolyte increases with increasing EMI TFSI content and then the ionic conductivity too. However, adding EMI TFSI increases also the viscosity of the electrolyte from 6.5 cP for ET-0 to 81.4 for ET-100, due to the increased ion-solvent interactions and Coulombic interactions between ionic species[7]. Thus, the decrease of the ionic conductivity from 50% of EMI TFSI content can be attributed to the increase of the viscosity. It is shown then that the addition of a small amount of RTIL in the electrolyte can increase its ionic conductivity, which may be beneficial for the battery.

To verify the compatibility of these new electrolytes with the lithium anode, Li/Li stripping/plating test is realized within the different electrolyte at 10 mA cm^{-2} and 25 °C. The cell is charged at constant current for 1 hour at 10 mA cm^{-2} and subsequently discharge for 1 hour at -10 mA cm^{-2}. A typical voltage profile is shown in the Figure 3-A. Since the cell is symmetric, it is not affected by parasitic chemical or electrochemical reactions and the cycles are symmetrical. The evolution of the overpotential of the Li/Li cell is shown for each electrolyte (Figure 3-B). With the ET-0 as electrolyte, the cell voltage is seen to be very low, around 9 mV vs. Li^+/Li and stays constant upon cycling for at least 200 cycles. This low voltage amplitude indicates that no passivation layer is formed. Concerning both blended electrolytes (ET-30 and ET-50), the cell voltage varies between 0.2 and 0.5 V vs. Li^+/Li, which is due to the formation of a solid electrolyte interphase (SEI) layer. A cell voltage around 0.1 V vs. Li^+/Li for ET-100 is observed, showing that the lithium surface is passivated in the presence of the EMI TFSI, probably due to molecule adsorption at the surface within lower voltage amplitude with respect to blended electrolytes. In all cases, the electrolyte enables the stripping/plating of the lithium.

The full discharge capacities of the Li-O_2 cells were measured at a constant specific current of 200 mA g^{-1}. The first full discharge curves obtained with the different electrolytes are shown in the Figure 4. The cell with ET-30 presents the highest capacity with 7618 mAh g^{-1}, whereas the cell with RTIL-free electrolyte (ET-0) has a capacity of 5651 mAh g^{-1}. This improvement by adding 30% of EMI TFSI can be explained by the higher ionic conductivity and a better wettability of the ET-30. However, adding more EMI TFSI in the electrolyte increases the viscosity, which leads to lower capacity. An optimization of the electrolyte content is then needed to achieve high battery performance. The four electrolytes are then tested in Li-O_2 cells to obtain discharge/recharge cycles at a controlled depth

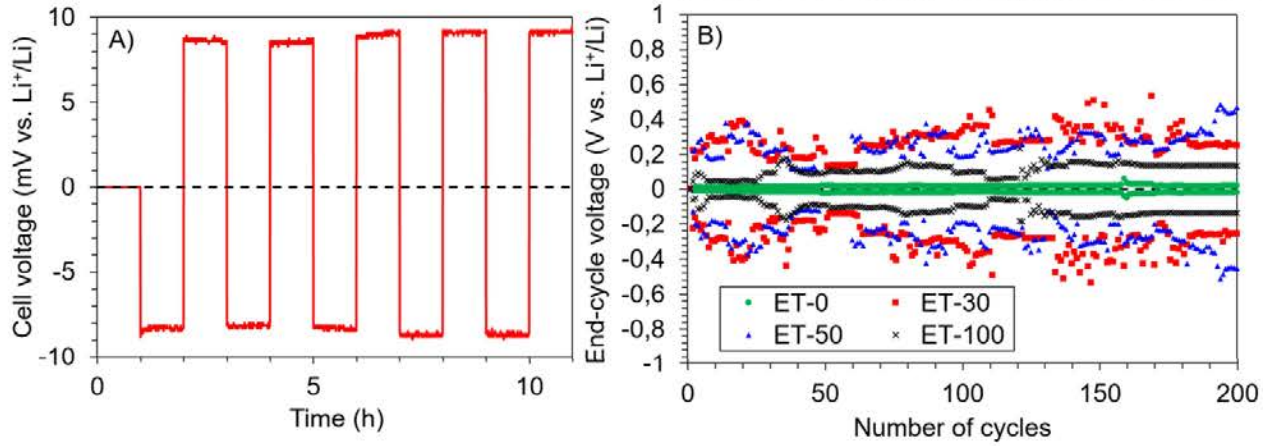

Figure 3. A) Typical voltage behavior of Li-Li cell during galvanostatic lithium stripping/plating cycle test (case of ET-0). A current of 10 mA cm^{-2} was applied for 1 hour in each direction. B) Evolution of the cell-voltage cutoff with the number of cycles for the different electrolytes studied.

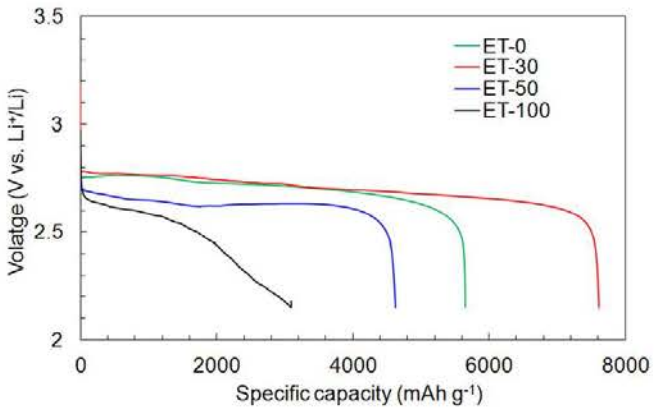

Figure 4. Initial full discharge curves of Li-O_2 cells with ET-0, ET-30, ET-50 and ET-100 electrolytes.

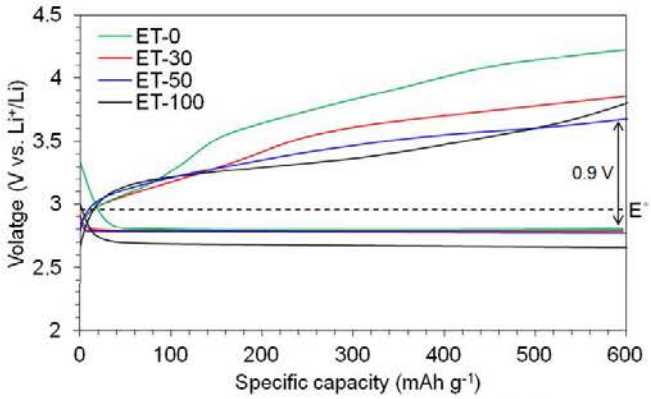

Figure 5. First cycle galvanostatic discharge and recharge of Li-O_2 cell with the different electrolytes studied, at the applied current of 200 mA g^{-1} and limited capacity of 600 mAh g^{-1}.

of discharge of 600 mAh g^{-1} and constant current of 200 mA g^{-1}. On the first cycle (Figure 5), the oxidation potential decreases with increased content of EMI TFSI. Indeed, the higher ionic conductivity of ET-30 and ET-50 compared to ET-0 enables faster kinetics of the oxidation reactions. The difference between ET-30 and ET-50, 3.86 and 3.68 V vs. Li^+/Li respectively, may be ascribed to a better wettability of the ET-50 electrolyte.[7] The higher EMI TFSI content makes the electrolyte more hydrophobic, wetting then more effectively the hydrophobic carbon cathode. Concerning the ET-100, the discharge plateau has a lower voltage (2.66 V vs. Li^+/Li) than for the electrolytes containing DMSO (2.80 V vs. Li^+/Li). Despite its high viscosity, the ET-100 show low oxidation potential of only 3.82 V vs. Li^+/Li, which may be due its hydrophobicity.[7] However, this potential rapidly increases with the cycles (Figure 6-D). The evolution of the overpotential with the cell cycling is shown in the Figure 6. Although it shows the highest overpotential, ET-0 has better cycling stability with 98 cycles whereas the ET-30 and ET-50 work for 69 and 18 cycles respectively. The overpotential of ET-0 is the highest observed at the first cycle and the charge voltage increases rapidly to 4.35 V vs. Li^+/Li after only 12 cycles. On the other hand, the ET-30 shows charge voltage below 4.35 V vs. Li^+/Li until the 54th cycle. As shown previously, the addition of EMI TFSI enables to increase the ionic conductivity of the electrolyte but it may also enhance the O_2 solubility.[18,19] Thus a better reversibility is observed for the electrolytes containing the ionic liquids for the first cycles. Indeed, the charge potential increases with the number of cycles until the battery fails, which occurs earlier when the electrolyte contains EMI TFSI. This can be ascribed to the

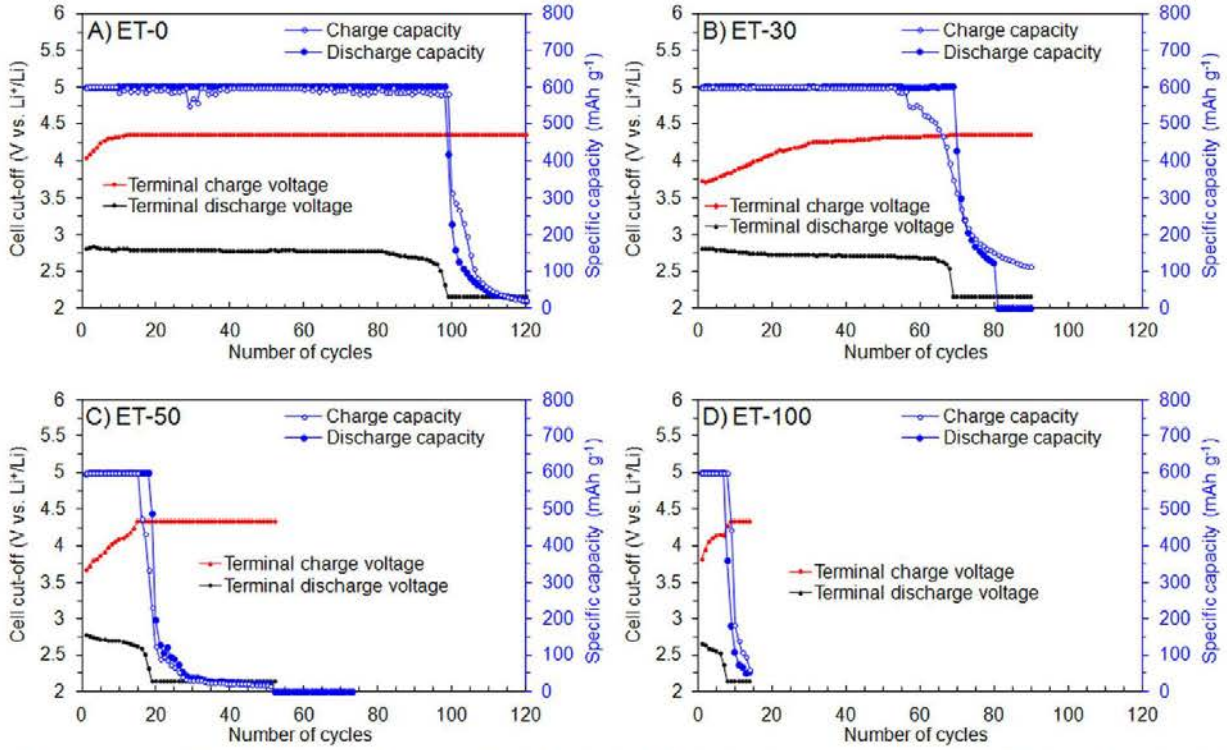

Figure 6. Cycling performance (blue curves) and corresponding cell-voltage cut-off (red and black curves) of Li-O_2 cells with A) ET-0, B) ET-30, C) ET-50 and D) ET-100 electrolytes at a constant current of 200 mA g^{-1} and 600 mAh g^{-1} capacity limit.

degradation products formation which was proved in previous work, that it is faster in presence of EMI TFSI than in DMSO without RTIL.[20] It was observed indeed that with cycling, LiOH concentration increases more rapidly in presence of ionic liquids, due to the high reactivity of the C2 proton of imidazolium cations, especially in presence of radical peroxide.[6,21] Concerning the DMSO, Sharon *et al.*[22] observed the formation of side products when exposed to superoxide. This would explain the battery cycling being limited at 98 cycles when using the ET-0.

In summary, it is important to remark that for blended DMSO/EMI TFSI electrolytes, significant improvements are observed concerning the thermal stability with a degradation/evaporation occurring at a temperature 80° higher and the ionic conductivity increasing from 7.88 to 13.1 mS cm^{-1} by adding 30% in weight of EMI TFSI. The Li-O_2 battery performance is also improved with a 35% higher full discharge capacity and an overpotential reduced to 1.06 V versus 1.43 V for the DMSO electrolyte. Reasonable cycling performance are also obtained, although the electrolyte without RTIL shows higher cycling life (98 cycles), 69 cycles are obtained with the blended electrolyte. The use of a RTIL more stable against peroxide radical attack and in presence of lithium may enable a longer cycle life. Besides, this study shows that the bulk electrolyte parameters (ionic conductivity, viscosity) have more influence on the battery performance than the cathode surface parameters (cell overpotential, wettability) and the anode surface parameters (Li/Li overpotential).

The STABLE project received funding from the European Union's FP7 research and innovation program under grant agreement Nº 314508. G. G. thanks financial support from project CTQ2015-65439-R from the MINECO.

Notes and references

1 G. Girishkumar, B. D. McCloskey, A. C. Luntz, S. Swanson and W. Wilcke, *J. Phys. Chem. Lett.*, 2010, **1**, 2193–2203.
2 C. J. Allen, J. Hwang, R. Kautz, S. Mukerjee, E. J. Plichta, M. a. Hendrickson and K. M. Abraham, *J. Phys. Chem. C*, 2012, **116**, 20755–20764.
3 S. Ferrari, E. Quartarone, C. Tomasi, M. Bini, P. Galinetto, M. Fagnoni and P. Mustarelli, *J. Electrochem. Soc.*, 2014, **162**, A3001–A3006.
4 G. A. Elia, J. Hassoun, B. Scrosati, F. Mueller, D. Bresser, S. Passerini, P. Oberhumer, N. Tsiouvaras and J. Reiter, *Nano Lett.*, 2014, **14**, 6572–6577.
5 D. Bresser, E. Paillard and S. Passerini, *J. Electrochem. Sci. Technol.*, 2014, **5**, 37–44.
6 S. Das, J. Højberg, K. B. Knudsen, R. Younesi, P. Johansson, P. Norby and T. Vegge, *J. Phys. Chem. C*, 2015, **119**, 18084–18090.
7 S.-M. Han, J.-H. Kim and D.-W. Kim, *J. Electrochem. Soc.*, 2015, **162**, A3103–A3109.
8 Y. Li, Z. Zhang, D. Duan, Y. Sun, G. Wei, X. Hao, S. Liu, Y. Han and W. Meng, *J. Power Sources*, 2016, **329**, 207–215.
9 P. Lou, C. Li, Z. Cui and X. Guo, *J. Mater. Chem. A*, 2016, **4**, 241–249.
10 W. Ni, S. Liu, Y. Fei, Y. He, X. Ma, L. Lu and Y. Deng, *ACS Appl. Mater. Interfaces*, 2017, **9**, 14749–14757.
11 S. Matsuda, K. Uosaki and S. Nakanishi, *J. Power Sources*, 2017, **356**, 12–17.
12 M. Olivares-marín, A. Sorrentino, E. Pereiro and D. Tonti, *J. Power Sources*, 2017, **359**, 234–241.
13 H. Nakamoto, Y. Suzuki, T. Shiotsuki, F. Mizuno, S. Higashi, K. Takechi, T. Asaoka, H. Nishikoori and H. Iba, *J. Power Sources*, 2013, **243**, 19–23.
14 K. Cai, H. Jiang and W. Pu, *Int. J. Electrochem. Sci.*, 2014, **9**, 390–397.
15 L. Cecchetto, M. Salomon, B. Scrosati and F. Croce, *J. Power Sources*, 2012, **213**, 233–238.
16 C. O. Laoire, S. Mukerjee, K. M. Abraham, E. J. Plichta and M. a. Hendrickson, *J. Phys. Chem. C*, 2009, **113**, 20127–20134.
17 P. Bonhôte, A.-P. Dias, N. Papageorgiou, K. Kalyanasundaram and M. Grätzel, *Inorg. Chem.*, 1996, **35**, 1168–1178.
18 Y.-F. Hu, Z.-C. Liu, C.-M. Xu and X.-M. Zhang, *Chem. Soc. Rev.*, 2011, **40**, 3802.
19 S. Monaco, A. M. Arangio, F. Soavi, M. Mastragostino, E. Paillard and S. Passerini, *Electrochim. Acta*, 2012, **83**, 94–104.
20 E. Knipping, C. Aucher, G. Guirado, F. F. Fauth and L. Aubouy, *New J. Chem.*, 2017, **41**, 7267–7272.
21 M. Hayyan, F. S. Mjalli, M. A. Hashim and I. M. Alnashef, *J. Mol. Liq.*, 2013, **181**, 44–50.
22 D. Sharon, M. Afri, M. Noked, A. Garsuch, A. a Frimer and D. Aurbach, *J. Phys. Chem. Lett.*, 2013, **4**, 3115–3119.